The origin of rhythmic magmatic layering in coarse-grained porphyritic S-type granite of the Peninsula pluton, Cape Granite Suite, South Africa

by

Priscilla L. Ramphaka

Thesis presented in partial fulfilment of the requirements for the degree of Master of Science in the Department of Earth Sciences, University of Stellenbosch

Supervisor: Prof Gary Stevens

Co-supervisor: Dr Federico Farina

Faculty of Science

November 2013

DECLARATION

By submitting this thesis, I declare that the entirety of the work contained therein is my own original work and that I am the sole author thereof (save to the extent explicitly otherwise stated). The reproduction and publication thereof by Stellenbosch University will not infringe any third party rights and that I have not previously submitted it either in its entirety or in part at any university for obtaining a qualification.

Signature: ……..

Date: November 2013

ABSTRACT

Rhythmic magmatic layering in granites is an intriguing feature that has been reported from plutons with contrasting chemical compositions from a wide range of tectonic settings. Layered granites are rare and occur in association with volumetrically dominant non-layered rocks having similar composition. Understanding the origin of such layering in granites, particularly from well exposed outcrops, may give crucial insights on the physical-chemical conditions and processes (such as fractional crystallization, size and composition of individual magma batches, efficiency of mixing between batches etc.) within magma chambers during their construction. In the Cape Granite Suite, rhythmic layering is exceptionally well preserved in outcrops of the S-type granodioritic to monzogranitic Peninsula pluton along the coastline of the small town of Llandudno.

At Llandudno, the granodioritic facies of the Peninsula pluton is exposed as a coarse-grained, cordierite and K-feldspar phenocrystic granite (referred to as Llandudno granodiorite in this study). Layering within the Llandudno granodiorite occurs within several lens-shaped bodies, of which the largest, with a thickness of about 5 m. The studied rhythmic sequence comprises 50 layers with thicknesses ranging between 5 and 50 cm. Each layer is typically characterised by a sharp lower contact overlain by a biotite-rich portion containing approximately 50 vol. % biotite. This mafic lower portion, grades upwards into a strongly leucocratic upper portion enriched in quartz, plagioclase and K-feldspar. The layered rocks host a substantially lower abundance of K-feldspar megacrysts and cordierite than the surrounding Llandudno granodiorite. In particular, cordierite crystals are five times less abundant in the layered zone than the un-layered Llandudno granodiorite. The K-Feldspars megacrysts that do occur within the layering are generally concentrated in the mafic part of some of the layers and are commonly oriented parallel to the layering. The K-feldspar megacrysts are significantly smaller than those in Llandudno granodiorite, but were found to be similar in composition.

The whole rock compositions of the layered rocks are peraluminous with A/CNK >1.4. They have lower Mg#s (51 to 58) than the Llandudno granodiorite (51 to 65). The Na_2O/CaO ratio of mafic and leucocratic portions is higher than in the Peninsula pluton. The mafic portions show an enrichment of trace and rare earth elements relative to the leucocratic portions and Peninsula pluton. The difference in bulk rock composition as well as trace and rare earth

elements composition shows that the layered rocks were not formed by magmas produced by differentiation of the Llandudno granodiorite. The differences in biotite composition in basal sections of adjacent layers suggest that each layer represents a separate magma pulse, with the mafic portions of the layers largely representing an accumulation of the crystals in the magma batch at the time of injection and that these crystals mostly consist of orthopyroxene and biotite. This is in agreement with the findings based on the whole rock chemistry of the layers compared with the Llandudno granodiorite. The inclusion of K-feldspar megacrysts from the host granite into the layering, as well as the exceptional state of preservation of the layering, suggests that the layering formed relatively late in the crystallization sequence of the granite. This, in combination with the evidence for subtle differences in the chemistry of the magmas that formed separate layers, suggests that the layers represent a frozen feeder zone in the Peninsula pluton recording small successive pulses of magma addition. Frequent occurrence of the less-preserved layered biotite schlieren in the pluton may represent the equivalents of the layering that have become partially digested and texturally equilibrated with the host magma.

OPSOMMING

Ritmiese magmatiese gelaagdheid in graniet is ’n interessante kenmerk van plutone met teenstellende chemiese samestellings in ’n wye verskeidenheid tektoniese omgewings. Gelaagde graniet is seldsaam en kom saam met volumetries dominante, niegelaagde gesteentes met soortgelyke samestellings voor. ’n Begrip van die oorsprong van hierdie gelaagdheid in graniet, veral in goed sigbare dagsome, kan belangrike insig verleen in die fisies-chemiese omstandighede en prosesse (soos fraksionele kristallisasie, die grootte en samestelling van individuele volumes magma, die doeltreffendheid van volume-vermenging, ensovoorts) in magmakamers gedurende die vorming daarvan. In die Kaapse granietgroep het ritmiese gelaagdheid besonder goed behoue gebly in dagsome van die S-tipe granodioritiese tot monsogranitiese Skiereilandse plutoon langs die kuslyn van die voorstad Llandudno.

Die granodioritiese fasies van die Skiereilandse plutoon by Llandudno manifesteer in die vorm van ’n grofkorrelrige, kordiëritiese en K-veldspatiese fenokris-graniet (wat in hierdie studie Llandudno-granodioriet genoem word). Gelaagdheid in die Llandudno-granodioriet kom voor in verskeie lensvormige massas, waarvan die grootste sowat 5 m dik is. Die bestudeerde ritmiese opeenvolging bestaan uit 50 lae met diktes van tussen 5 cm en 50 cm. Elke laag word gekenmerk deur ’n skerp onderste kontakvlak wat bedek is met ’n biotiet-ryke gedeelte wat uit sowat 50 vol % biotiet bestaan. Hierdie mafiese onderste gedeelte gradeer opwaarts in ’n sterk leukokratiese boonste gedeelte wat ryk is aan kwarts, plagioklaas en K-veldspaat. Die gelaagde gesteentes bevat beduidend minder K-veldspatiese megakriste en kordiëriet as die omliggende Llandudno-granodioriet. Die kordiëritiese kristalle in besonder kom vyf keer minder in die gelaagde sone as in die niegelaagde Llandudno-granodioriet voor. Die K-veldspatiese megakriste wat wél in die gelaagdheid voorkom, is oor die algemeen in die mafiese gedeelte van sommige lae gekonsentreer, en ~~lê~~ is meestal parallel met die gelaagdheid georiënteerd. Die K-veldspatiese megakriste is aansienlik kleiner as dié in die Llandudno-granodioriet, maar het ’n soortgelyke samestelling. Die heelrots-samestellings van die gelaagde gesteentes is peralumineus, met A/CNK >1,4. Dit toon ook laer Mg#s (51 tot 58) as die Llandudno-granodioriet (51 tot 65). Die Na_2O/CaO-verhouding van die mafiese en leukokratiese gedeeltes is hoër as in die Skiereilandse plutoon. In die mafiese gedeeltes is daar ‘n verryking in spoor- en skaarsaarde-elemente relatief tot die leukokratiese gedeeltes sowel as die Skiereilandse plutoon. Die verskil in heelrots-samestelling sowel as spoor- en seldsame-aardelementsamestelling toon dat die gelaagde gesteentes nié gevorm is deur

magmas wat uit differensiasie van die Llandudno-granodioriet ontstaan het nie. Uit die verskille in die biotiet-samestelling van basissnitte uit aanliggende lae word afgelei dat elke laag ’n afsonderlike magmapuls verteenwoordig, terwyl die mafiese gedeeltes van die lae hoofsaaklik ‘n versameling van kristalle verteenwoordig wat tydens inplasing van die magma volume gevorm het, meestal ortopirokseen en biotiet. Dít stem ooreen met die bevindinge rakende die heelrots-chemie van die lae in vergelyking met die Llandudno-granodioriet. Die insluiting van K-veldspatiese megakriste vanaf die moedergraniet by die gelaagdheid, dui daarop dat die gelaagdheid betreklik laat in die kristallisasie-orde van die graniet gevorm het. Dít, tesame met bewyse van subtiele verskille in die chemie van die magmas waaruit afsonderlike lae gevorm is, dui daarop dat die lae ’n bevrore toevoersone in die Skiereilandse plutoon uitmaak wat kort, opeenvolgende pulse van magmatoevoeging vasgevang het. Die gereelde voorkoms van swakker bewaarde, gelaagde biotiet-sliere in die plutoon kan moontlik dui op sones van die gelaagdheid wat gedeeltelik verteer is en tekstureel met die moedermagma ge-ekwilbreer het.

ACKNOWLEDGEMENTS

I would like to acknowledge support from my supervisors Prof Gary Stevens and Dr Federico Farina for their continuous support and encouragement never to give up throughout the research; this thesis wouldn't be possible without your continuous ideas to help complete it. Throughout our discussions I have grown immensely in the knowledge of Igneous Petrology and the Cape Granite Suite. Thank you for Prof Gary Sevens for sponsoring my studies and making me feel welcome and being part of the Stellenbosch geology community. Thank you to Madelaine Frazenburg, Dirk Frei, Riana Rossouw and Esme Spicer for your help with my analytical acquisitions. Thank you to George Olivier for the field equipment required and Fundisile for helping me with the sample preparation instruments.

I would like to thank my fellow research students; Cedric and Kathryn for going with me to the field, Risa and Wasiu your support was just unforgettable. A big thank you to all my friends (Joanna and Jane) and my brethren from church for praying with and for me, your continuous prayers and the word your minister really kept me going. My deepest appreciation to my Pastor, there is no way I would have been here without your teachings. I would like to thank my parents and family for their continuous support, I really appreciate and love each one of you a lot.

TABLE OF CONTENTS

LIST OF FIGURES

Figures **Page**

LIST OF TABLES

Tables **Page**

CHAPTER ONE

INTRODUCTION

The volume of individual magma batches involved in the construction of granitoid plutons is currently the subject of substantial scientific debate. The formation of plutons has been assumed to be a consequence of large ascending molten blobs of magma which intruded the upper crust (Paterson et al., 1996). In this view magmas are considered to accumulate at depth and to rise diapirically (Paterson and Fowler, 1993; Weinberg, 1996; Alexander et al., 1998). Vigneresse et al., 1996 concluded that if plutons were emplaced as large magma bodies, melt fraction should be at least 30-50 % during emplacement. Recently there has been a change of paradigm regarding the way plutons are emplaced and grown in the upper crust. Many researchers now interpret the formation of plutons to occur at emplacement level, and to be a result of incremental growth by pulsed injections of magma, over extended periods of time (Glazner et al., 2004; Farina et al., 2012). Wiebe and Collins, (1998) suggested the steeply dipping sheets at the margins of some plutons were subhorizontal during growth of the pluton but later tilted due to the sagging floor, in order to make space for the growing magmatic pluton body. Other plutons such as McDoogle near the eastern margin of the Sierra Nevada batholith show a series of dykes which show emplacement through these conduits (Mahan et al., 2003).

In the case of Monte Capanne pluton, Elba Island Tuscany, cryptic internal contacts, evidence for incremental assembly of the pluton was determined through geochemical data differences in major elements, trace elements and isotopic compositions as well as the biotite composition within the different facies (Farina et al., 2010). Additionally, in the Monte Capanne pluton, textural and geochemical data have also revealed cryptic internal contacts between the pulses and the lack of sharp contacts could be attributed to the fact that the sharp contacts never existed, due to short time span between magma injections (Farina et al., 2010). The incremental growth of plutons has been questioned by authors who describe a complex range of widespread magmatic structures interpreted to indicate the accumulation of mafic minerals and large K-feldspar crystals with diverse magma history and ages (Weinberg et al., 2001; Zak and Klomínský, 2007; Paterson, 2009). These structures include stationary and migrating tubes, pipes, troughs, diapirs, mafic schlieren and schlieren channels, cross-beds, ladder dikes, magmatic folds, layering and melt segregation structures (Clarke and Clarke, 1998; Reid et al., 1993; Wiebe and Collins, 1998; Weinberg et al., 2001; Paterson et al.,

2005; Zak and Klomínský, 2007). Such structures are interpreted to be formed by local magma flow through crystal-rich magma often associated with the formation of schlieren rich in accessory and mafic minerals, and associated with filter pressing and accumulation of crystals (Paterson, 2009). Why the existence of such structures has been interpreted as incompatible with incremental pluton assembly is unclear and seemingly without logic. The formation of structures such as layering and pluton formation may be closely related, as some authors argue that the layering represents the viscous flow of the magma that is related to mingling of heterogeneous magmas in dynamically evolving systems (Seaman et al., 1995). In some cases layering is thought to be as a result of the repeated influx of new magma into the growing magma chamber (Barbey, 2009). In fact, all structures that are interpreted to require magma flow to form are compatible with the interpretation of incremental pluton assembly as the incoming batches of magma must be associated with some degree of magma flow in the chamber.

Layering in igneous intrusions is defined by repetitive changes in mineralogy with often superimposed cryptic chemical change in the compositions of the minerals over a distance larger than the scale of the layering (Rockhold et al., 1987). Layering is reported to be the product of an interplay between numerous processes which include; diffusion, heat loss and accumulation of crystallizing minerals (Irvine, 1987 as cited in Solgadi and Sawyer, 2008 p .2010). In mafic intrusions layering occurs on a pluton-wide scale and the low viscosities and high diffusion rates relevant to mafic magmas are interpreted to permit these processes (e.g. diffusion, heat loss and accumulation of crystals) to occur efficiently (Rockhold et al., 1987). In granitic rocks layering is rare, possibly due to the relatively low temperatures and high viscosities of these magmas which act to inhibit crystal settling, chemical diffusion and nucleation of crystals (Rockhold et al., 1987).

In the Peninsula pluton of the Cape Granite Suite, layered biotite schlieren structures are very common within the pluton; they are continuous for distances from few centimetres to tens of meters. Repetitive, rhythmic biotite layered structures are exceptionally well preserved in outcrops of the S-type granodioritic to monzogranitic Peninsula Pluton at the town of Llandudno. Layering occurs within several parallel lenses the largest of which is approximately 5 m thick by 30 m long. Understanding the origin of layering in granites is important as this may give crucial insights on the physical-chemical conditions within magma chambers during their construction. Within the large range of magmatic structures described,

this study is focussed on the origin of layered structures within the coarse grained cordierite and K-feldspar megacrystic granite exposed along the coast at Llandudno. In this paper we examine a phenomenally well preserved layered structure and use field evidence, mineral textural evidence, whole rock geochemical and mineral chemical data to interpret the magmatic processes that formed the layering.

Magmatic structures and layering: a literature review

Structures involving curved and cylindrical layering

Complex arrays of magmatic structures have been observed in many plutons around the world. These structures include stationary and migrating tubes, pipes, troughs, diapirs, mafic schlieren, layering and melt segregation structures (Fig.1&2) (Clarke and Clarke, 1998; Reid et al., 1993; Wiebe and Collins, 1998; Weinberg et al., 2001; Paterson et al., 2005; Zak and Klomínský, 2007). Although numerous researchers have observed and described layered structures in a relatively small number of granite plutons in the world, such as the Ploumanac'h pluton, France (Barriére, 1981), the South Mountain batholith, Nova Scotia (Abbott, 1989; Clarke and Clarke, 1998), the Tavares pluton, Brazil (Weinberg et al., 2001), the Vinalhaven intrusive complex (Wiebe et al., 2007), and several plutons in the Sierra Nevada, California (Reid et al., 1993; Žák and Paterson, 2005; Žák et al., 2007) there are only a few investigations that have focussed specifically on the petrogenesis of these structures (e.g. Solgadi & Sawyer, 2009). Consequently, our knowledge of how these structures form is relatively poorly developed. However, several different hypotheses have been put forward to explain their formation, though the proposed mechanisms for the formation of these structures represent interpretations with little consensus in some cases.

Magma tubes are defined as cylindrical or tube shaped structures in three dimensions, that in sections perpendicular to tube axes, display numerous, elliptical schlieren bounded layers (Paterson, 2009). Two types of tubes were noted in the Tuolumne batholith namely: stationary and migrating tubes. In the case of stationary tubes, the tube axis is interpreted to not have migrated with time (Fig. 1A), while in the case of a migrating tube, the tube axis moves and develops along a path length of typically meters to tens of meters (Fig.1B) (Reid et al., 1993; Paterson, 2009). In the case of migrating tubes, the displacement of tube centres results in crescent-shaped patterns of alternating light and dark schlieren along the path lengths (Burgess and Miller, 2008; Paterson, 2009). Some or occasionally all layers within

the tubes are reported to have compositions and/or textures distinct from the surrounding host magma (Paterson, 2009). Pipes are enclosed, sometimes funnel-shaped to more commonly cylindrical-shaped bodies (Fig. 1C-E), geometrically similar to tubes, but distinct from tubes in that they have a single, dominant composition distinct from and typically more felsic than the surrounding magma (Paterson, 2009). Unlike pipes, troughs are open and asymmetrical schlieren bounded channels with curvatures commonly less than tubes (Fig. 1F) (Paterson, 2009). As the trough curvature decreases, they grade into and are commonly associated with layered schlieren (Burgess and Miller, 2008; Paterson, 2009). Small scale diapirs are noted to be highly irregular in shape often with narrow tails and bulbous or mushroom shaped heads (Fig. 1G), these structures are reported to be mature due to the separation from their origin, while immature diapirs are cylindrical if still connected to layering that is interpreted to represent the magma which fed the diapir (Paterson, 2009).

The formation of all these magmatic structures is reported to involve multiphase magmatic flow during cooling and crystallization of the magma (Paterson, 2009). Tubes were reported to represent cylindrical channels of magma flow through crystal mushes, with the main flow direction parallel to the tube walls (Fig. 2A&B) (Weinberg et al., 2001). Migrating tubes resulted from the superposition of sequential cylindrical magma pathways in which each new curved schlieren represents the walls of a former cylindrical magma path (Fig. 2B) (Paterson, 2009). Magma flow through the tubes, either down or up is proposed to be driven by thermal or compositional buoyancy (Weinberg et al., 2001). Combined flow sorting and filter pressing are proposed to form the schlieren along the tube walls (Paterson, 2009). Pipe formation is suggested to occur immediately after juxtaposition of magma with different compositions which produce a density inversion, the less dense magma rises up through the more dense magma, largely as a result of Raleigh-Taylor instability (Wiebe et al., 1996), which results due to the varying viscosity and density contrasts (Vigneresse and Clemens, 2000). Weinberg et al., 2001 also suggested that pipes form when the flow necking led to a megacryst “logjam” which continued to grow by the filtering out megacrysts upstream (Fig. 2C).

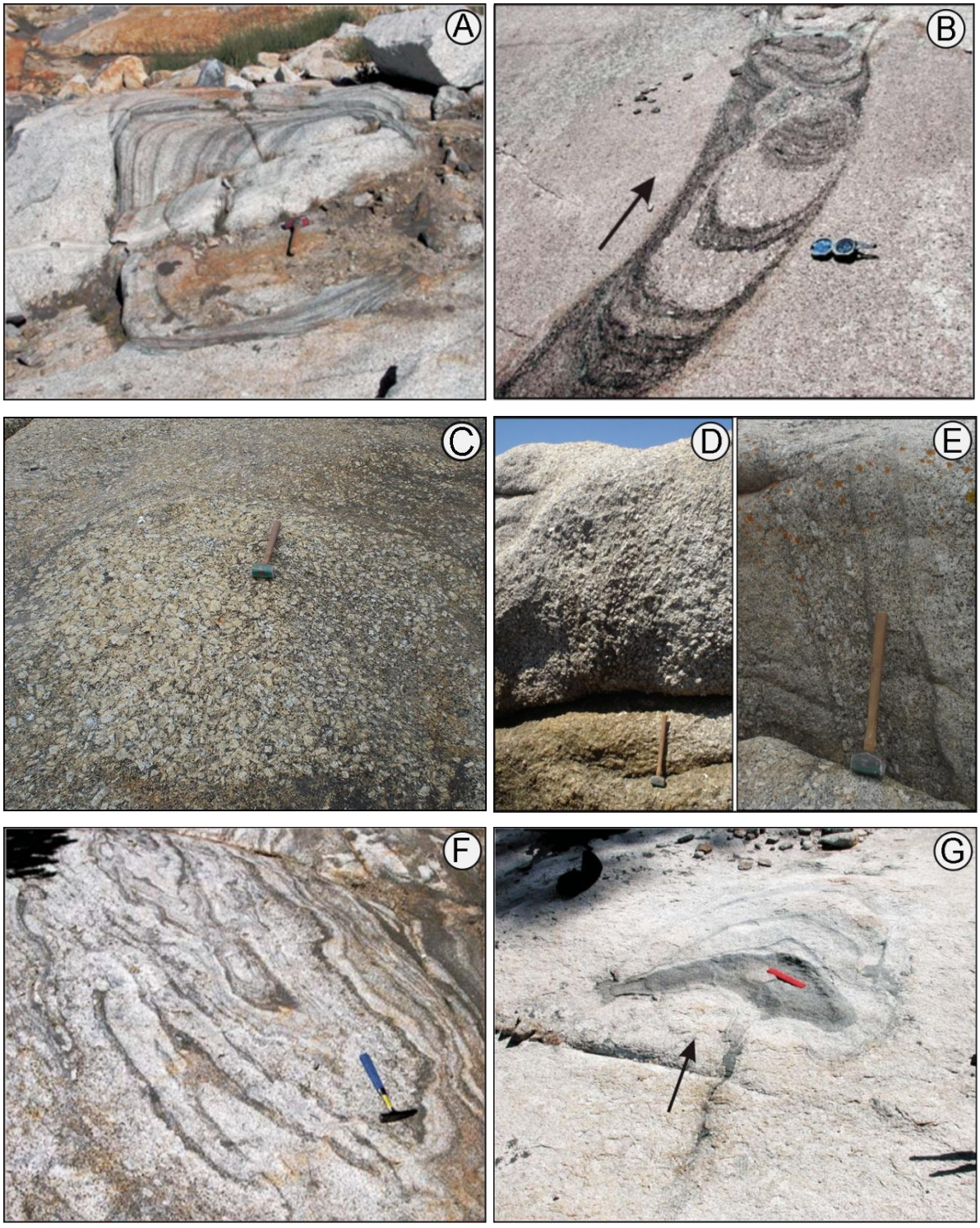

Fig.1 Images showing examples of magmatic structures in the granitic plutons. (A&B) show two different types of tubes: stationary tubes, (A) where the tube axis is stationary and migrating tubes (B), with the tube axis moving to develop path lengths of meters to tens of meters (Images after Paterson, 2009). (C-E) show pipes within the Peninsula pluton, (C) Subhorizontal section through a steeply orientated pipe, with the bioite schlieren showing the margin of the pipe. (D&E) show a vertical sectionm through a steeply orientated pipe, with (E) illustrating complexity within the pipe, possibly reflecing injection of different magma batches (Images after Farina et al., 2012). F Subhorizontal trending schlieren bounded trough exposed in three dimensions, (G) Laterally moving diapir of quartz diorite with arrow showing direction of movement (Images after Paterson, 2009 in the Tuolomne batholith, Sierra Nevada, California).

Troughs are considered to be analogous to sedimentary flow channel in which channels have a bed-load and formed in porous media (Solgadi and Sawyer, 2008). These channels in the Tuolumne batholith vary from fairly localized with similar width/depth ratios to broad gently curved surfaces (large width/depth ratios), interpreted to be associated with broad sheet flows along an internal crystal mush boundary (Paterson, 2009). Magma flow is probably parallel to trough axes, as inferred by aligned hornblende crystals in basal schlieren. Host magmas, including earlier troughs, were stiff enough to allow local erosion followed by redeposition and associated filter pressing and local lag deposits to form (Paterson, 2009). The similar material in the troughs and in the host magmas is interpreted to suggest local sources: the highly variable orientation of trough axes suggests variable processes driving magma flow in troughs, such as crystal mush avalanches, gravity-driven channelized flows, convection driven flow along irregular mush zone margins, and downward return flow during ascent of new magmas (Fig. 2D) (Paterson, 2009). Diapirs and plume heads are interpreted to represent magma batches that moved through the host magma, which was displaced around the diapir and potentially incorporated into plume heads (Fig. 2E&F) (Paterson, 2009). The thin tails, broad heads, and compositions as noticed in the host magmas of most Tuolumne batholith diapirs indicate that they were detached (typically from unobserved sources) batches of magma moving through but not significantly incorporating host magma (Miller and Paterson, 1999).

The formation of schlieren in granitoids is explained by several proposed mechanisms: partial assimilation of mafic enclaves; crystal settling; shearing out of chemical inhomogeneities; steep physicochemical gradients at flow margins (Barriere, 1981), which results in crystallisation of ferromagnesian minerals and the suppression of crystallisation of felsic

minerals (Naney et al., 1980); as well as, shear sorting against an effectively rigid wall (Barriere, 1981). Thus, magmatic structures potentially record information about the processes by which crystals and melt are sorted, separated and/or mixed within granitic plutons (Zak and Klomínský, 2007). Magmatic structures represent a network in which channelized flow occurred in an existing chamber of crystal rich magma resulting in compositional and structural diversity (Paterson, 2009). They reveal important information about the processes which operated within in a magma chamber in the time interval between emplacement of the first batch of magma (multi-batch emplacement) and the complete crystallization of the system.

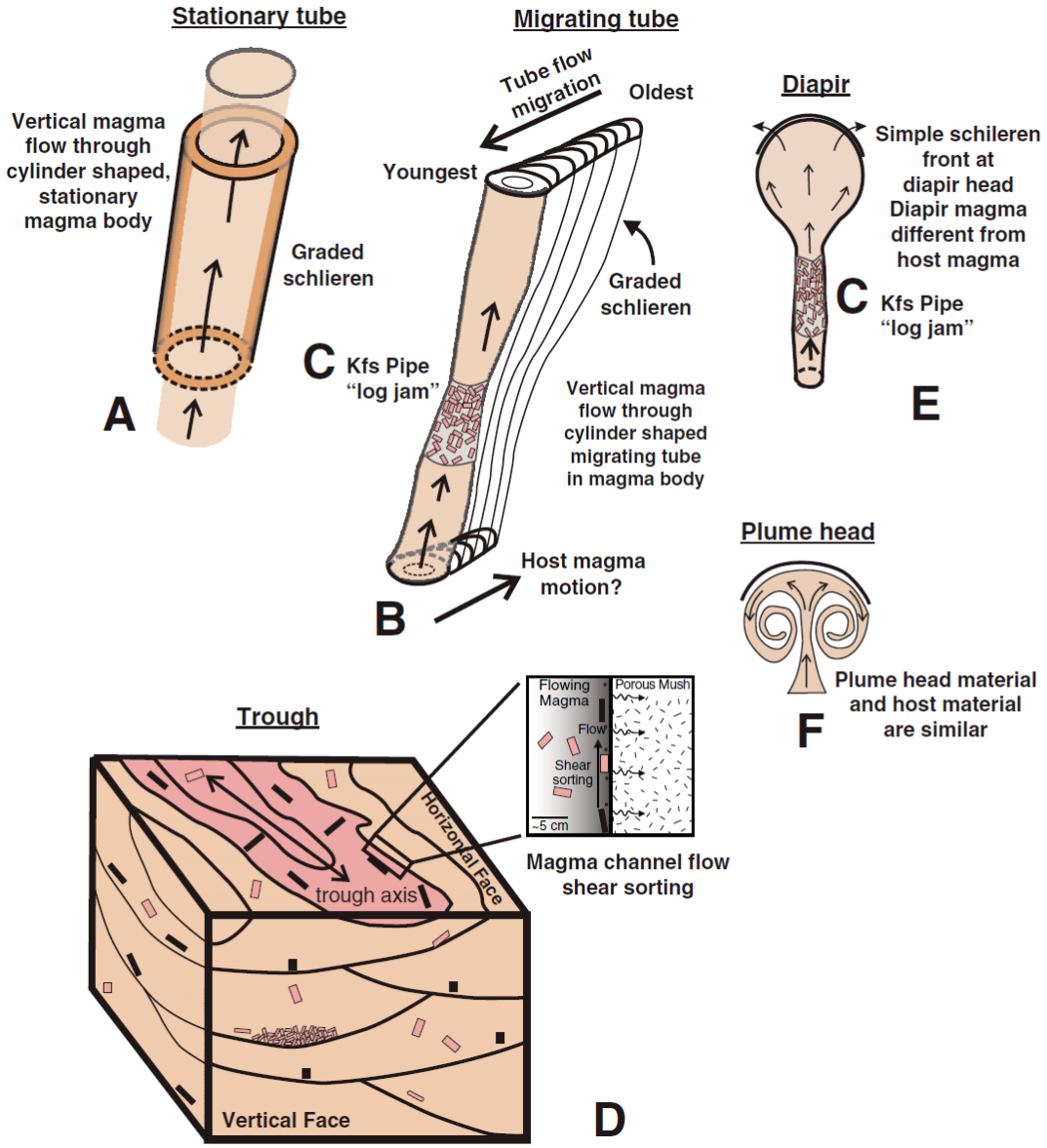

Fig.2 Schematic images showing the three dimensional form of the structures discussed above, as well as some petrogenetic interpretation of how the structures form. (A&B) shows the two different tubes; stationary and migrating tubes respectively. (C) shows a pipe feature with K-Feldspar megacrysts. (D) Trough, this structure usually shows relationship between trough cutoffs, mineral fabrics, magma flow direction as well as the crystal accumualtion. (E) Diapir. (F) Plume head. Arrow in the structures indicate implied magma flow direction. (Images after Paterson, 2009 in the Tuolomne batholith, Sierra Nevada, California).

Planar layering

Planar layering in granitic plutons, occurs at different scales, but is generally a relatively small scale feature relative to the size of the hosting magma body. Consequently, such layering is thought to be dependent on the interplay of magma injection and magma chamber processes (Barbey et al., 2008; Barbey, 2009). Different mechanisms for the formation of this layering have been proposed from studies performed on felsic plutons world-wide. Weinberg et al., (2001) outlined a filter process for the formation of the layering with more complex, non-planar morphologies driven by the gradient in magma pressure across an interface in a crystal mush undergoing compaction; they proposed that the residual melt moves out through the more crystallised magma, thus crystals accumulate at the interface on the less crystallised side. Several mechanisms proposed for the formation of the layers includes gravitational settling of crystals (Clarke and Clarke, 1998) and growth of convection boundary layer (Irvine et al., 1998), [summary by Naslund and McBirney, (1996)]. Solgadi and Sawyer, (2008) listed several mechanisms for the formation of layering in felsic plutons and divided these into 5 broad categories: 1. Processes related to crystallisation of the magma such as crystal fractionation; 2. Growth of crystals in a boundary layer; 3. Injection and attenuation (transposition) of different batches of magmas with or without mixing; 4. Mingling or diffusive exchange between magma batches; 5. Hydrodynamic processes which redistribute crystals, including, but are not restricted to, various kinds of density flows, erosion and slumping processes. In their study on the Tuolumne Intrusive Suite Solgadi and Sawyer, (2008) concluded that layering was due to the gravity flow of melt and crystals initiated by syn-magmatic tectonic deformation and seismic shaking. Pupier et al. (2008) proposed in situ fractional crystallisation at boundary layers to be responsible for the formation of layering in the Dolbel Batholith, SW Niger. In this process the crystallisation of phases is controlled by the composition of magma close to the interface between the crystal pile and relatively crystal

free magma and fine scale modal layering parallel to the crystallisation front form as the magma composition evolves (Pupier et al., 2008).

CHAPTER TWO

GEOLOGICAL SETTING

The Saldanha belt and the Cape Granite Suite

The Saldania Belt is one of a number of Neoproterozoic mobile belts that formed during the formation of Gondwana, due to the convergence of the Rio de la Plata and Kalahari Cratons (Fig. 3A)(Da Silva et al., 2000, Scheepers, 2000). It is proposed to be a continuation of the Gariep and Damara Belts to the north on the African continent and with the Dom Feliciano Belt in southern Brazil (Gresse et al., 1996). It is composed of a number of inliers unroofed in mega-anticlinal hinges of the Permo-Triassic Cape Fold Belt along the southern tip of Africa (Fig.3). The main exposure, in the area of Cape Town and surroundings consists of the supracrustal Malmesbury Group and the Cape Granite Suite rocks which intrude the Malmesbury group. The Malmesbury Group is considered to be an accretionary melange from the closure of the Adamastor Ocean between the Kalahari and Rio de la Plata Cratons (Rozendaal et al., 1999). It consists of greywackes, shales, limestones, conglomerates and mafic metavolcanic rocks which are metamorphosed up to lower greenschist facies grades. The group is divided into three terranes by prominent northwest-trending fault and shear zones, namely southwestern Tygerberg terrane separated from Swartland terrane by the Colenso (Saldanha-Stellenbosch) Fault; the central Swartland and the northeastern Boland terrane are separated by the Piketberg-Wellington fault zone (Rozendaal, 1999). The granite plutons of the Cape Granite Suite intrude all these terranes (Scheepers, 2000).

The Cape Granite Suite, crops out over a distance of more than 500 km along the Southern and Western Cape coast and predominantly consists of I- and S-type granites (Scheepers, 2000). There are three major phases of granite magmatism postulated by Scheepers and Rozendaal, (1992); Scheepers, (1995). The first phase of syn- to post tectonic granites to form is the S-type granite that intrudes the folded Malmesbury rocks of the Tygerberg terrane. The Peninsula pluton constitutes part of this first phase of syn- to post tectonic S-type granite magmatism. The inferred emplacement age for the pluton is in the range of 552± 4Ma to 539± 4Ma (SHRIMP U-Pb zircon and monazite ages; Scheepers and Armstrong, 2002). These ages are in agreement with those determined by Villaros et al., (2011) (538.2±1.9 and 538.3± 1.5 Ma) for the Peninsula Pluton and the Darling Batholith respectively, which are

assumed to have crystallised during the same magmatic event at c. 537 Ma. The strongly peraluminous nature of these S-type granites, their relatively K_2O-rich compositions and their abundant inherited zircons spanning an age range of some 600Ma indicate that they formed primarily as peraluminous melts from the clay rich sediments sourced from old recycled crust (Villaros et al., 2011). This crust records several episodes of crustal recycling (Villaros et al., 2011) during period of increased heat flow possibly by introduction of basaltic magma in the crust (Scheepers and Rozendaal, 1992).

The second phase of post-tectonic granite intrusions into the Malmesbury metasediments consists of I-type granites with emplacement ages of 536±5 Ma; SHRIMP U-Pb zircons (Da Silva et al., 2000; Scheepers and Armstrong, 2002). These granites occur in the Swartland and Boland Terranes. The last phase of granite magmatism is represented by the post-tectonic anorogenic A-type granites which intrude the S and I-type as well as the Malmesbury group metasediments and are found in the Tygerberg and Swartland terranes (Da Silva, 2000). They have ages that vary between 525 and 510 Ma (Scheepers and Armstrong, 2002). Apart from obvious major element differences expresses in A/CNK, Na:Ca etc, the minor and trace element compositions also set the three groups of granites apart. The S-type granites are relatively high in P_2O_5 (>0.1 wt. %) with low Th content (<40 ppm); the A-type granites have low P_2O_5 (<0.1 wt. %) with high Th content (>40 ppm); whilst the I-type associations have low P_2O_5 (Harris et al., 1997) and intermediate Th content (Scheepers, 2000).

The S-type plutons of the Cape Granite Suite (CGS) form a suite of strongly peraluminous ($1<A/CNK<2$), K-rich granites with a substantial range in total FeO + MgO values between (0.8 and 9 wt. %) (Stevens et al., 2007). The rocks typically contain cordierite, biotite, muscovite, plagioclase and large K-feldspar phenocrysts (Villaros et al., 2009b). There are four major S-type plutons in the CGS namely: Saldanha, Darling, Stellenbosch and Peninsula; located south of the NW-SE trending Colenzo Fault (Villaros et al., 2009b). These plutons are believed to be sourced from a higher grade equivalent of the Malmesbury Group metasediments (Harris et al., 1997).

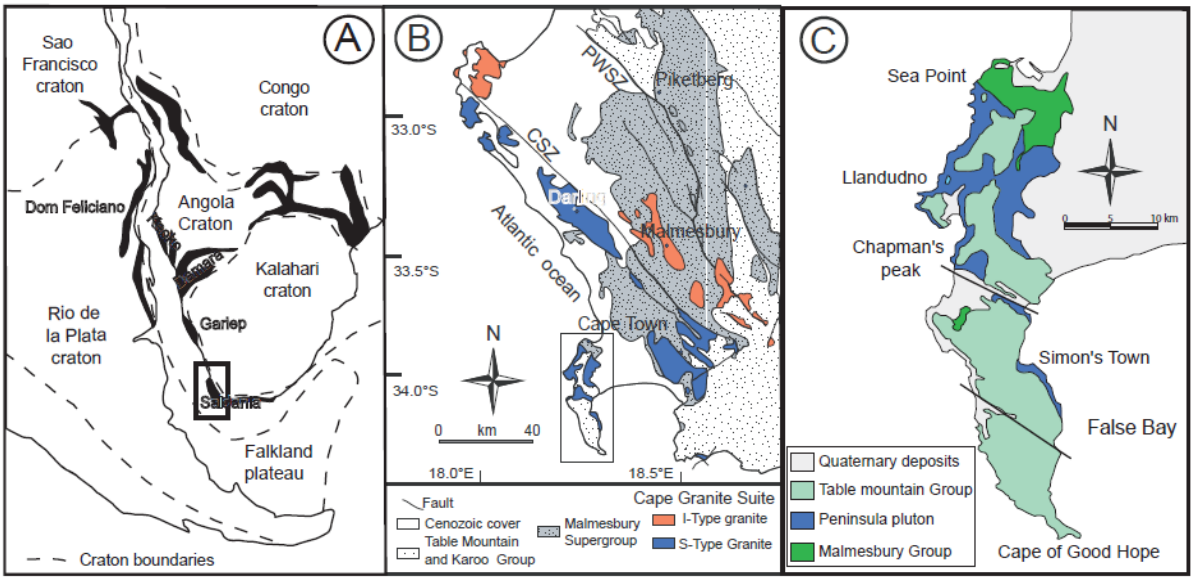

Fig. 3 (A) Palaeogeographic reconstruction of the Saldania orogeny at 550 Ma. (B) Geological map of the area around Cape Town illustrating the distribution of the I- and S-type granites of the Cape Granite Suite; CSZ stands for Colenzo Shear Zone, PWSZ for Piketberg-Wellington Shear Zone. (C) The distribution of the Peninsula pluton (Figure modified after Villaros et al., 2009a, b).

The Peninsula pluton

The Peninsula pluton forms the southernmost pluton of the CGS, and crops out along the Cape Peninsula from Cape Town to Cape Point (Fig. 3B&C). It is undeformed with little alteration and contains rocks which record the full range of S-type CGS compositions, from leucogranites to granodiorites (Scheepers, 2000; Villaros et al., 2009b). The main chemical features of the pluton have been described by Villaros et al. (2009a, b), while the chemical variability of the pluton as a whole has been examined by Farina et al. (2012). The Peninsula pluton is typically K_2O-rich and peraluminous with SiO_2 content varying from 61.1 to 76.7 wt. %; high Al_2O_3 (12.9-17.1 wt. %) and variable FeOt, MgO and TiO_2 (1.15-10.38, 0.32-3.5 and 0.14-1.91 wt. % respectively) (Villaros et al., 2009b). The pluton is generally cordierite rich, with rocks containing in excess 10% cordierite being common (Villaros et al., 2009b). The presence of cordierite, garnet and tourmaline confirms the inference of an aluminous metasedimentary source (Stevens et al., 2007). The pluton is characterized by the occurrence of 5-15 vol% of large K-feldspar crystals reaching up to 20 cm in length. Cordierite and biotite commonly either completely or partially replace garnet (Villaros et al., 2009b). Compositional variation within the Peninsula pluton compositional variation is expressed in variations in the proportions of biotite, cordierite, garnet and K-feldspar phenocrysts (Villaros

et al., 2009b). Schoch (as cited in Villaros et al., 2009b, p. 546) defined four main facies within the Peninsula; a dominant leucocratic K-feldspar porphyritic granite (Cape Granite) as well as three minor mafic facies: biotite rich K-feldspar porphyritic granite (Biotite Porphyritic Granite), biotite non porphyritic granite (Biotite granite) and granodioritic facies (Cape Granodiorite). The nature of the contacts between these facies is diffuse, indicating that the different facies are co-magmatic (Villaros et al., 2009b). The outcrops at Llandudno that are the focus of this study are part of the Peninsula pluton. The facies of the Peninsula pluton that is exposed along the coast at Llandudno is the granodioritic facies (Cape Granodiorite) and layering is developed within this facies. This thesis refers to the coarse grained, cordierite and K-feldspar porphyritic Cape Granodiorite which hosts the layering in the Llandudno area as the Llandudno granodiorite; the layered rocks are referred to as the layered granites or the layering

According to Stevens et al., (2007) and Villaros et al., (2009b), 1st order geochemical diversity in S-type granites is produced within the source by three different mechanisms: (a) The composition of the source controls of the melt composition by determining the composition and proportions of the minerals consumed by the melting reaction. Geochemical variation in the source is reflected in variations in the concentration of elements that are compatible within the melt (e.g. K_2O, Na_2O, Sr, and Ba). Within granites, these elements typically show a substantial range in concentration at any given bulk rock MgO+FeO^T value (Farina et al., 2012); (b) The degree of peritectic assemblage entrainment controls a number of magma compositional parameters. Stevens et al., 2007 concluded that the strong positive correlation between Ti and Mg+ Fe in S-type granites was the result of the entrainment of the peritectic assemblage produced on incongruent melting of biotite into the magma, with proportions ranging approximately from 0 to 30 mol% of the peritectic assemblage produced. This mechanism is proposed to most strongly control the concentration of CaO, TiO_2, FeO and MgO in S- and I-type granite magma, as well as ratios such as Mg# and A/CNK, through the entrainment of peritectic plagioclase, garnet, ilmenite, cordierite, orthopyroxene and clinopyroxene, as determined by the PT conditions of anatexis and the bulk composition (Stevens et al., 2007; Clemens et al., 2011; Clemens and Stevens, 2012); (c) Co-entrainment of the accessory mineral suite controls the trace element composition of the magma. Monazite and zircon commonly occur as inclusions in biotite in high grade metamorphic rocks. Thus, it is likely that they were co-entrained with the peritectic assemblage because of their proximity to the sites of melting. Villaros et al., (2009b) proposed that during biotite

incongruent melting zircon and monazite are liberated and entrained as peritectic assemblages. The rock compositions which appear to be saturated with zircon and monazite were produced as a result of this entrainment and not through the enrichment of Zr or LREE in the melt via dissolution of zircon and monazite in the source. This is evidenced by the very large fraction of inherited zircon in such granites (Villaros et al., 2009). The co-entrainment of the peritectic assemblage and the accessory suite hosted in biotite was proposed to account for the close correlation between the major and trace elements that have low solubility in the melt, such that between Zr and Mg + Fe (Stevens et al., 2007; Villaros et al., 2009b). Villaros et al., (2009b) modelled major and trace elements variations within different phases of the Peninsula pluton. In particular, they noted that some leucocratic Peninsula pluton magmas have Zr concentrations below saturation levels at the proposed source melting temperature of 850C, despite the fact that these rocks contain xenocrystic zircon. Known rates of zircon dissolution allowed Villaros et al., (2009b) to constrain the residency of such zircons in the high temperature magma to less than 500 years. Thus, it has been proposed that the magmas which constructed the Peninsula pluton were sourced from rocks of different compositions, with the magmas generated by trace element disequilibrium melting. Due to little mixing during the growth of the pluton the original chemical character of the different magma batches was retained (Villaros et al., 2009b).

The Peninsula pluton is characterised by a wide range of mesoscopic magmatic structures that have been described from other plutons worldwide (Barriere, 1981; Zak and Klomínský, 2007; Paterson, 2009). These structures include; pipes, high concentrations of K-feldspar megacrysts adjacent to enclaves, flow alignment of K-feldspar megacrysts, biotite accumulation in schlieren, metamorphic xenoliths, magmatic enclaves and troughs. These structures are widespread within the pluton. In the Peninsula pluton, pipes are enclosed cylindrical shaped accumulations of megacrysts consisting of more than 70 vol. % of K-feldspar megacrysts and have a vertical or steeply plunging axis (Farina et al., 2012). The K-feldspar megacrysts in the coarse grained mafic enclaves and pipes are reported to be similar to the host granite in size, shape and internal structure (Farina et al., 2012). The pipes have been proposed to have formed by localised magma flow and melt crystal separation occurring at temperature not exceeding 750˚C in a crystal rich magma chamber (Farina et al., 2012). This relatively low temperature of formation is required because K-feldspar crystallises late in the history of these magmas. This is shown by the experimental work of Clemens and Wall, 1981 where K-feldspar starts to crystallise at 760-780˚C in peraluminous granitic melts

having 4 wt% water at pressures of 3-5 kbars. This is supported by the work of Moore and Sisson, (2008), in I-type magmas, using the zirconium in titanite geothermometer, calculated the crystallization temperature of titanite crystals within K-feldspar megacrysts. Temperatures ranged from 735 to 760˚C. Despite the proposal by Glazner et al., (2007) for subsolidus growth of K-feldspar megacrysts in granites, a magmatic origin for K-feldspar megacrysts remains the preferred interpretation in many instances (e.g. Paterson, 2008; Moore and Sisson, 2008, Farina et al., 2010). The evidence in support of this conclusion is commonly that: i) crystals display major and trace elements oscillatory zoning that is consistent with crystallization from a magma; ii) K-feldspar commonly contain plagioclase and biotite inclusions which are smaller than these minerals within the general framework of the rock; iii) inclusions are concentrically arranged parallel to crystallographic planes; iv) the occurrence of resorption surfaces in megacrysts impinged by other megacrysts indicates, in rocks with no evidence of solid-state deformation indicates that the megacrysts were transported in a magma (Farina et al., 2012). Moore and Sisson, (2008) related the origin of K-feldspar megacrysts to the incremental growth of plutons. They noted from their study of four K-feldspar megacrysts in the Sierra Nevada Batholith that the K-feldspar megacrysts are phenocrysts that grew in contact with the granitic melt, and that their growth was attributed to the repeated influx of the new magma within the batholith. This continuous influx of new magma creates temperature fluctuation just above alkali-feldspar stability for long periods, providing necessary elements for the growth of the megacryst (Moore and Sisson, 2008). Mafic mineral aggregates, which consist of cordierite, biotite-quartz clots, also bearing abundant xenoliths and microgranular granodioritic enclaves are widespread within the pluton. Some of this mafic mineral aggregates contain K-feldspar megacrysts and are irregular shapes occupying area from 1 to up to 30 m^2 (Farina et al., 2012). Planar to curved biotite schlieren also occur and are sparsely distributed, these occur along margins of pipes and also occur as isolated features. Some schlieren are planar and laterally continuous up to a meter while others are wispy, folded and highly irregular in shape and continuous over few meters (Farina et al., 2012).

CHAPTER THREE

FIELD CHARACTERISTICS OF THE LLANDUDNO GRANODIORITE

The Peninsula pluton exposed along the coast at Llandudno and termed the Llandudno granodiorite in this study, is a coarse-grained, cordierite and K-feldspar phenocrystic granodiorite. The rock consists of plagioclase, quartz, alkali feldspar, biotite and cordierite which is strongly pinnitised (Fig. 4A). Garnet is a rare mineral in the granodiorite and is commonly pseudomorphed by cordierite. Tourmaline nodules are widespread in the Llandudno granodiorite (Fig. 4B); these nodules are not only constrained in Llandudno but are found throughout the Peninsula pluton. K-feldspar phenocrysts are mostly rectangular in section and are up to 10 cm long, while the pinnitised cordierite grains are mostly rounded and range from 1 to 1.5 cm in diameter. In some areas the Llandudno granodiorite is characterised by the alignment of K-feldspar megacrysts, this is interpreted to be due to magma flow within the chamber (Farina et al., 2012). This flow fabric is not continuous but is changeable on a metre scale. The Llandudno granodiorite is also characterised by some mesoscopic magmatic structures that are widespread in the Peninsula pluton. These structures are defined by anomalously high concentrations of K-feldspar megacrysts, and biotite accumulation in schlieren. Within the Llandudno area such schlieren are wispy, folded and highly irregular in shape and laterally continuous over a few meters. They are modally graded with sharp bottoms and diffusive tops, and vary in thickness from a few centimetres to tens of centimetres. They are associated with K-feldspar megacrysts showing preferential alignment parallel to the schlieren margin. Magmatic enclaves and metasedimentary xenoliths are also common in the granodiorite. These magmatic enclaves vary in size from mm to several meters in diameter and vary greatly in degree of assimilation. Within the Peninsula pluton in general, magmatic enclaves are reported to account less than 1 vol. % of the pluton (Farina et al., 2012). These enclaves were subdivided into five types according to their field appearance, mineralogy and chemical composition (Farina et al., 2012); these are (i) leucogranitic enclaves, (ii) megacryst-free enclaves, (iii) porphyritic granodiorite enclaves, (iv) microgranitoid enclaves and (v) coarse grained mafic enclaves. In the Llandudno granodiorite, enclaves present are coarse grained mafic enclaves. These are rounded to bean-shaped bodies with dimensions ranging from 0.5 to 1 meter and contain abundant large pseudomorphs of cordierite replacing former garnet as well as fine-grained symplectitic clots of biotite and quartz. They consist mainly of biotite, quartz, cordierite, and plagioclase with almandine rich garnet preserved in the pseudomorphs. They also contain K-feldspar

megacrysts (about 30 vol. %) which are similar in size and texture to those in the Llandudno granodiorite (Fig. 4C) (Farina et al., 2012). The relative modal abundance and size of cordierite pseudomorphs, biotite + quartz clots and plagioclase is strongly variable (Farina et al., 2012). The accessory phases present are apatite, zircon, ilmenite, monazite and rare titanite. Cordierite in the pseudomorphs is pinnitised with a mineral assemblage of biotite, white mica and kaolinite.

Metasedimentary xenoliths are also common in the Llandudno granodiorite, with sizes varying between 3-4 cm and 30 cm in length (Fig. 4D). According to Farina et al., (2012) their concentration within the pluton is variable with 1 xenolith every 5 m^2 observed being a typical average. The metamorphic mineral assemblages in the xenoliths range in grade from lower greenschist facies up to garnet-bearing amphibolite facies (Villaros et al., 2009b). The xenoliths of low metamorphic grade preserve their original sedimentary bedding while those at amphibolite facies grades have metamorphic fabrics defined by preferential biotite orientation (Villaros et al., 2009b). Villaros et al., (2009b) identified two types of garnet bearing metasedimentary xenoliths: a biotite-dominated metapelite and a quartz and feldspar-dominated metapsammite. These xenoliths contain well developed foliation defined by aligned biotite crystals and continuous quartzo feldspathic layers with a metamorphic texture wrapping garnet crystals. Garnet-biotite thermometry produced temperature estimates of 715 °C and 735 °C (±25 °C) for the metapelite and metapsammite xenoliths respectively (Villaros et al., 2009b).

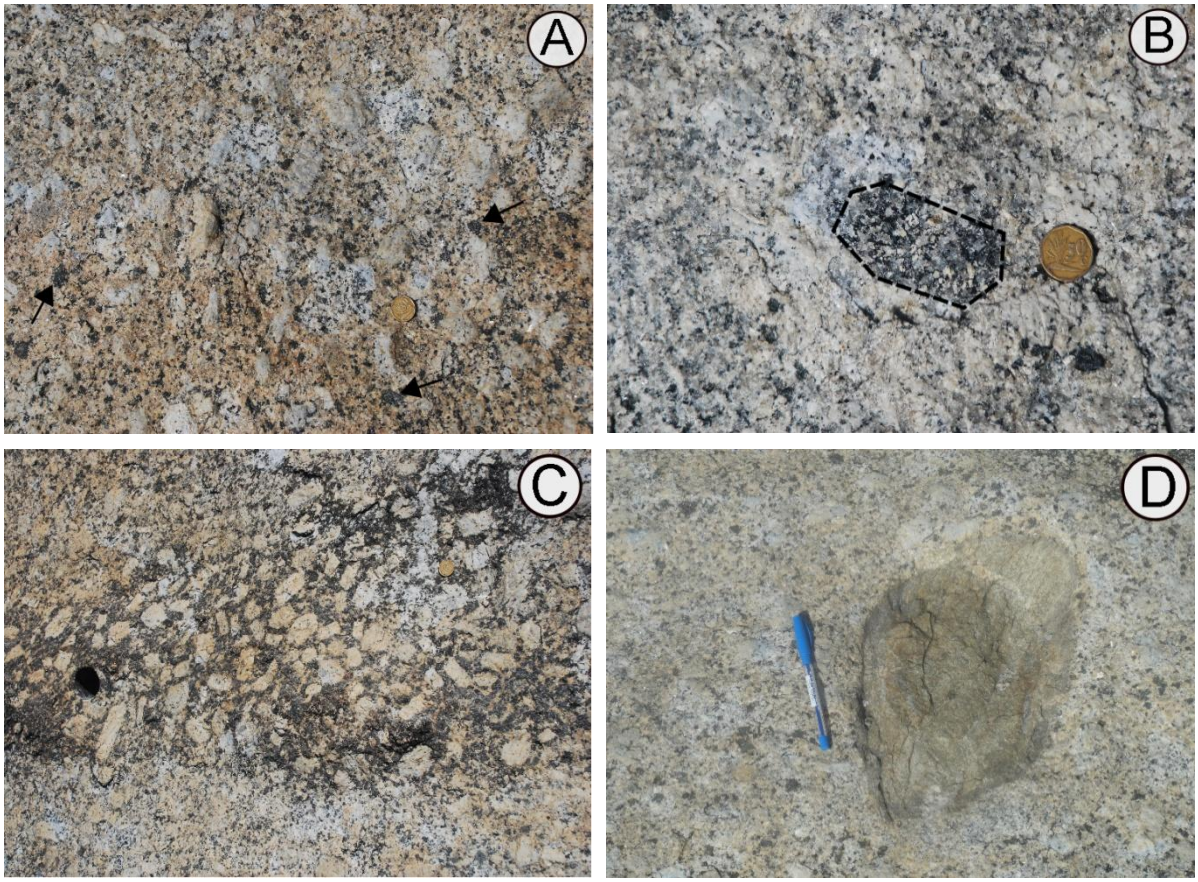

Fig. 4 Relevant images showing the structures present in the Llandudno granodiorite. (A) show typical K-feldspar and cordierite megacryst textured Llandudno granodiorite, black arrows indicate cordierite megacrysts. (B) Image shows tourmaline nodule, tourmaline is widespread in the pluton. (C), a coarse grained mafic enclave with K-feldspar megacrysts that are similar to those in Llandudno granodiorite. The coin is 2cm in diameter. (D) illustrates metasedimentary xenolith that is present in the area. The pen is 15 cm in length.

The layering in the Llandudno granodiorite

Layering within the Llandudno granodioritic body occurs within several lens-shaped bodies (Fig. 5A-C). The largest of these lenses has a thickness of some 5 m and consists of 50 layers with thickness ranging between 5 and 50 cm (Fig. 5D&E). Each layer is characterized by a sharp lower contact and a biotite rich lower portion containing approximately 50 vol. % biotite (Fig. 5E). This mafic lower portion, grades upwards into a strongly leucocratic upper portion enriched in plagioclase, quartz and K-feldspar (Fig. 5G). The mafic-leucocratic pair is interpreted to represent one single complete layer; this is because of the sharp bottom contact between the complete mafic-leucocratic layers which eventually moves to gradational upper contact. The leucocratic portion of the layering is different from the Llandudno granodiorite,

this portion shows that it is not only the case of biotite accumulation but it is fundamentally different in texture and composition. The texture in the leucocratic portion is quartz porphyritic which is not seen in the Llandudno granodiorite, which is mainly K-feldspar porphyritic. Where layers cross-cut each other there is always a mafic-leucocratic pair, there is no mafic portion seen in the layering without the leucocratic portion or vice versa, so wherever a single portion is seen the other portion is present also, suggesting that they were formed together.

The layers are mostly planar extending for tens of meters and terminate by joining with layers that formed earlier on to form one single layer which eventually dissipates in the Llandudno granodiorite. In one case the layers are wispy and folded with high concentration of mafic minerals, showing a trough (Fig. 5F). The leucocratic portions of the layers in this layered package are enclosed within the mafic portion of the layers and are not continuous as in the general case. Cordierite crystals are commonly concentrated in the bottom part of the leucocratic portion of the layer. K-feldspar megacrysts within the layered rocks commonly show preferential alignment parallel to the layering in the mafic lower portion but much weaker alignment in the leucocratic portion of the layers. In one particular area, the mafic portion of the layers display extreme biotite enrichment (Fig. 5F&H), with the mafic portion of the layers thicker compared to the main layered sequence. Sedimentary like structures such as flames and slumps characterize the layering in the area. Flame-like structures are finger-like protrusions of felsic material derived from the top of the underlying layer, occurring either in the convex portions of the undulate layers or on the flanks of the concentrations of mafic minerals (Solgadi and Sawyer, 2008). These structures closely resemble ‘flame” structures in the sedimentary rocks and seem to have formed before the melt in the layers had solidified (Solgadi and Sawyer, 2008). In three places, several layers have been affected by magmatic faulting, one particular area the layers below and above appear not to have been affected by this process (Fig. 5I). These layers were cut into several small rectangular layered clasts and were tilted possibly due to the magma flow. The fact that only a few layers have been affected suggests that this deformation is only recorded in the more completely solidified rocks. These clasts could mean that while they were solid the Llandudno granodiorite was still relatively mush. Sedimentologically, the deformed layers might be slump structures. A sense of magma flow direction may be deduced from these clasts, as the clasts seem to be tilted to the direction of the flow of magma. In another

location, faulting is only restricted to one layer (Fig. 5J), and also shows it was formed synchronous with the formation of the layer.

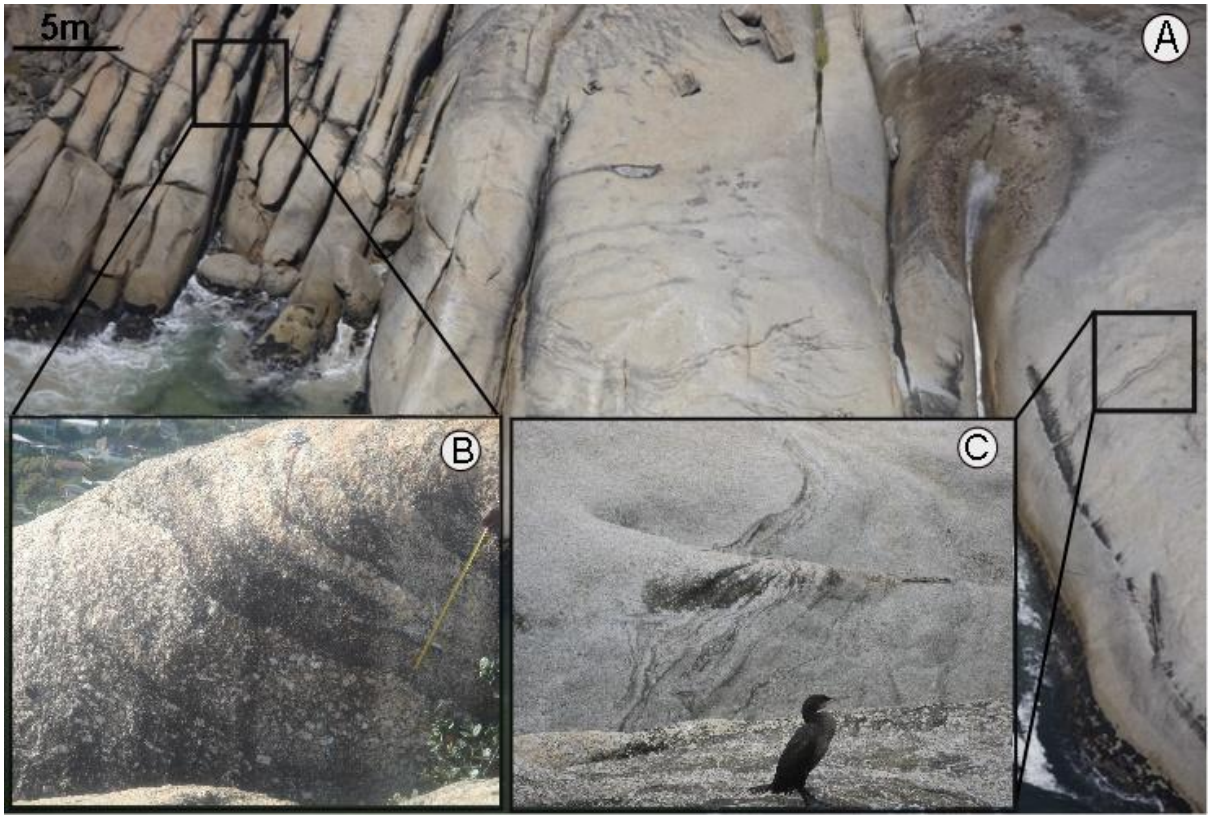

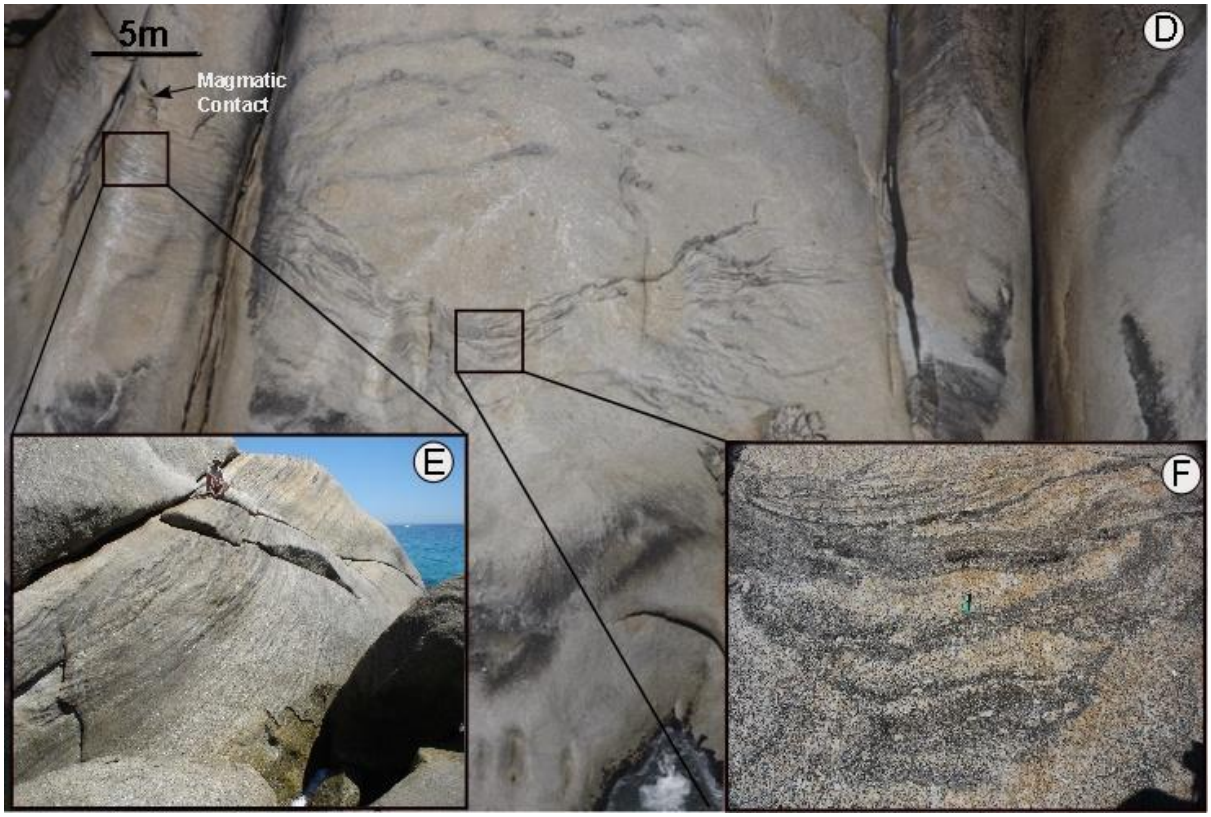

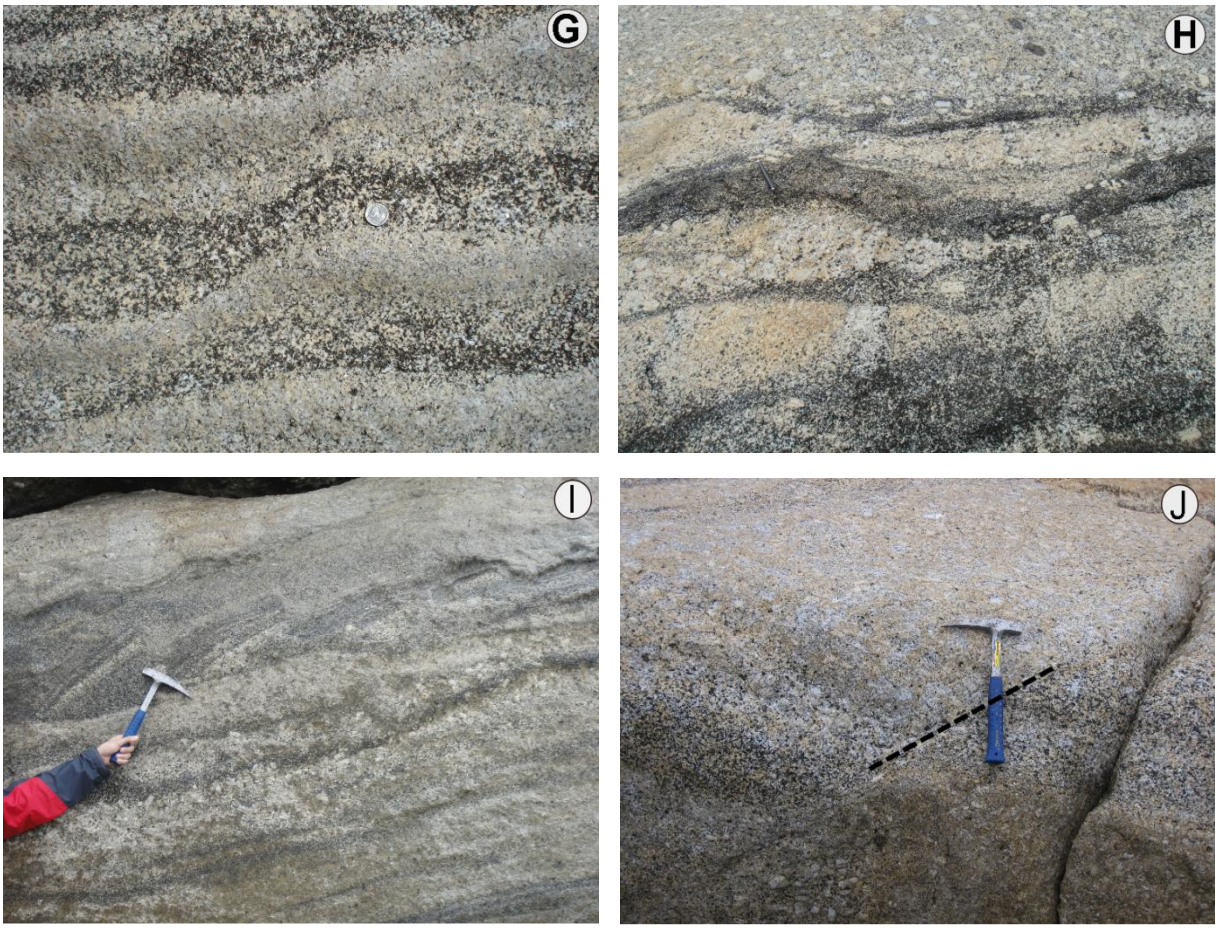

Fig. 5 Different field appearance for the Llandudno granodiorite. (A-C) illustrate the outcrop with several lenses of layering; measuring tape is 45cm in length. (D-F) show the layering within the outcrop. (E&F) show a close up of the layering, with (E) showing the main layering. The orientation of the layering is variable; striking 50 to 100˚ and dipping 35 to 65˚ towards the NW. (G) shows a close up of layering characterised by sharp contact at the bottom and a diffuse contact at the top, coin is 2 cm in diameter. (H) layering with extreme biotite enrichment and K-feldspar megacrysts with preferred orientation to the layering, pen is 15 m in length. (I&J) fault structures within the layering. Hammer is 32 cm in length.

Summary of interpretation of field relation

Magmatic structures in the Llandudno granodiorite record a variety of physical processes which occurred within a weak and partially crystallised magma. The magmatic enclaves may present evidence of incipient disruption indicating that, at the time the structure formed, they were not completely solidified. These are more mafic as compared to the Llandudno granodiorite and vary in sizes and shapes ranging from rounded, equigranular to spherical. Some enclaves have sharp contacts with the host granodiorite, an indication that they were

solid material during magma flow. Farina et al., (2012) noted that cordierite and some K-feldspar megacrysts accumulate at the edge of the enclave, suggesting that during magma flow the enclave was already crystallised to act as solid object. In some instances the K-feldspar make up to 30 vol. % of the magmatic enclaves these are reported to be similar to those in the Llandudno granodiorite (Farina et al., 2012). The layered sequence occurs within the Llandudno granodiorite; it appears that the layering formed within a magma that was partially crystallised. This is supported by the fact that within this layering the K-feldspar megacrysts are similar in size to those in the Llandudno granodiorite, although they are significantly lower in abundance. It is noteworthy that these megacrysts do not occur in all the layers but in a few. K-feldspar megacrysts show preferential orientation within the layering which is interpreted to show the flow direction of the magma. The mafic portion of the layering shows cumulate texture which resulted from the settling of early formed crystals of biotite and plagioclase. This texture is different from the leucocratic portion and the granodiorite which are quartz porphyritic and K-feldspar porphyritic respectively. The leucocratic portion shows textural and compositional difference from the Llandudno granodiorite, meaning that this difference could possibly be an indication of a different composition from that of Llandudno granodiorite, possibly another facies different from the Cape Granodiorite which Llandudno forms part of. Whether the layering formed sequentially from bottom to top or by underplating it is not evident within this sequence, though there is evidence of sequential formation indicated by the sharp contacts between the mafic-leucocratic pair with the subsequent mafic-leucocratic pair. The mafic-leucocratic pair are always seen together, even where there are cross cutting structures, these always appear in pairs, never a single portion. Each layer (mafic-leucocratic portions) shows that it was formed by one individual magma batch; this is because of the sharp to diffuse contacts between the pairs. The layering initially seems to be a part of some larger layered structure within the Peninsula pluton and within the Llandudno outcrops three layered lenses are preserved. In one of the best exposed of these lenses, the lens very clearly fingers out into the Llandudno granodiorite to the south, giving the impression that it was digested out by the granodiorite. In many parts of the Peninsula pluton there are biotite schlieren that exhibit layering and may represent the digested remnants of larger layered structures. If this is true, layering was a common part of the Peninsula pluton during earlier phases of its development.

CHAPTER FOUR

PETROGRAPHY

The Llandudno granite

The Llandudno granodiorite is coarse grained and consists mainly of plagioclase (25-30%), quartz (30-40%), alkali feldspar (15-20%), biotite (<10%) and cordierite (5-10%) which is pinnitised (Fig. 6A). The accessory mineral assemblage consists of apatite, zircon, monazite and ilmenite. The granodiorite is characterised by euhedral and inclusion rich K-feldspar megacrysts, giving the rock a porphyritic texture. Some K-feldspar crystals are commonly dusty in appearance and display simple Carlsbad twins. These crystals host numerous inclusions of biotite, plagioclase, quartz and rarely cordierite. Myrmekite, an intergrowth of quartz and plagioclase, is also visible mostly along boundaries of plagioclase and K-feldspar crystals. There are three biotite generations observed in these rocks; (which are described in detail below in section 5.4) the first type is euhedral to subhedral (Fig. 6B&C), the second type replaces orthopyroxene and the third type occurs together with muscovite and pinnite as replacements product for cordierite and has a symplectic texture. Similarly to biotite, muscovite also occurs as two generations, the first as replacement of cordierite with biotite and secondly as interstitial anhedral crystals, the second type is not common and is rarely seen in the layering. Quartz was the last phase to grow filling in the interstitial spaces with some anhedral K-feldspar crystals. The crystals are small to large anhedral crystals reaching 8mm (Fig. 6B&C). Quartz has a very distinct undulatory extinction. Plagioclase grains are euhedral to subhedral, and mostly medium (about 5 mm) with a few large grains which can reach up and above 1cm. Some plagioclase crystals are characterised by multiple twinning with oscillatory zoning evident (Fig. 6D). Zircon, monazite and apatite are commonly associated with biotite (Fig. 6E).

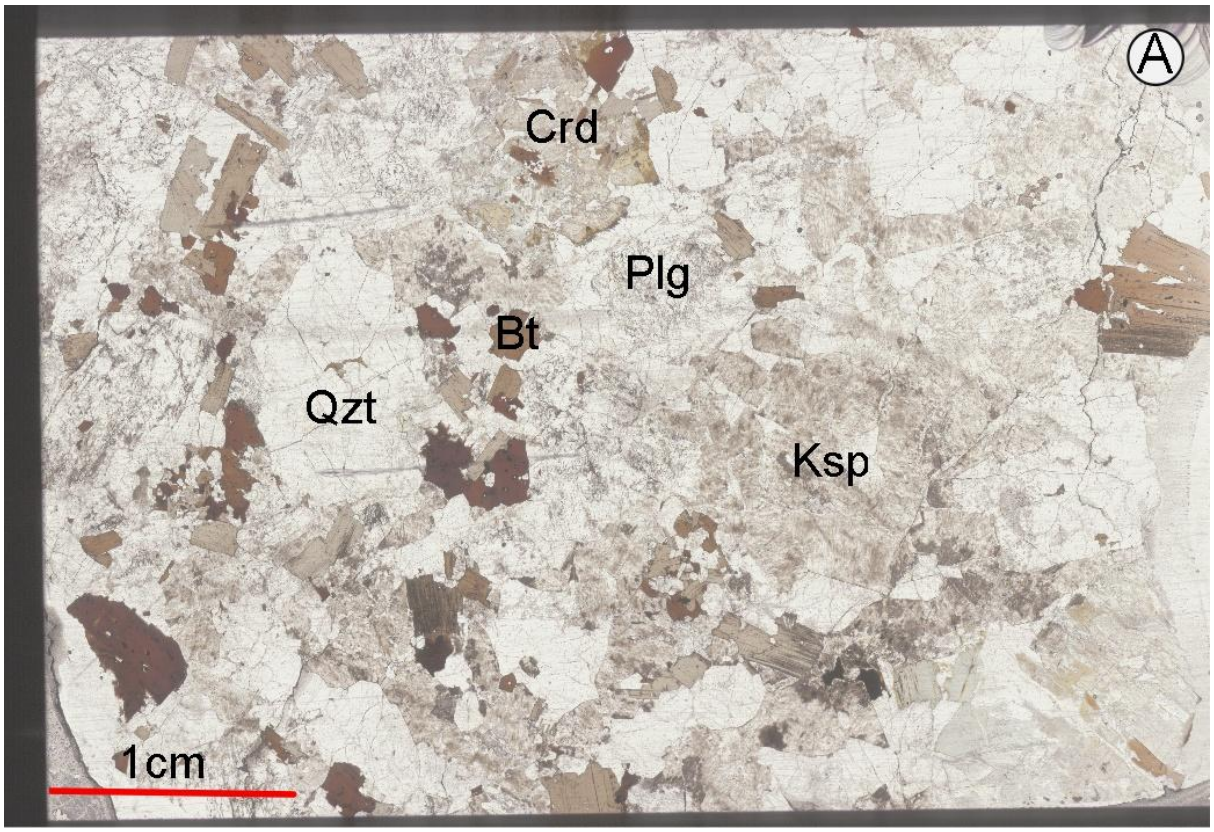

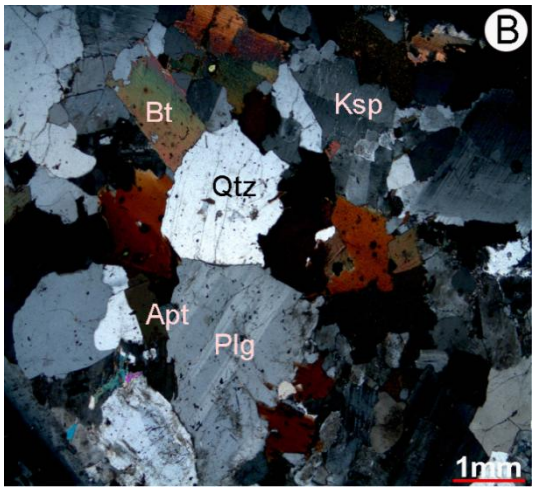

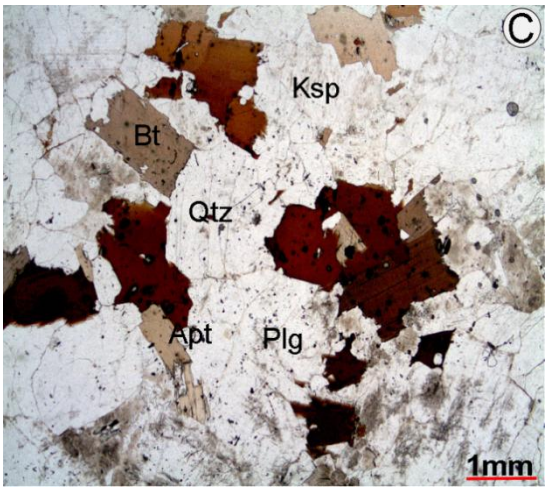

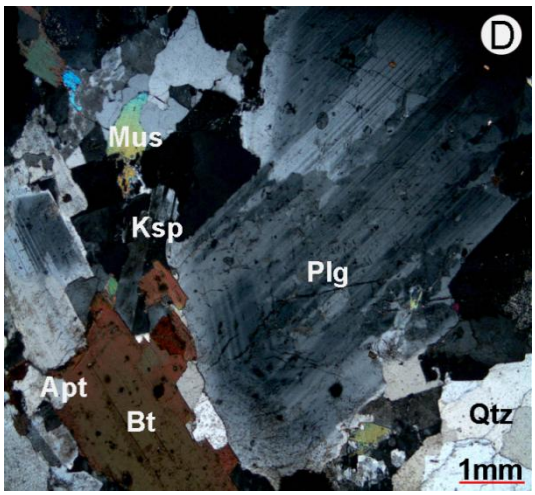

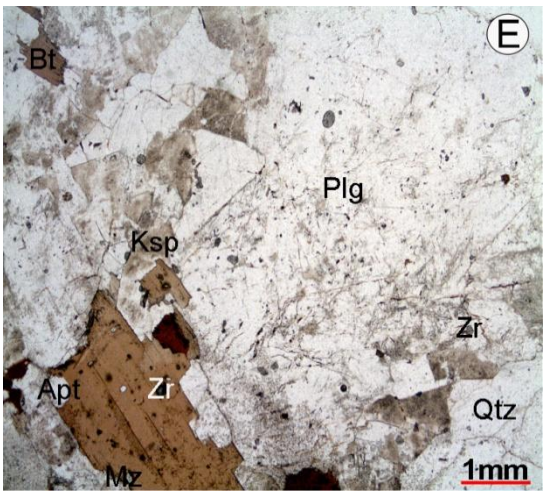

Fig. 6 Images from a thin section taken from the Llandudno granodiorite. (A) Nikon scan of the thin section, showing different minerals within the Llandudno granodiorite. (B-E) show the texture of the Llandudno granite seen under crossed polars and plane polars. (B&C) shows the euhedral and subhedral biotite crystals, with interstitial anhedral quartz. (D&E) show subhedral plagioclase crystals showing multiple twinning and oscillatory zoning; accessory minerals found in biotite, (E).

The mafic portion of the layers

The mafic portions of the layers are generally thinner than their corresponding leucocratic portion. The ratios are variable, but on average the mafic portions of the layer make up approximately one third of the thickness of each layer. The thickest mafic portion of layers recorded in this study was 28 cm thick. The minerals in the thin sections show cumulate texture, characterized by euhedral to subhedral mineral grains (Fig. 7A). The mineralogy which consists of biotite, plagioclase, K-feldspar, quartz and some cordierite within the portions that were investigated is consistent throughout the entire sequence of layering. Biotite is the most abundant ferromagnesian mineral forming individual crystals up to 8 mm in length, and within the mafic portions of layers the percentage of biotite differs from 30-50 vol. %. It has a light to deep brown colour in the plane polarized light view (Fig. 7B&C) and is strongly pleochroic. Some mafic portions contain biotite that is fine grained, while in some cases it is medium grained. In the case where biotite occurs as replacement product of cordierite, it is fine grained and does not contain any inclusions. Accessory minerals such as zircon, monazite, apatite and ilmenite are present in abundance within the biotite of mafic portions, as compared to biotite within the leucocratic portions. Obvious features of biotite are the inclusions of zircon and monazite that occur on the rim of the grain (Fig. 7D&E). These accessory minerals seem to separate the euhedral original biotite crystal from the overgrowth. This overgrowth could be as a result of the interstitial liquid crystallisation and the reactions consuming orthopyroxene and cordierite as the melt crystallises. Replacements products of orthopyroxene consisting of biotite, quartz and ilmenite are present. Plagioclase displays typical multiple twinning as well as oscillatory zoning. In some cases plagioclase as seen in the case of K-feldspars in all the layered rocks is cloudy. K-feldspar occurs as medium grained crystals, but megacrysts occasionally occur in some mafic portions but this is the exception rather than the norm.

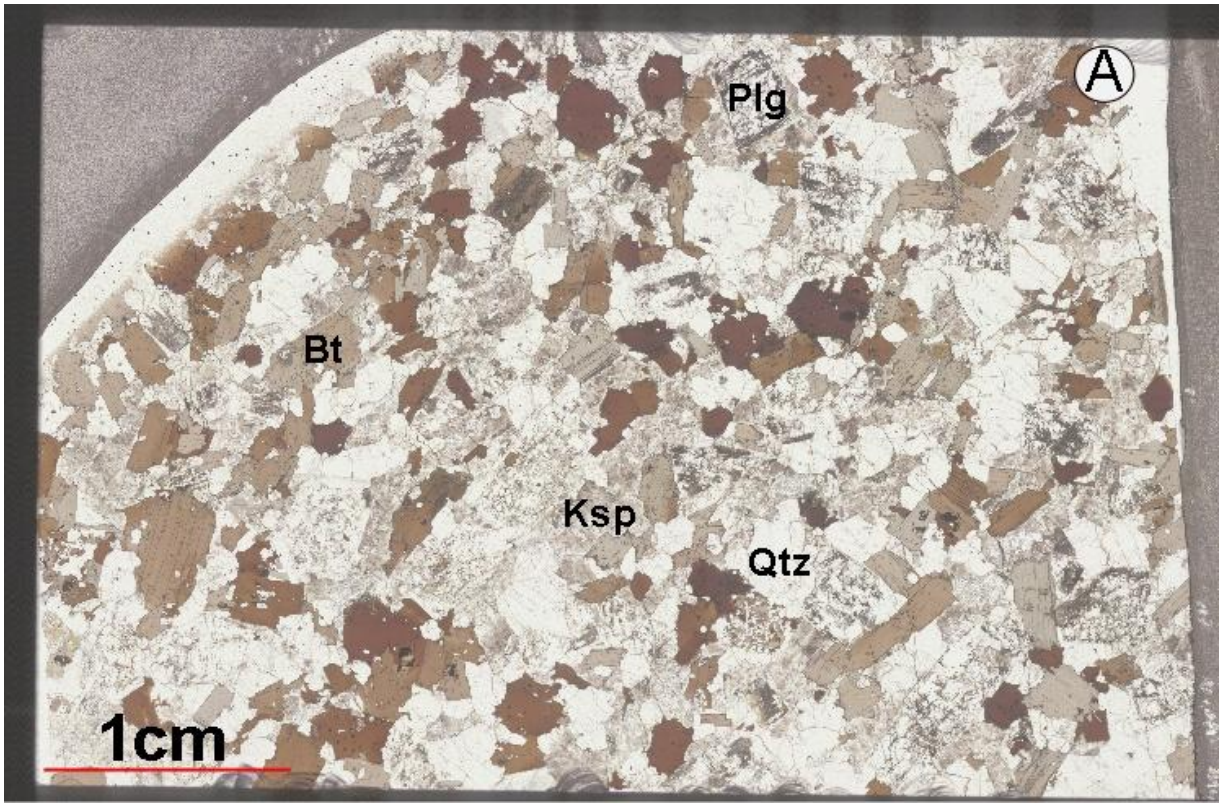

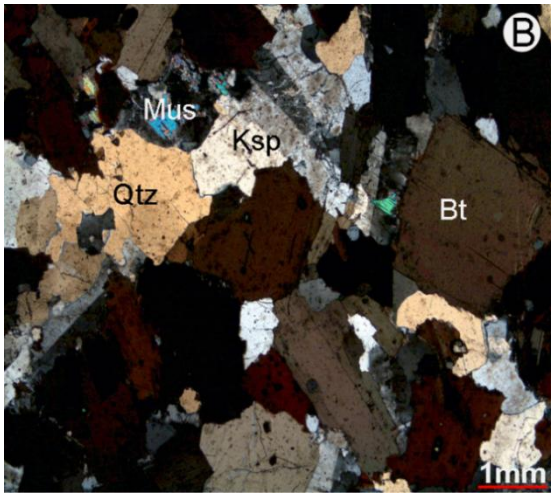

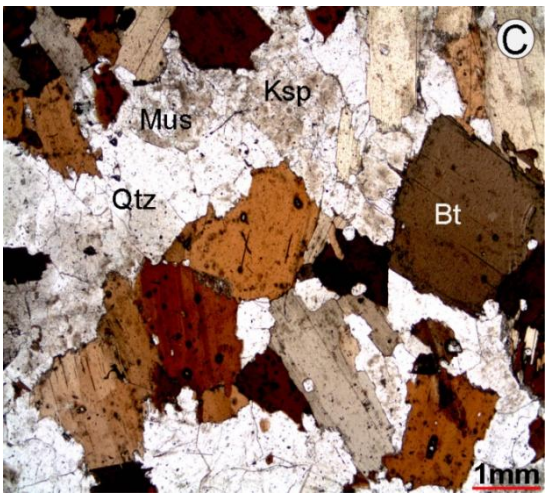

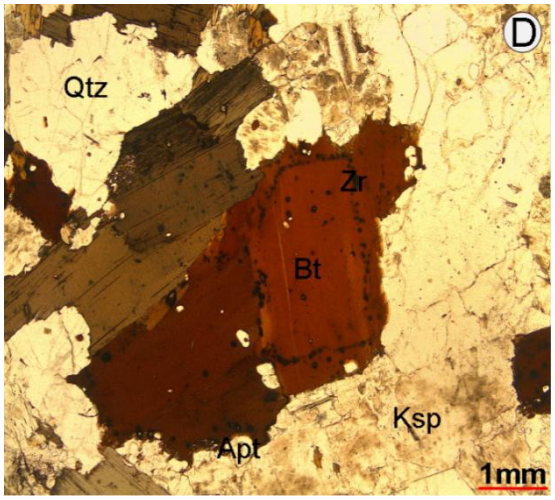

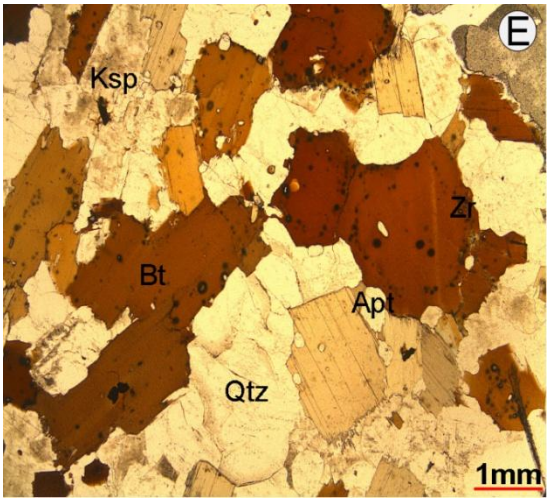

Fig.7 Images taken from a thin section in the mafic portion of the layering. (A) Nikon scan of the thin section from the mafic portion of the layering. (B&C) show the texture of the mafic portion under crossed and plane polars. (D&E) show the accessory minerals (zircon) forming a rim on the biotite seeming to mark the start of the overgrowth of biotite.

The leucocratic portion of the layers

The leucocratic portions of the layers differ in thickness substantially within the package of layering. In some areas these portions can reach up to 40 cm in thickness. Crystals in the leucocratic portions are course grained relative to those in the mafic portions. Some leucocratic portions are medium grained, but most portions show a porphyritic texture. The samples are predominately composed of K-feldspar, quartz, plagioclase and biotite with accessory minerals such as zircon, ilmenite and apatite (Fig. 8A). K-feldspar crystals are subhedral with inclusions of biotite and plagioclase. K-feldspar megacrysts occasionally occur in these portions, but they are slightly smaller in size to those in the Llandudno granodiorite. Muscovite which is rarely seen as replacement of biotite is present (Fig. 8B&C).Biotite is mostly subhedral but is also euhedral. Muscovite is also present as a product of the alteration of cordierite, as well as a replacement of biotite (Fig. 8B&C). The biotite content of the leucocratic portions is variable; some contain less than 1 vol. % biotite, whilst the most biotite-rich leucocratic portions contain approximately 10 vol. % biotite. Plagioclase grains seen in this image have a cloudy dirty appearance. In some cases plagioclase poikilitically encloses biotite as well as inclusions of apatite and zircon present. Plagioclase is characterized by multiple twinning, with some crystals showing very distinct normal zonation that is concentric with euhedral crystal faces. Quartz occurs with a variety of forms. Medium to coarse grained subhedral crystals form part of a porphyritic texture, whilst fine grained, anhedral interstitial quartz is also an important component of the leucocratic portions.

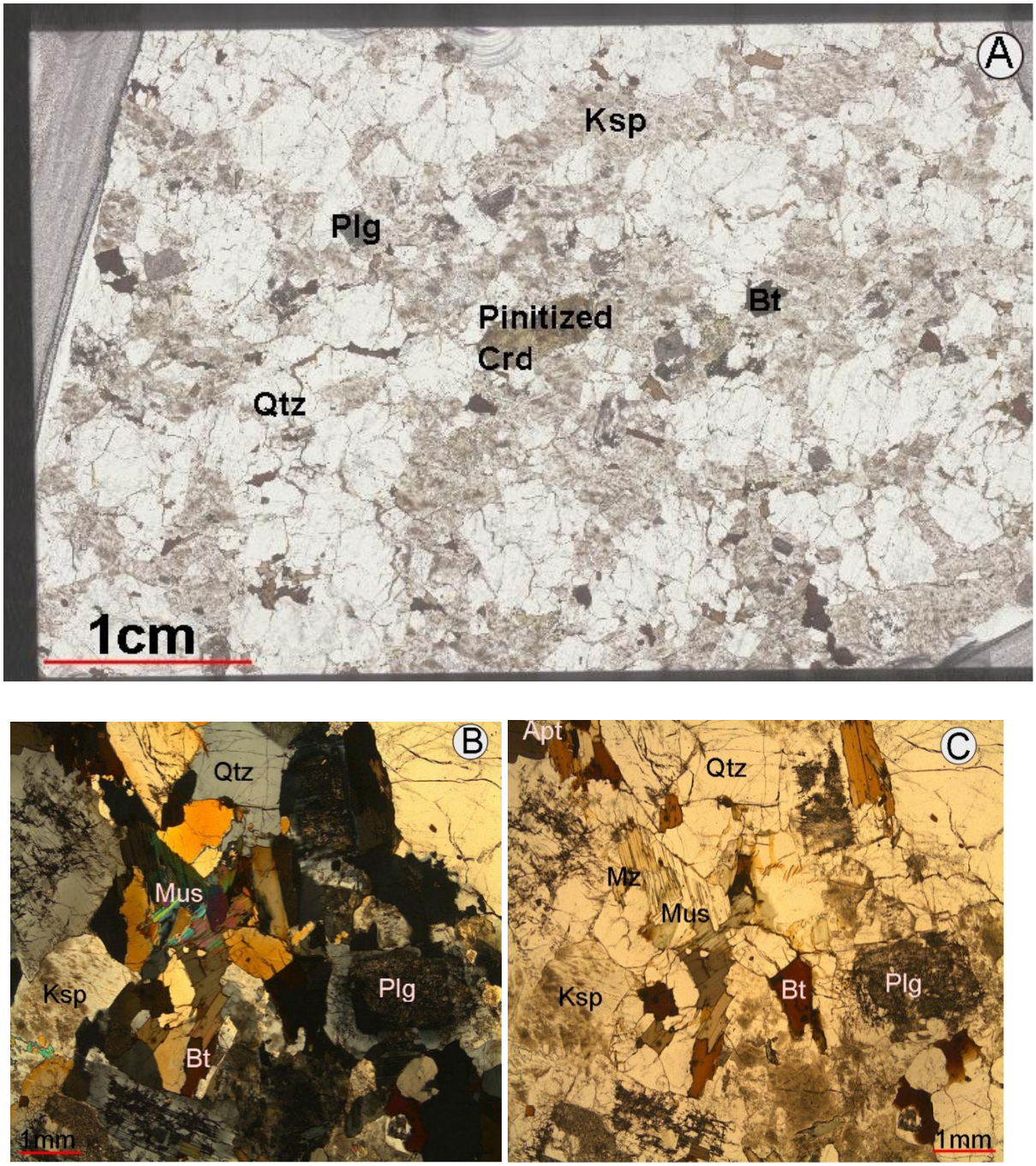

Fig. 8 Images taken from a thin section in the leucocratic portion of the layering. **(A)** Nikon scan of the thin section showing quartz porphyritic texture. (B&C) showing characteristic minerals in the leucocratic portion, K-feldspar and plagioclase crystals with their dusty apprearence.

Reaction textures

The Llandudno granodiorite and the layered zones are characterised by reaction textures which provide information on mineral reactions that occurred in the crystallizing magma.

Cordierite (Fig. 9A), a common mineral in these rocks and is highly pinnitised and has been replaced by a mineral assemblage of pinnite, muscovite and biotite. Under the microscope cordierite is not visible, the crystals are completely replaced by aggregates of green-brown Ti- poor biotite and white mica with very fine grained mats of phyllosilicate which vary from grey to typical first order blue of muscovite (Fig. 9B&C); they are both colourless under plane polars (Fig. 9D). Most K-feldspar grains have a cloudy appearance, and some grain have a brown colour (Fig. 9E). Biotites in the Llandudno granodiorite and the layering represent three generations. The first generation is the normal matrix biotite that is mostly euhedral. The second generation occurs when the melt reacts with orthopyroxene to form biotite, mainly associated with quartz and ilmenite. At this rate the cordierite is still in equilibrium with the melt. This biotite is dark red in colour showing that it was formed during high temperature. This biotite form clots which are up to 1 cm in diameter (Fig. 9F). These clots mostly occur in the mafic portions of the layering. The biotite and quartz crystals are finer grained relative to those in the Llandudno granodiorite. Biotite hosts many large ilmenite inclusions (up to 400um), in some cases making it by far the most abundant inclusion in these structures. These structures have two different textures that are recognised and in both cases the rim of the clot consists of biotite crystals enclosing both quartz and biotite. In the first type, the core of the structure consists of euhedral to subhedral biotite and quartz crystals of the same size to that of biotite crystals forming the rim. The second texture is characterised by symplectic intergrowths, which are mostly known from the more mafic granites. These clots are thought to represent alteration products of orthopyroxene, though pyroxene was not found in any of the thin sections. This is supported by experimental studies on S-type granites predicting stability of orthopyroxene at high temperatures (Clemens and Wall, 1981). These clots have been described elsewhere by Clemens and Benn, (2010) for Australian S-type granites in Mt Disappointment pluton. In these granites the remnants of pyroxene are preserved so the origin of these textures is unambiguous in this case; clino-pyroxene occurs with orthopyroxene in Mt. Disappointment pluton. The third generation of biotite occurs when the melt reacts with cordierite and the water content and the temperature decrease and this form is a dark green low temperature biotite. Crystals of K-feldspar and plagioclase have a dusty appearance; this could be as a result of small crystals of sericite and/or opaque minerals that exsolved Fe^{3+}. The Fe that plagioclase takes up at high temperatures, is exsolved at low temperatures creating this dusty appearance. This appearance doesn't seem to show alteration in that the LOI of the whole rock chemistry is quite low and while the water content is < 1.

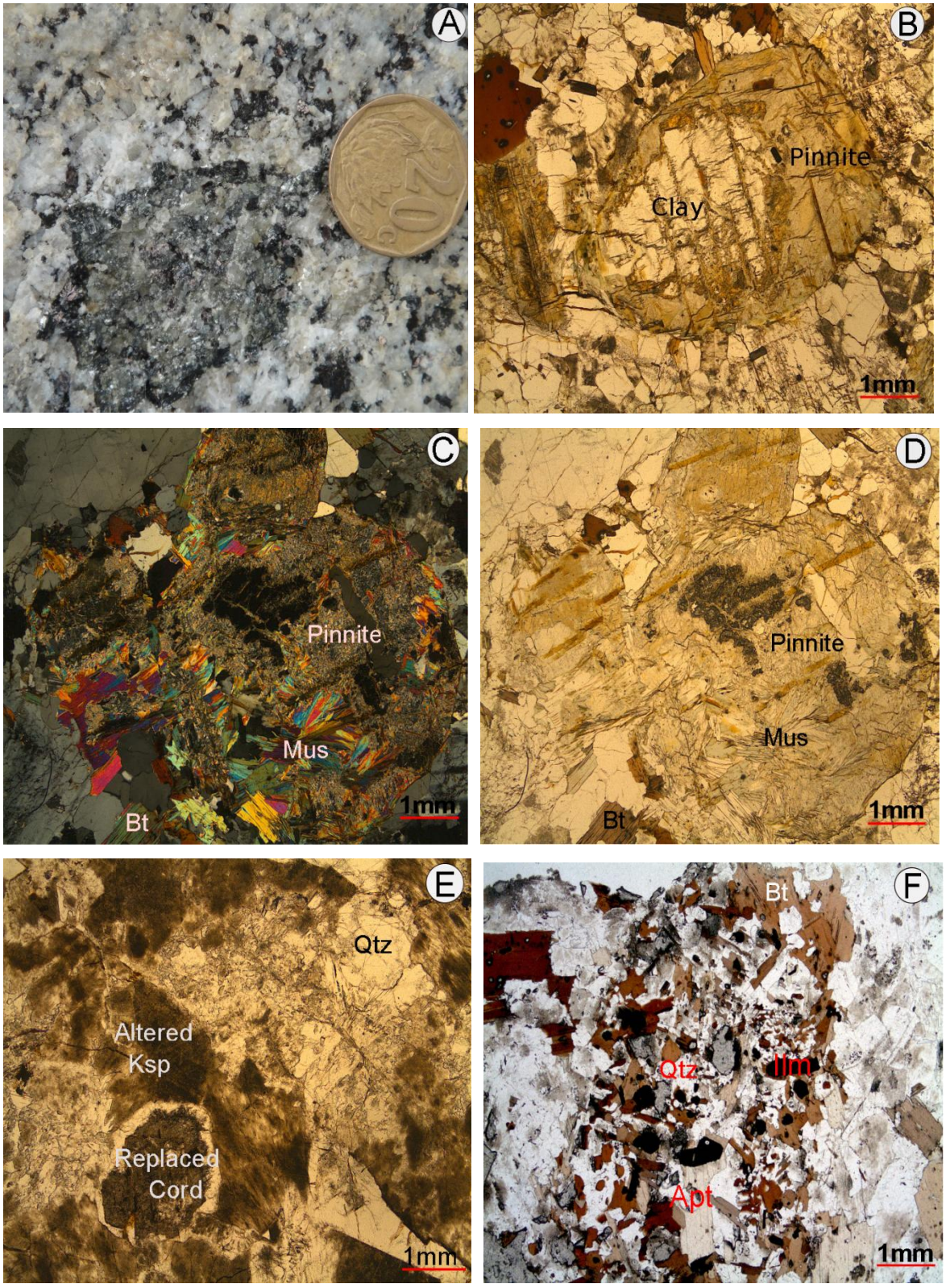

Fig. 9 Images showing reaction textures that are common in the Llandudno granodiorite and layering. (A) show cordierite grain as seen in the field, clearly rimmed by biotite, coin is 18 mm in diameter. (B-D) show the cordierite grain that has been replaced by muscovite, biotite, pinnite and clay mineral. (E) illustrate a completely pseudomorphed grain of cordierite by some clay mineral, which has a powdery texture, as well as K-feldspar crystal with cloudy appearance**.** (F) show orthopyroxene crystal that was replaced by biotite, quartz and ilmenite with minor apatite.

CHAPTER FIVE

GEOCHEMICAL ANALYSIS

Database

Samples from the Llandudno granodiorite were collected and analyzed for major and trace element composition (the analytical methods are detailed below). Due to the location of the area on a prominent wave eroded shore-front, samples were difficult to obtain by hammer due to the smooth, whale-back nature of the outcrops. Consequently a limited number of samples were collected, generally by rock drill (40 mm cores) and by portable rock saw with which blocks were cut and then chiseled free. The study area is also a prominent area of considerable natural beauty, so care was take to sample as sensitively as possible, with the sample sights selected away from the most prominent and striking outcrops. The samples were handled in such a way as to get the maximum amount of information out of each sample. As individual layers are characterised by biotite rich lower portions which grade upwards into a strongly leucocratic upper portion each of these components were either sampled separately, or where cores of entire layers were obtained, these were split in order to collect information on the composition of each of the paired components. In such cases the composition of the entire layer was established by integrating the two compositions proportional with their true thickness. Thirteen samples were collected from the bottom to the top of the layered sequence (Fig. 10) and two samples were collected from the host granodiorite. The samples from the layered rocks comprise the following: Two samples of mafic and leucocratic material from the same layer; Seven samples were collected from the biotite rich lower portion of the layering (these are referred to as mafic portions); Four samples were also collected from the upper leucocratic portion of the layering (referred to as leucocratic portion). The remaining two samples were collected from the host granodiorite, one from the bottom granite and the other from the top granite which bound the layering. Additionally compositions from the Peninsula pluton in general were obtained from Farina et al., (2012). The major and trace element geochemical data from the Llandudno granodiorite is presented in Table 1.

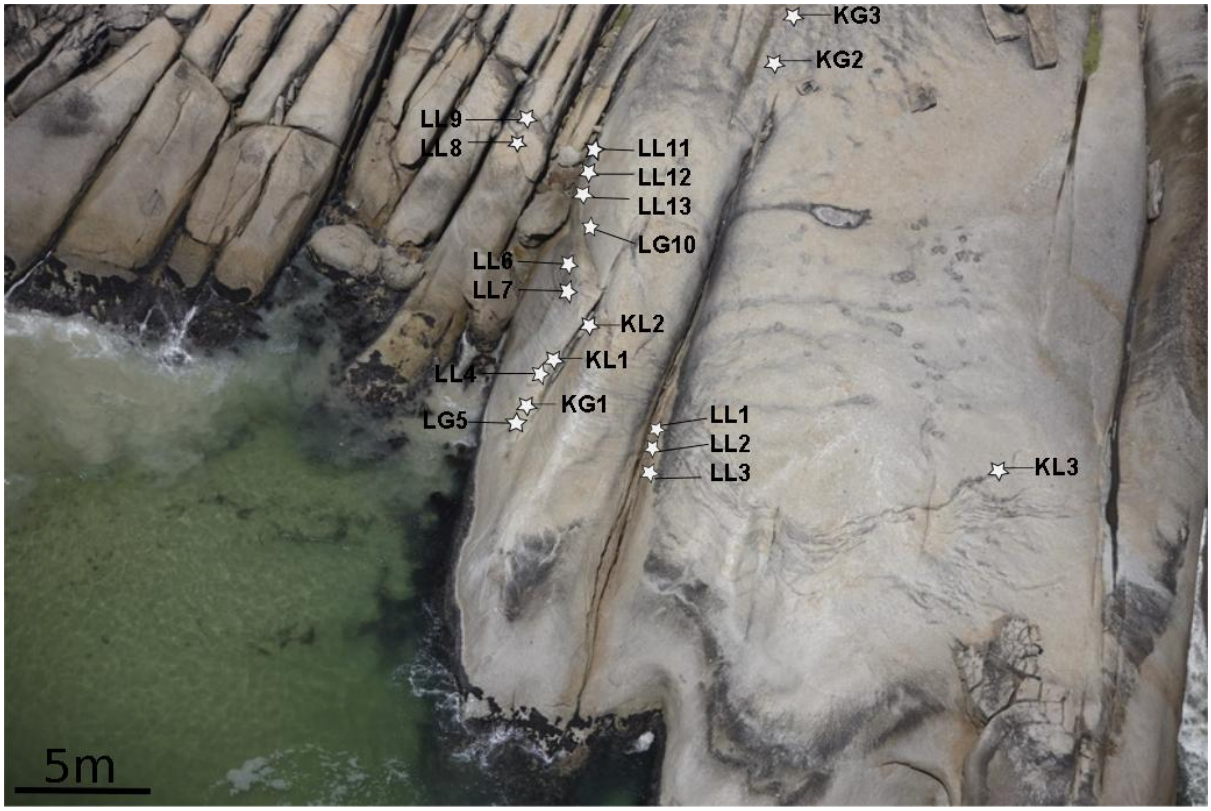

Fig.10 Aerial Image showing sites where samples were collected, LG for Llandudno granite, LL for layering, KG for K-feldspar in granite and KL for K-feldspar in layering.

Analytical methods

Whole rock geochemistry

Thin sections were prepared at the Department of Geological Sciences, University of Cape Town. Samples were also crushed for major and trace elements analyses at the Central Analytical Facility, University of Stellenbosch, South Africa. Loss on ignition values was calculated by placing powdered samples in an oven at 1000 °C for 1 hour. Major element compositions were analysed by X-ray fluorescence spectrometry (XRF) on glass beads prepared with La-free flux. Internal standards were basalt BHVO-1 and granite NIM-G. For the granite, calculated uncertainties (twice the measured deviations for the granite standard expressed in wt%) are: 0.35 for SiO_2, 0.02 for TiO_2, 0.12 for Al_2O_3, 0.15 for FeOT , 0.01 for MnO, 0.02 for MgO, 188 0.07 for CaO, 0.10 for Na_2O, 0.02 for K_2O and 0.01 for P_2O_5. Results are plotted after normalization to 100 wt % volatile-free. Trace element compositions have been obtained from the same fused beads used for major element determination by applying the method described by Eggins, (2003) and analysed using an Agilent 7500ce ICP-MS coupled with a Nd-YAG 223 nm New Wave LASER ablation (LA) system operating at a

12 Hz frequency with a mixed He-Ar carrier gas. Three analyses (each comprising a 30 s blank followed by data collection for 60 s) on each whole rock fused disc were obtained using a 100 µm diameter aperture, and the results averaged. After every three samples (i.e. every 10th 195 analysis) NIST612 (Pearce et al., 1997) glass bead was analysed as a calibration standard, in addition to fused discs of NIM-G (granite) and BHVO-1 (basalt) that were analysed as secondary standards. Data were collected in time-resolved mode and were reduced using the SiO_2 content measured by XRF as the internal standard. For each element, the reproducibility of replicate analyses of the samples, and deviation from the certified values of the secondary standards are less than 10%, and mostly less than 5% relative.

Mineral chemistry

The major element compositions of the rock-forming minerals in selected samples were analysed using a Leo® 1430VP Scanning Electron Microscope at the Department of Earth Sciences, Stellenbosch University, South Africa. Mineral compositions were quantified by EDX (Energy Dispersive X-ray) analysis using an Oxford Instruments 133 keV ED X-ray detector and Oxford INCA software. Beam conditions during the quantitative analyses were 20 kV accelerating voltage and 1.5 nA probe current, with a working distance of 8.5 mm and a specimen beam current of−4.0 nA. X-ray counts were typically ~7000 cps, and the counting time was 50 s live-time. Analyses were quantified using natural mineral standards, and mineral chemical compositions were recalculated to mineral stoichiometries to obtain resultant mineral structural formulae. Comparisons between measured and accepted compositions of control standards within this laboratory, as a reflection of the accuracy of the analytical technique, have been published by Moyen et al. (2006).

Table 1. Representative whole rock composition of the layering and hosting Llandudno granodiorite.

Rock Type	Mafic portions									Leucocratic portions						Composite Layer		Llandudno granodiorite	
Sample	**LL1**	**LL3**	**LL4**	**LL7**	**LL11B**	**LL13B**	**LG2**	**LG4**	**LG11**	**LL2**	**LL6**	**LL8**	**LL11A**	**LL12**	**LL13A**	**LL11**	**LL13**	**LL5**	**LL10**
Wt%																			
SiO_2	63.85	62.58	65.82	60.48	66.66	66.63	67.58	65.28	65.01	77.56	78.07	80.88	79.31	79.97	80.02	76.78	75.33	72.18	70.57
TiO_2	1.31	0.83	1.06	1.54	0.83	0.94	0.89	0.97	1.12	0.25	0.23	0.16	0.2	0.22	0.15	0.33	0.43	0.29	0.42
Al_2O_3	14.19	17	14.61	14.7	14.85	14.76	14.71	15.28	14.64	11.43	11.74	9.06	10.71	10.52	11.16	11.54	12.42	15.01	14.79
Fe_2O_3	8.58	7.6	6.99	10.28	6.07	6.32	5.8	6.72	7.31	1.84	1.84	1.21	1.59	1.69	1.17	2.49	2.97	2.47	3.03
MnO	0.1	0.16	0.1	0.12	0.09	0.09	0.08	0.09	0.09	0.03	0.03	0.02	0.03	0.03	0.03	0.04	0.05	0.05	0.05
MgO	2.52	2.7	1.95	2.88	1.68	1.7	1.62	1.81	1.95	0.52	0.5	0.24	0.47	0.43	0.29	0.71	0.78	0.73	0.84
CaO	1.14	0.54	1.49	1.22	1.11	1.63	1.68	1.58	1.46	1.05	1.22	0.38	0.48	0.77	1.12	0.61	1.30	2.02	1.44
Na_2O	1.81	1.44	2.29	1.7	2.31	2.53	2.31	2.2	1.98	2.38	2.46	1.67	1.97	2.03	2.36	2.04	2.42	3.3	2.8
K_2O	5.52	5.44	4.84	6.08	5.46	4.45	4.27	4.76	4.87	4.01	3.87	4.42	5.02	4.23	3.85	5.11	4.06	3.44	5.4
P_2O_5	0.37	0.18	0.33	0.45	0.38	0.3	0.31	0.33	0.34	0.16	0.15	0.13	0.14	0.15	0.11	0.19	0.18	0.17	0.19
LOI	1.33	2.3	1.08	1.15	1.35	1.35	1.12	1.19	1.28	0.75	0.93	0.84	0.84	0.72	0.66	0.94	0.90	0.98	0.86
H_2O-	0.2	0.12	0.09	0.08	0.14	0.16	0.08	0.08	0.08	0.12	0.14	0.09	0.14	0.11	0.1	0.13	0.11	0.13	0.1
Sum	100.93	100.9	100.66	100.69	100.93	100.86	100.45	100.3	100.13	100.1	101.17	99.1	100.91	100.87	101.02	99.82	99.94	100.77	100.49
MgO + FeO	11.1	10.3	8.94	13.16	7.75	8.02	7.43	8.53	9.26	2.36	2.34	1.45	2.06	2.12	1.46	3.20	3.76	3.2	3.87
A/CNK	1.29	1.84	1.25	1.27	1.27	1.24	1.28	1.31	1.31	1.12	1.12	1.1	1.12	1.13	1.11	1.16	1.16	1.17	1.13
Na_2O/CaO	1.59	2.67	1.54	1.39	2.08	1.55	1.38	1.39	1.36	2.27	2.02	4.39	4.10	2.64	2.11	3.36	1.86	1.63	1.94
Mg#	37.29	41.84	36.10	36.19	35.91	35.26	36.12	35.29	35.07	36.39	35.49	28.65	37.44	34.00	33.42	36.70	34.80	37.44	35.95
ppm																			
Sc	26	22	24	27	20	19	18	19	20	18	18	18	17	11	11	18	14	17	16
V	127	102	97	145	81	85	90	97	106	25	24	17	21	25	18	33	42	27	40
Ni	34	24	27	34	23	21	22	29	26	8	7	6	9	9	7	12	12	9	13
Zn	147	115	125	167	95	119	107	131	123	40	48	26	38	38	33	50	63	57	56
Rb	446	362	373	516	406	381	334	371	372	200	197	192	234	210	181	268	251	203	242
Sr	53	50	61	45	58	71	66	60	49	50	61	29	42	42	58	45	62	80	87
Y	89	31	77	123	109	68	57	66	68	23	26	17	21	24	16	39	34	25	26

Table 1 (continued)

Rock Type	Mafic portions									Leucocratic portions						Composite Layer		Llandudno granodiorite	
Sample	**LL1**	**LL3**	**LL4**	**LL7**	**LL11B**	**LL13B**	**LG2**	**LG4**	**LG11**	**LL2**	**LL6**	**LL8**	**LL11A**	**LL12**	**LL13A**	**LL11**	**LL13**	**LL5**	**LL10**
Zr	472	257	417	612	390	373	353	357	372	99	112	61	80	92	66	142	173	124	149
Nb	51	27	42	60	37	38	36	40	42	11	11	7	9	10	6	15	17	12	15
Sn	16	12	15	17	16	16	28	34	28	8	9	6	8	8	6	10	10	9	7
Cs	25	35	26	29	31	32	28	34	27	12	12	10	11	13	10	15	18	18	12
Ba	174	435	156	193	172	147	129	140	133	108	109	103	168	119	141	169	143	108	462
La	83	48	75	104	74	68	63	63	65	20	23	12	16	18	16	27	34	27	28
Ce	179	96	157	213	153	142	137	142	143	46	48	29	35	42	35	59	72	60	64
Pr	21	12	19	26	19	17	16	16	17	5	6	3	4	5	4	7	8	7	7
Nd	81	44	70	102	72	65	60	62	64	19	21	12	15	17	14	26	32	24	25
Sm	17.3	9.2	15.9	22.9	16.6	14.5	12.9	13.9	14.1	4.1	4.5	2.8	3.4	3.9	3.1	6.1	7.1	5	5.7
Eu	0.6	0.8	0.6	0.6	0.7	0.8	0.7	0.7	0.6	0.5	0.6	0.4	0.4	0.5	0.6	0.5	0.7	0.8	0.9
Gd	17.7	8.9	15.4	23.3	17.4	12.8	12.1	13.2	12.6	4.3	4.9	3.1	3	3.9	2.8	5.9	6.3	4.8	5.2
Tb	2.7	1.2	2.6	3.7	2.9	2.2	1.8	2.1	2.1	0.7	0.8	0.4	0.6	0.7	0.5	1.0	1.1	0.8	0.8
Dy	17.2	6.4	14.3	22.7	19.1	12.7	11.2	12.6	12.6	4.3	4.5	3	3.6	4.3	2.8	6.7	6.2	4.6	4.8
Ho	3.3	1.1	2.7	4.4	3.8	2.5	2	2.4	2.5	0.8	0.9	0.6	0.8	0.9	0.6	1.4	1.2	0.9	0.9
Er	8.9	2.9	8.1	11.7	10.9	6.7	6	6.6	6.7	2.4	2.8	1.7	2.1	2.4	1.5	3.9	3.3	2.3	2.6
Tm	1.2	0.3	1.1	1.7	1.4	0.9	0.8	0.9	0.9	0.3	0.4	0.2	0.3	0.3	0.2	0.5	0.5	0.3	0.4
Yb	7.6	2.3	6.6	10.3	10	6.1	5.1	6.1	5.8	2.1	2.4	1.7	1.9	2.2	1.5	3.6	3.1	2.2	2.3
Lu	1.1	0.3	0.9	1.4	1.4	0.8	0.7	0.9	0.8	0.3	0.3	0.2	0.3	0.3	0.2	0.5	0.4	0.3	0.3
Hf	13.5	7.1	12	17.1	12	10.7	10.6	10.5	10.9	2.9	3.5	2	2.5	2.7	2.1	4.4	5.1	3.6	4
Ta	3.9	1.6	3.5	4.9	3.6	3.2	3.1	3.5	3.3	1	1.1	0.9	1.2	1.1	0.8	1.7	1.7	1.3	1.1
Pb	19	21	18	17	20	20	21	21	18	26	28	26	29	28	28	28	25	29	37
Th	45	21	40	59	44	36	34	36	36	11	12	7	9	10	8	16	18	13	14
U	8.4	3	5.5	7.3	8.9	5.7	5.2	5.3	5.4	9.8	2.4	8.8	3.8	3.7	2.4	4.8	3.6	2.8	3.1
Eu/Eu*	89	45	78	117	88	64	61	67	64	22	25	16	15	20	15	30	62	24	26

Major element distribution

Major elements data is used to determine the composition of the rock as well as in the construction of variation diagrams to determine the relationship between elements in the dataset so as to infer the geochemical processes involved in the formation of this rocks. Large compositional variation in the Peninsula pluton and most predictably within the Llandudno layered samples can be observed (Fig. 11), emphasizing some heterogeneity of the samples. The Peninsula pluton granites are strongly peraluminous (A/CNK 1.2-1.4), and are plotted for reference. Llandudno samples are peraluminous (A/CNK 1.1-1.8) with variability in major and trace elements (SiO_2 60-81wt%, FeO^T + MgO 1.45- 13.16 wt. %, Al_2O_3 9.06-17.00 wt. %, K_2O 3.44-6.08 wt. %). The samples show a strong positive linear correlation between FeO^T+ MgO and TiO_2, Al_2O_3 and P_2O_5. In contrast SiO_2 displays a strong negatively correlation while Na_2O shows a poorly negative correlation with FeO^T+ MgO. CaO, Na_2O and K_2O are scattered showing a great degree of variation. P_2O_5, CaO and Na_2O are not illustrated but data is available in the Table 1. The strong positive variation of Ti and Al with FeO^T+ MgO is attributed to the peritectic assemblage entrainment of garnet and ilmenite. Within the Peninsula pluton, this strong correlation is a function of variable degrees of peritectic assemblage entrainment (garnet and ilmenite) that occurred as a consequence of biotite incongruent melting in the source. These phases combined with a melt of leucogranitic composition, with very low TiO_2, FeO and MgO contents, to form the S-type magmas of the Cape Granite Suite. Consequently the TiO_2: FeO^T+ MgO ratio inherent to all these S-type rocks was inherited from the stoichiometry of the biotite that melted in the source (Stevens et al., 2007). Zr and P_2O_5 show strong positive correlation with FeO^T+MgO is due to the entrainment of accessory phases zircon, apatite and monazite. In the case of P_2O_5, this strong correlation is unusual for S-type granites which usually demonstrate a poor correlation between P_2O_5 and FeO^T+ MgO due to the strong solubility of P_2O_5 in peraluminous melts.

The mafic portions of the layering have higher FeO^T + MgO than any of the Peninsula pluton compositions reported by Farina et al., (2012). Similarly, the leucocratic portions have higher SiO_2 than any common Peninsula pluton compositions (Fig. 11). The compositions of complete individual layers have higher SiO_2 contents and have lower Al_2O_3 contents than any common Peninsula pluton compositions. This compositional difference could be attributed to the lesser amount of cordierite that is found in the layering than in the granites. Cordierite was found to be five times less in the layering than in the host granites. The Na_2O/CaO ratios

for the leucocratic and mafic portions of the layers, as well as entire layers, suggest that this ratio is generally higher in the layered rocks than in the hosting granites. Na_2O/CaO ratios vary substantially between the mafic and leucocratic portions of layers, with the six leucocratic portions analysed having an average value of 2.92, whilst the average for the nine mafic layers analysed was 1.66. These observations are in good agreement with the petrographic findings. The high FeO^T + MgO values and low Na_2O/CaO ratios are largely accounted for by the textures indicating accumulation of biotite and plagioclase. The high SiO_2 values in the leucocratic portions are in agreement with the presence of phenocrystic quartz in these rocks.

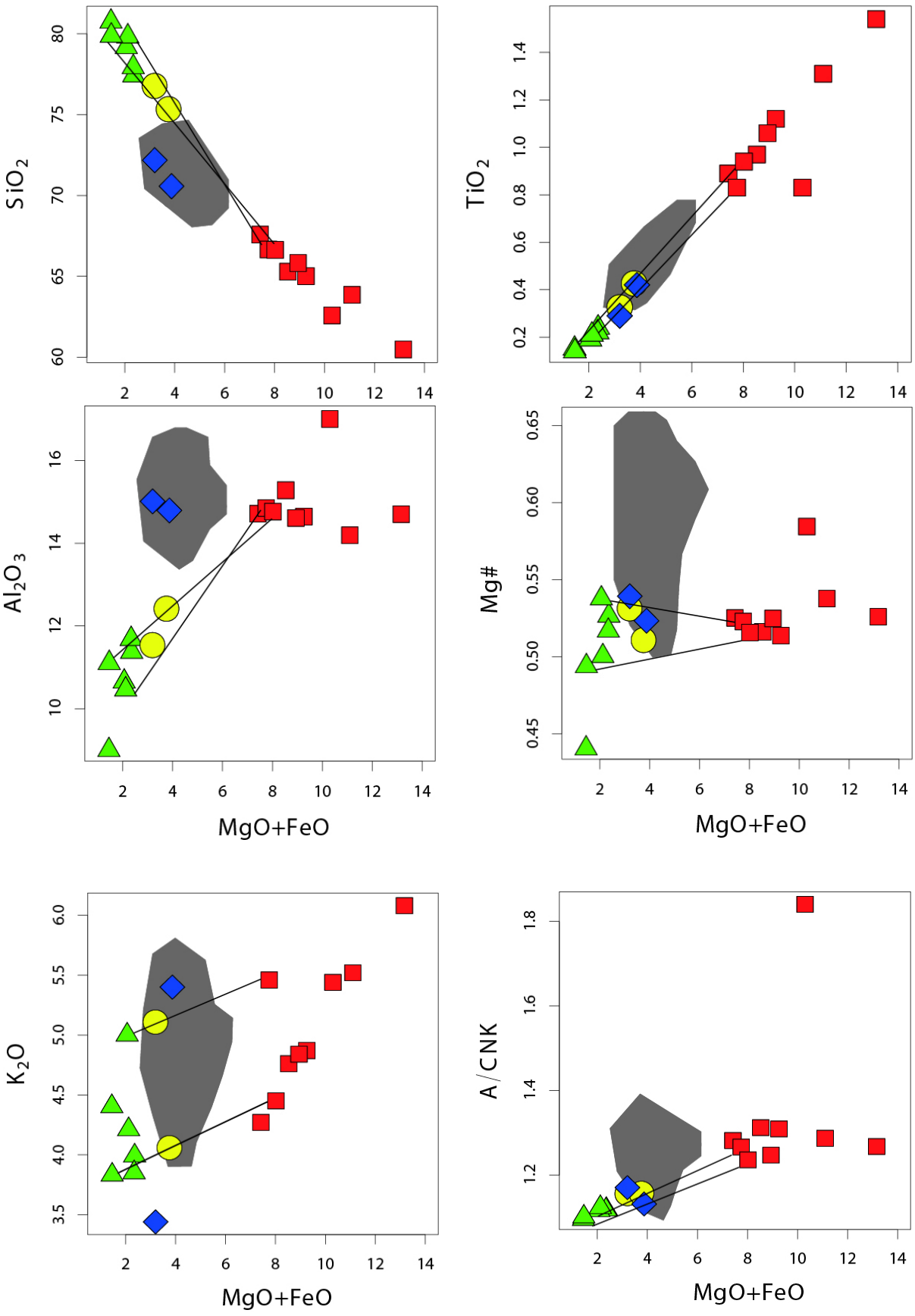

Fig. 11 Major element compositional variation of the layered zones relative to the Llandudno granodiorite and the Peninsula pluton in general. The green triangles represent the leucocratic portions, the red squares represent the mafic portions, the blue diamonds represents the Llandudno granodiorite and the yellow circles represent complete layers (mafic-leucocratic portions). The grey field represents the compositional range of the Peninsula pluton from the data of Farina et al., (2011). The lines represent tie lines between samples that have a mafic portion and a leucocratic portion of the layers. These samples when combined represent a complete layer, indicated by yellow circles.

Trace element chemistry

Most trace elements are strongly enriched in the mafic portions of layers relative to the leucocratic portions (Fig. 12). This is consistent with the abundance of accessory minerals in the mafic portions relative to the leucocratic portions. The enrichment of middle and heavy rare earth elements shows the abundance of zircon, while the enrichment of light rare earth elements reflects the abundance of monazite. High field strength elements such as Zr, Hf, Nb and Ta are compatible in ilmenite, which is mostly present in the mafic portions of the layers associated mostly with biotite; this is the similar case with zircon and monazite. Apatite contains most rare earth elements with other elements such as Y, Sr and Th. Apatite like other trace elements phases is mostly enriched in mafic portions of the layers than in leucocratic. This is reflected in the high concentration of rare earth elements (REEs) in the mafic portions than in the leucocratic portions. Rb which is preferentially partitions in biotite is higher mostly in the mafic portion than in the leucocratic portions of the layers. This is the same case with Ba which is compatible with plagioclase. Sr shows similar concentration in both mafic and leucocratic portions.

Within the layered rocks trace element variation diagrams of FeO^T+MgO against Rb, Zr, Nb and Eu/Eu* show a very strong linear positive within both mafic and leucocratic samples. Ba and Sr commonly show poor correlation with maficity, this is due to the fact that these elements are not affected by entrainment of accessory phases and are hosted within feldspars which largely enter the melt on anatexis. The scatter of the data with FeO^T +MgO is thought to reflect variations in source mineralogy and trace element composition. Sr for layers, mafic and leucocratic portions is lower than for Peninsula pluton and Llandudno granodiorite. Samples from the mafic portions are enriched in Rb, Nb and Zr, while Peninsula pluton is enriched in Sr and Ba.

The rare earth elements (REEs) pattern for the layered rocks normalised to Llandudno granodiorite are shown in Fig. 13. Relative to the Llandudno granodiorite, the mafic samples are enriched in light rare earth elements (LREEs) and in heavy rare earth elements (HREEs). This is interpreted to reflect greater abundance of zircon and monazite in the mafic portions of the layers, as is consistent with their relatively Zr- and P_2O_5-rich character. This may reflect greater degrees of co-entrainment of accessory phases monazite and zircon along with the peritectic assemblage during the formation of these magmas. Importantly, this work demonstrated that trace element disequilibrium is to be expected during the formation of the magma because zircon is slow to dissolve in the melt. The mafic portions have a deep negative anomaly relative to the Llandudno granodiorite. Leucocratic portions are depleted in both light rare earth and heavy rare earth elements. They have a slight negative Eu anomaly. The REE compositions of complete layers are similar to those of the mafic portions showing enrichment in HREEs than in REEs as well as the deep europium anomaly. The abundance of rare earth elements in the mafic portions of the layering is reflected by the abundance of zircon, monazite and ilmenite associated with the biotite as seen in the petrography. This seems to explain the composition of these rocks. This enrichment is consistent with the texture which shows the accumulation of biotite and plagioclase. The accumulation of plagioclase might be seen as inconsistent with the fact that the mafic layers have the deepest Eu anomaly. The mafic portions though have higher Eu concentration compared to the leucocratic portions, thus the deep Eu anomaly rises from the fact that zircon and monazite entrained in the source contain high concentration of REE adjacent to the Eu in the REE spectrum.

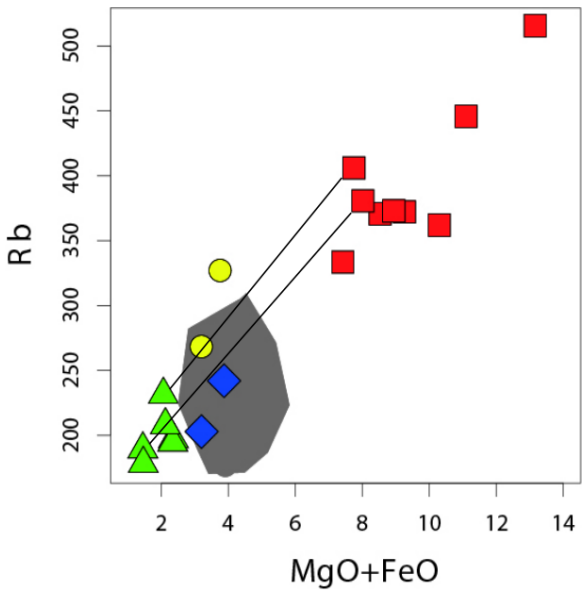

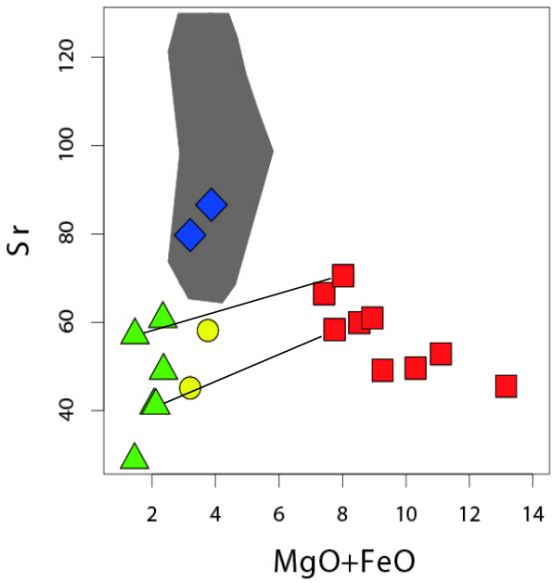

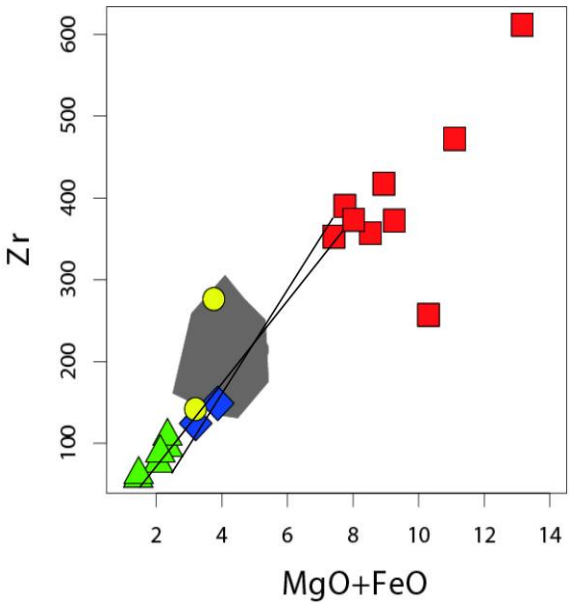

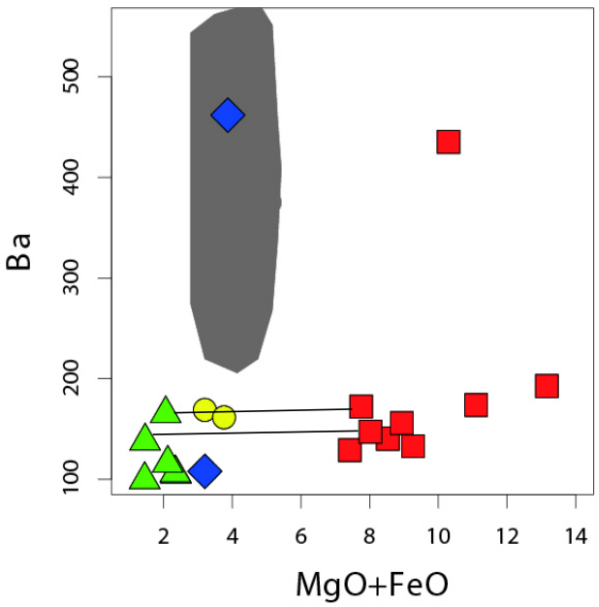

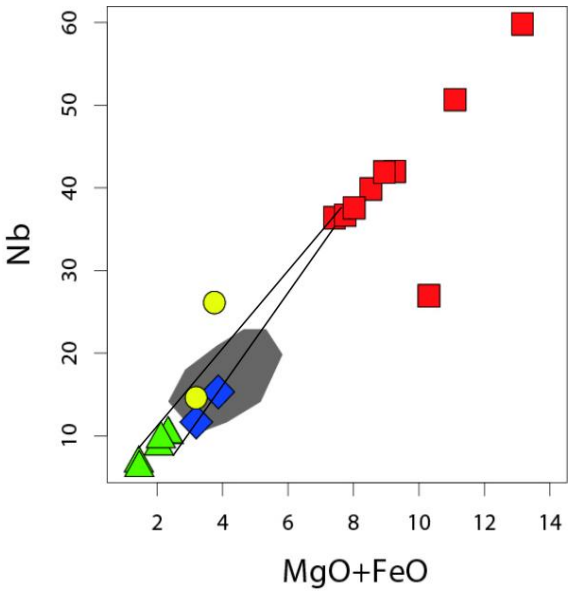

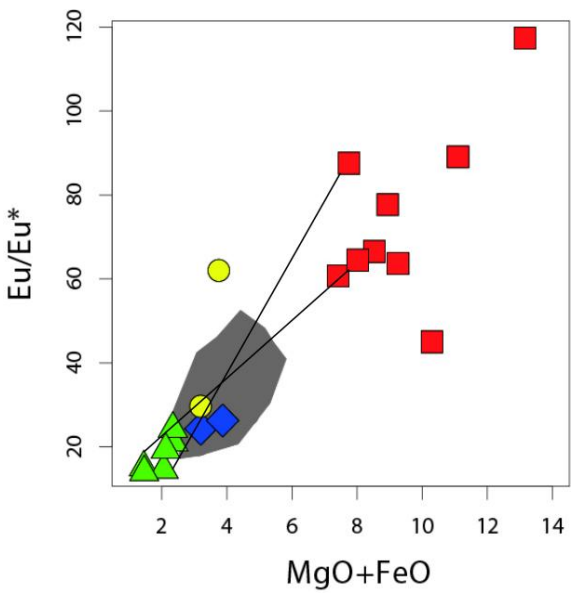

Fig. 12 Trace elements versus MgO + FeO variation diagrams for the layered rocks, Llandudno granodiorite and the Peninsula pluton. The green triangles represent the leucocratic portions, the red squares reflect the mafic portions, and the blue diamonds indicate the compositions of the Llandudno granodiorite samples, whilst the yellow circles reflect the compositions of the complete layers. The grey field represents the compositional range for the Peninsula pluton. The lines represent tie lines between samples that have a mafic portion and a leucocratic portion of the layers. These samples when combined represent a complete layer, indicated by yellow circles.

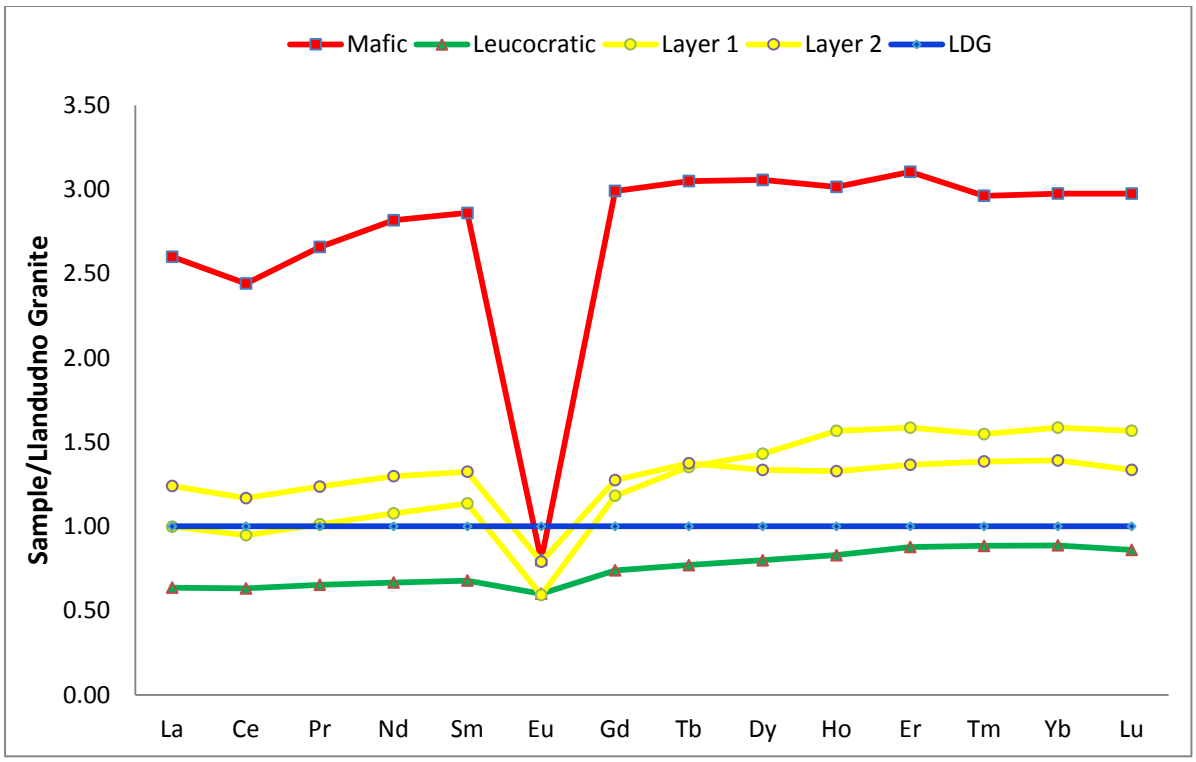

Fig. 13 REE-spider plots normalized to Llandudno granodiorite showing average patterns for the mafic portions (red) and leucocratic portions (green) of the layering as well as the two complete layers analysed (yellow) and an example of the Llandudno granodiorite (blue).

CHAPTER SIX

MINERAL CHEMISTRY

The mineral chemistry of biotite, plagioclase, K-feldspar and the trace element composition of monazite and apatite in the layering and in the granodiorite were analysed. These show some variability in the different layers and in the granites also.

Biotite

Biotites were analysed from the mafic and leucocratic portions of the layered rocks, Table. 2. The graphic representation of this data is illustrated in Fig. 14 for biotite in the mafic portions and Fig. 15 showing biotite in leucocratic portion of the layering. The matrix biotite with red-brown pleochroism was analysed. Biotite in the mafic portions displays a significant range of Mg# (34 to 44) (Fig. 14). Importantly, biotite Mg# in the mafic portions varies from layer to layer, whilst in the leucocratic portions Mg# variability is more limited (34 to 40) (Fig. 15) and the variation within layers is similar to that between layers. Biotites from the basal parts of the layered sequence show high Mg# (38-44) while in those from the top of the sequence show a low Mg# (34-36).

Table 2. Mineral chemistry of biotite in the mafic portions of the layers.

Sample Name		SiO_2	TiO_2	Al_2O_3	FeO	MnO	MgO	CaO	Na_2O	K_2O	Total	Si	Ti	Al	Fe	Mn	Mg	Na	K	Al VI	Mg#
LL1	1	37.03	3.64	19.39	19.19	0.39	7.11	0.07	0.21	8.97	96.02	5.56	0.41	3.43	2.41	0.05	1.59	0.06	1.72	0.99	0.43
	2	37.34	3.53	19.82	20.27	0.35	7.16	0.03	0.24	9.13	97.86	5.52	0.39	3.45	2.51	0.04	1.58	0.07	1.72	0.97	0.42
	3	36.83	3.88	18.99	19.82	0.40	7.36	0.04	0.26	8.75	96.32	5.53	0.44	3.36	2.49	0.05	1.65	0.07	1.68	0.89	0.43
	4	36.39	3.84	19.24	19.78	0.38	7.21	0.03	0.37	8.76	96.00	5.49	0.44	3.42	2.50	0.05	1.62	0.11	1.69	0.91	0.42
	5	37.29	4.03	19.33	19.53	0.34	7.51	0.01	0.32	8.88	97.23	5.53	0.45	3.38	2.42	0.04	1.66	0.09	1.68	0.91	0.44
	6	37.62	3.99	18.99	19.66	0.31	7.41	0.00	0.34	8.84	97.16	5.58	0.45	3.32	2.44	0.04	1.64	0.10	1.67	0.91	0.43
	7	37.49	4.34	20.00	19.34	0.40	6.68	0.06	0.26	9.35	97.93	5.52	0.48	3.47	2.38	0.05	1.47	0.07	1.76	0.99	0.41
	8	37.01	4.12	19.70	20.35	0.29	7.39	0.02	0.27	9.21	98.34	5.46	0.46	3.42	2.51	0.04	1.62	0.08	1.73	0.88	0.42
	9	37.75	4.10	18.95	19.69	0.30	7.63	0.00	0.15	9.00	97.56	5.57	0.46	3.30	2.43	0.04	1.68	0.04	1.69	0.87	0.44
LL3	1	36.18	4.88	17.83	21.88	0.19	7.29	0.03	0.21	9.01	97.49	5.44	0.55	3.16	2.75	0.02	1.63	0.06	1.73	0.60	0.40
	2	35.77	4.14	18.85	21.54	0.23	7.09	0.06	0.24	9.00	96.92	5.40	0.47	3.36	2.72	0.03	1.60	0.07	1.73	0.76	0.40
	3	36.08	4.84	18.20	21.87	0.32	6.99	0.13	0.24	8.95	97.62	5.42	0.55	3.22	2.75	0.04	1.57	0.07	1.72	0.64	0.39
	4	36.46	5.15	18.04	21.73	0.26	7.23	0.01	0.22	9.16	98.25	5.44	0.58	3.17	2.71	0.03	1.61	0.06	1.74	0.60	0.40
	5	36.06	5.14	18.07	22.14	0.38	7.05	0.05	0.17	8.98	98.04	5.40	0.58	3.19	2.77	0.05	1.57	0.05	1.72	0.59	0.39
	6	36.36	5.10	17.65	21.64	0.28	7.05	0.02	0.24	8.98	97.32	5.47	0.58	3.13	2.72	0.04	1.58	0.07	1.72	0.60	0.40
	7	36.87	5.20	17.60	22.01	0.22	7.09	0.00	0.26	8.99	98.23	5.50	0.58	3.09	2.74	0.03	1.58	0.07	1.71	0.59	0.39
	8	36.81	5.06	17.46	21.60	0.47	7.51	0.08	0.16	8.98	98.12	5.49	0.57	3.07	2.69	0.06	1.67	0.05	1.71	0.56	0.41
	9	36.07	4.38	18.76	21.65	0.37	7.18	0.07	0.24	9.10	97.83	5.40	0.49	3.31	2.71	0.05	1.60	0.07	1.74	0.71	0.40
LL6	1	35.17	3.76	19.20	22.79	0.54	6.11	0.01	0.19	9.51	97.29	5.35	0.43	3.44	2.90	0.07	1.38	0.05	1.85	0.79	0.35
	2	35.49	4.20	18.96	22.39	0.44	6.18	0.08	0.19	9.36	97.30	5.38	0.48	3.39	2.84	0.06	1.40	0.06	1.81	0.76	0.36
	3	35.62	4.08	18.66	22.47	0.41	6.29	0.06	0.26	9.29	97.14	5.41	0.47	3.34	2.85	0.05	1.42	0.08	1.80	0.75	0.36
	4	35.50	4.19	18.62	23.12	0.46	6.20	0.01	0.26	9.29	97.66	5.38	0.48	3.33	2.93	0.06	1.40	0.08	1.80	0.71	0.35
	5	35.48	4.30	18.47	22.61	0.48	6.17	0.05	0.22	9.38	97.15	5.40	0.49	3.31	2.88	0.06	1.40	0.07	1.82	0.71	0.36
	6	35.40	4.33	18.68	22.76	0.39	6.11	0.02	0.24	9.27	97.21	5.38	0.50	3.35	2.89	0.05	1.38	0.07	1.80	0.73	0.35
	7	35.25	4.30	18.71	22.68	0.47	6.28	0.08	0.25	9.33	97.36	5.35	0.49	3.35	2.88	0.06	1.42	0.07	1.81	0.70	0.36

	8	35.14	4.29	18.69	22.82	0.34	6.20	0.06	0.25	9.45	97.25	5.35	0.49	3.35	2.91	0.04	1.41	0.07	1.84	0.70	0.35
	9	34.83	4.22	18.68	23.50	0.45	5.87	0.04	0.20	9.61	97.40	5.32	0.49	3.36	3.00	0.06	1.34	0.06	1.87	0.68	0.34
LL13B	1	33.95	3.97	18.55	22.82	0.29	6.09	0.02	0.19	9.23	95.11	5.30	0.47	3.41	2.98	0.04	1.42	0.06	1.84	0.71	0.35
	2	34.37	3.73	18.54	22.71	0.46	6.32	0.06	0.22	9.06	95.46	5.33	0.43	3.39	2.95	0.06	1.46	0.07	1.79	0.72	0.36
	3	34.77	4.05	17.69	22.39	0.38	6.49	0.00	0.34	8.77	94.89	5.42	0.47	3.25	2.92	0.05	1.51	0.10	1.74	0.66	0.37
	4	34.09	3.93	18.23	22.86	0.27	6.24	0.03	0.28	8.87	94.80	5.33	0.46	3.36	2.99	0.04	1.45	0.09	1.77	0.69	0.36
	5	34.64	4.04	18.08	22.07	0.36	6.09	0.02	0.21	9.08	94.59	5.41	0.47	3.33	2.88	0.05	1.42	0.06	1.81	0.73	0.36
	6	35.05	4.08	18.18	22.08	0.29	6.47	0.02	0.25	9.07	95.49	5.41	0.47	3.31	2.85	0.04	1.49	0.07	1.79	0.72	0.37
	7	34.60	4.31	17.63	22.45	0.33	6.39	0.04	0.30	8.81	94.86	5.39	0.51	3.24	2.93	0.04	1.49	0.09	1.75	0.64	0.37
	8	34.16	3.64	18.64	22.76	0.30	6.13	0.05	0.16	9.06	94.89	5.33	0.43	3.43	2.97	0.04	1.43	0.05	1.80	0.76	0.35
	9	34.51	4.42	18.07	23.96	0.35	6.35	0.05	0.28	9.09	97.08	5.30	0.51	3.27	3.08	0.05	1.45	0.08	1.78	0.57	0.35

Table 3. Mineral chemistry of biotite in the leucocratic portions of the layers.

Sample Name		SiO_2	TiO_2	Al_2O_3	FeO	MnO	MgO	CaO	Na_2O	K_2O	Total	Si	Ti	Al	Fe	Mn	Mg	Na	K	Al IV	Al VI	Mg#
LL6	1	35.23	4.18	18.80	22.87	0.49	6.17	0.00	0.26	9.25	97.24	5.36	0.48	3.37	2.91	0.06	1.40	0.08	1.79	2.64	0.73	0.35
	2	34.57	4.24	18.01	24.27	0.44	6.33	0.08	0.16	9.02	97.11	5.31	0.49	3.26	3.12	0.06	1.45	0.05	1.77	2.69	0.57	0.35
	3	36.08	4.36	18.02	22.97	0.55	6.73	0.06	0.14	9.26	98.17	5.43	0.49	3.19	2.89	0.07	1.51	0.04	1.78	2.57	0.62	0.37
	4	35.82	4.40	18.24	23.19	0.52	6.41	0.05	0.23	9.23	98.10	5.40	0.50	3.24	2.93	0.07	1.44	0.07	1.78	2.60	0.65	0.36
	5	35.33	4.30	18.33	23.02	0.39	6.53	0.01	0.23	9.14	97.29	5.37	0.49	3.29	2.93	0.05	1.48	0.07	1.77	2.63	0.66	0.36
	6	34.99	4.39	18.12	23.93	0.49	6.56	0.01	0.18	9.04	97.70	5.32	0.50	3.25	3.04	0.06	1.49	0.05	1.76	2.68	0.57	0.36
	7	35.54	4.27	18.70	23.06	0.40	6.26	0.08	0.26	9.35	97.91	5.37	0.49	3.33	2.91	0.05	1.41	0.08	1.80	2.63	0.70	0.35
	8	34.90	4.36	18.31	23.94	0.44	6.15	0.05	0.11	9.06	97.31	5.33	0.50	3.29	3.06	0.06	1.40	0.03	1.76	2.67	0.62	0.34
	9	35.96	4.21	18.54	22.93	0.29	6.49	0.10	0.33	9.09	97.94	5.42	0.48	3.29	2.89	0.04	1.46	0.10	1.75	2.58	0.71	0.36
LL9	1	34.98	3.75	19.01	22.47	0.52	6.28	0.16	0.24	9.27	96.68	5.35	0.43	3.43	2.87	0.07	1.43	0.07	1.81	2.65	0.77	0.36
	2	35.21	4.15	18.89	22.80	0.39	6.00	0.07	0.17	9.13	96.80	5.37	0.48	3.39	2.91	0.05	1.36	0.05	1.78	2.63	0.76	0.35
	3	35.11	4.09	18.90	23.52	0.54	6.20	0.09	0.15	9.17	97.77	5.32	0.47	3.38	2.98	0.07	1.40	0.04	1.77	2.68	0.70	0.35

	4	34.78	3.99	18.75	22.90	0.59	5.88	0.10	0.24	9.29	96.51	5.34	0.46	3.40	2.94	0.08	1.35	0.07	1.82	2.66	0.74	0.34
	5	35.08	4.01	19.05	23.01	0.41	5.98	0.09	0.13	9.16	96.91	5.35	0.46	3.42	2.93	0.05	1.36	0.04	1.78	2.65	0.77	0.34
	6	35.05	4.14	18.88	22.70	0.51	6.09	0.01	0.12	9.30	96.81	5.35	0.48	3.40	2.90	0.07	1.39	0.04	1.81	2.65	0.75	0.35
	7	35.38	4.05	18.98	22.85	0.41	6.12	0.02	0.25	9.26	97.31	5.37	0.46	3.40	2.90	0.05	1.38	0.07	1.79	2.63	0.77	0.35
	8	35.05	4.01	18.84	22.74	0.46	6.31	0.04	0.25	8.89	96.59	5.36	0.46	3.39	2.91	0.06	1.44	0.07	1.73	2.64	0.75	0.36
	9	35.50	3.24	19.37	23.31	0.32	6.30	0.05	0.18	8.74	97.01	5.39	0.37	3.47	2.96	0.04	1.43	0.05	1.69	2.61	0.86	0.35
LL11A	1	35.98	4.10	19.10	22.76	0.48	6.42	0.07	0.20	9.07	98.19	5.39	0.46	3.37	2.85	0.06	1.44	0.06	1.73	2.61	0.77	0.36
	2	35.23	4.09	18.95	22.79	0.39	6.24	0.07	0.16	9.17	97.09	5.36	0.47	3.39	2.90	0.05	1.41	0.05	1.78	2.64	0.75	0.36
	3	35.93	3.99	18.66	22.48	0.33	6.55	0.00	0.30	9.32	97.56	5.43	0.45	3.32	2.84	0.04	1.47	0.09	1.80	2.57	0.75	0.37
	4	35.50	4.25	18.59	22.52	0.37	6.37	0.00	0.32	9.13	97.04	5.40	0.49	3.33	2.86	0.05	1.44	0.09	1.77	2.60	0.73	0.36
	5	35.72	4.24	18.83	22.05	0.46	6.52	0.09	0.23	9.15	97.29	5.40	0.48	3.35	2.79	0.06	1.47	0.07	1.76	2.60	0.75	0.37
	6	35.94	4.37	18.74	22.71	0.25	6.54	0.02	0.25	8.98	97.81	5.41	0.49	3.32	2.86	0.03	1.47	0.07	1.72	2.59	0.73	0.37
	7	35.75	4.30	18.71	22.86	0.53	6.73	0.09	0.27	8.99	98.24	5.37	0.49	3.31	2.87	0.07	1.51	0.08	1.72	2.63	0.68	0.37
	8	35.45	4.27	18.52	22.44	0.37	6.69	0.09	0.26	8.91	97.00	5.38	0.49	3.31	2.85	0.05	1.51	0.08	1.73	2.62	0.70	0.38
	9	35.28	4.08	18.94	23.05	0.49	6.45	0.10	0.27	9.04	97.70	5.34	0.46	3.38	2.92	0.06	1.45	0.08	1.75	2.66	0.72	0.36
LL13A	1	34.85	4.15	17.82	22.25	0.46	6.79	0.05	0.27	8.82	95.47	5.39	0.48	3.25	2.88	0.06	1.57	0.08	1.74	2.61	0.64	0.38
	2	34.63	4.28	17.95	21.41	0.48	6.78	0.04	0.25	9.00	94.82	5.38	0.50	3.29	2.78	0.06	1.57	0.07	1.78	2.62	0.67	0.39
	3	34.96	3.81	18.25	21.59	0.41	6.54	0.06	0.21	9.02	94.86	5.42	0.44	3.33	2.80	0.05	1.51	0.06	1.79	2.58	0.75	0.38
	4	34.70	3.74	18.71	21.89	0.35	6.55	0.03	0.17	9.06	95.20	5.37	0.43	3.41	2.83	0.05	1.51	0.05	1.79	2.63	0.77	0.38
	5	33.62	3.73	18.54	21.95	0.44	6.35	0.00	0.13	8.96	93.72	5.30	0.44	3.45	2.89	0.06	1.49	0.04	1.80	2.70	0.75	0.37
	6	35.46	3.69	18.43	21.57	0.46	6.27	0.03	0.22	9.02	95.15	5.47	0.43	3.35	2.78	0.06	1.44	0.07	1.78	2.53	0.82	0.37
	7	34.87	4.00	18.28	21.75	0.50	6.13	0.02	0.22	8.90	94.67	5.42	0.47	3.35	2.83	0.07	1.42	0.07	1.77	2.58	0.77	0.36
	8	34.77	3.45	19.03	21.79	0.21	6.29	0.00	0.29	8.95	94.79	5.39	0.40	3.48	2.83	0.03	1.45	0.09	1.77	2.61	0.87	0.37
	9	34.38	3.73	18.73	22.04	0.57	5.93	0.09	0.18	9.11	94.76	5.36	0.44	3.44	2.87	0.08	1.38	0.06	1.81	2.64	0.80	0.35

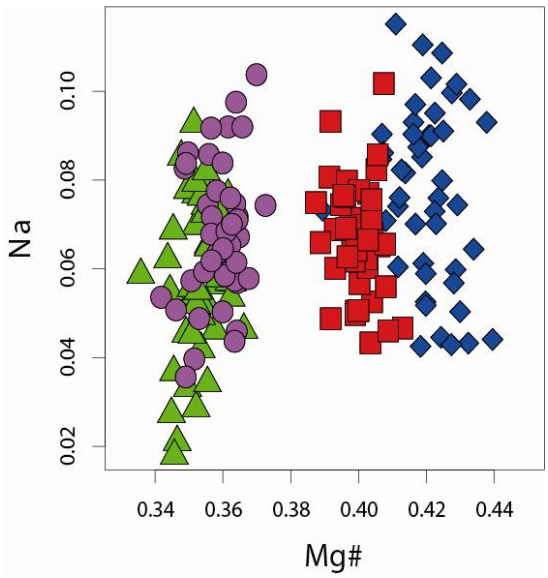

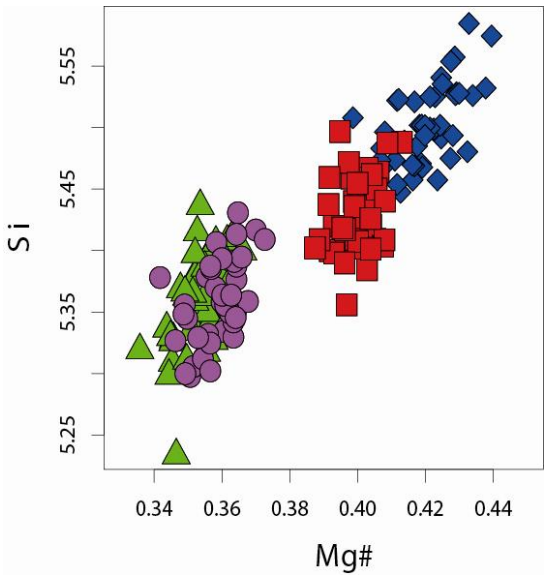

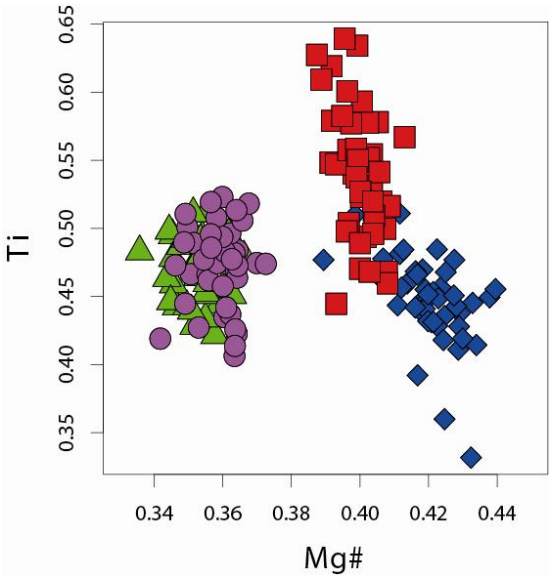

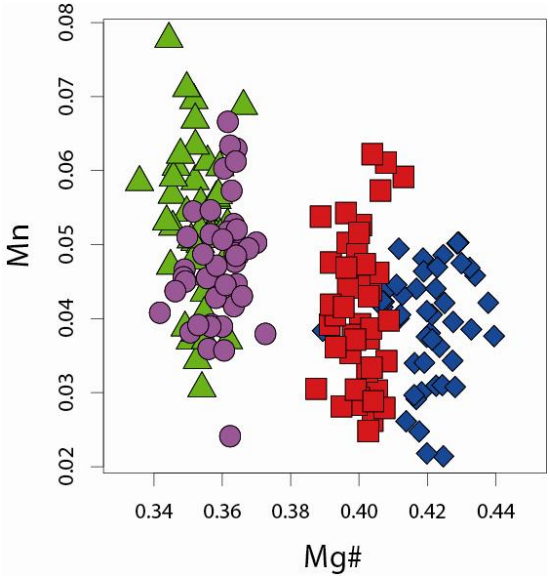

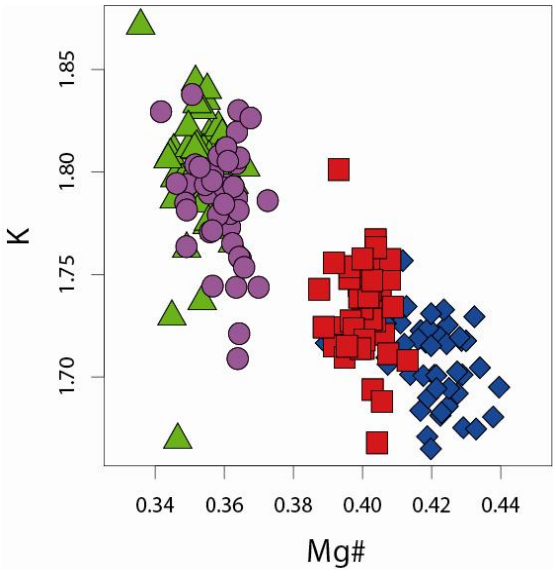

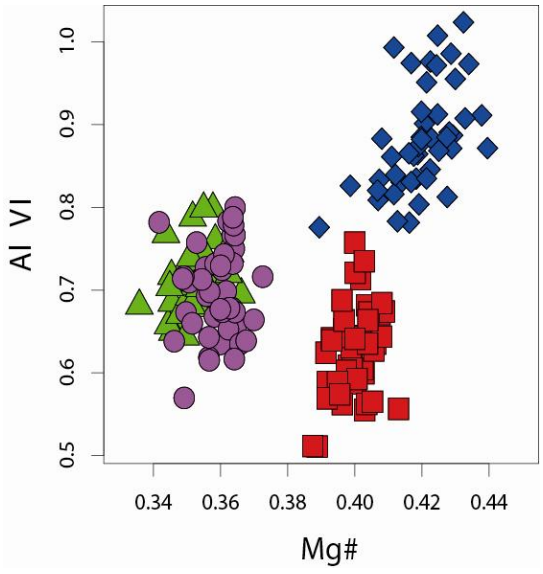

Fig. 14 The biotite composition from the mafic portions of layers plotted as mineral structural formula parameters against the Mg#. The blue diamonds represent LL1, the red square represents LL3, the green triangles represent LL6 and the purple filled circles represent LL13B.

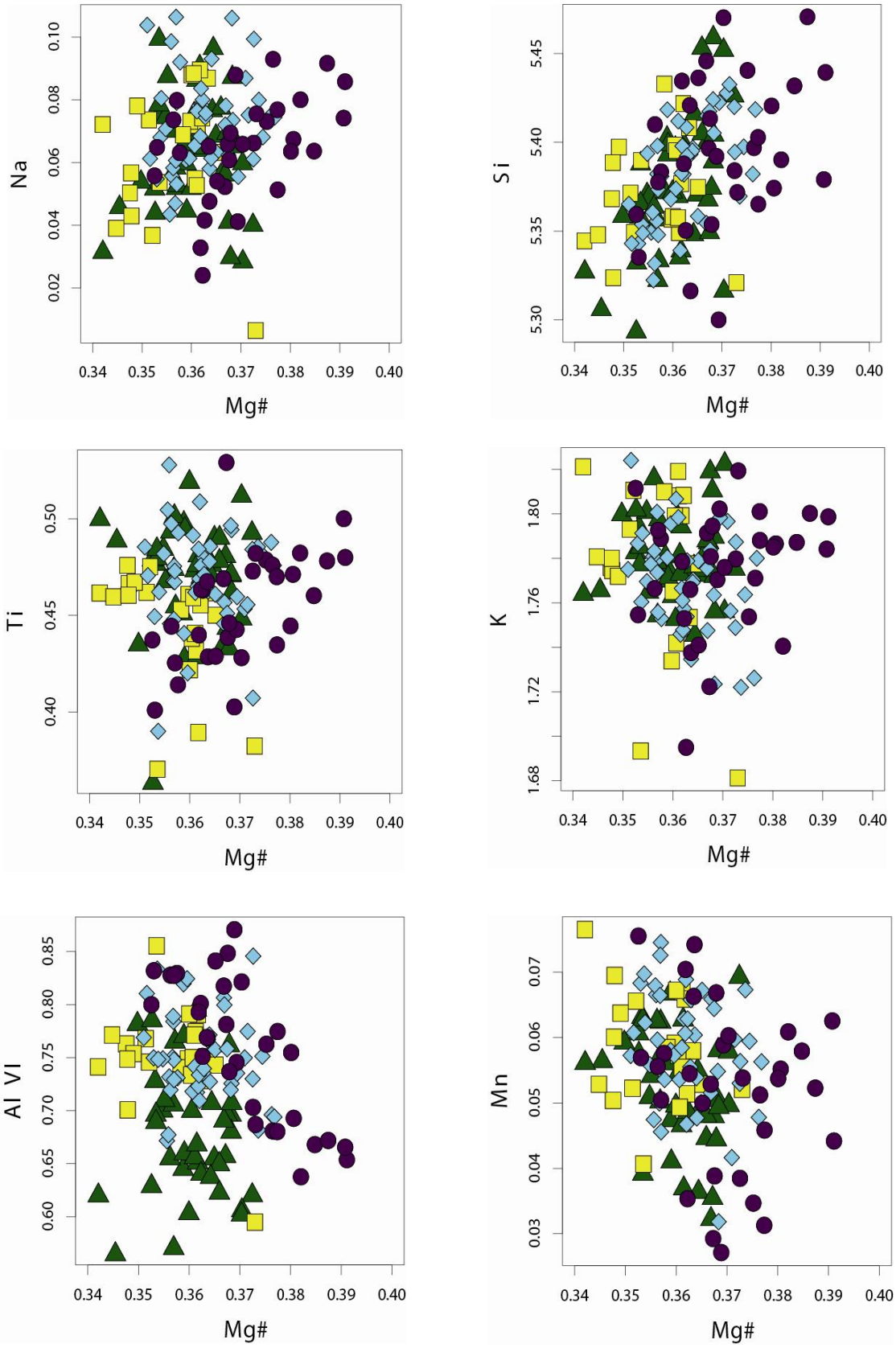

Fig. 15 The composition of biotite within the leucocratic portions of layers plotted as a function of Mg#. The green triangles represent LL6, purple circles represent LL13, the blue diamonds represent LL11 and the yellow squares represent LL9.

Plagioclase

Plagioclase was analyzed from the layered rocks and data is presented in Table. 3. Plagioclase crystals are euhedral, and reach up to 1 cm in length and crystals analysed display oscillatory zoning. This zonation is indicated in the chemical maps in Fig. 16 and 17. It is clear from the Fig. 16&17B that the crystals are rimmed with an albitic mantle. This is evident in the analyses done as the data show that the rim is Ab-rich while the core is An-rich. Plagioclase in both mafic and leucocratic portions of layers displays no significant difference in the range of compositions recorded, yet within each rock type range in composition is substantial (Figure 18&19). Similarly, plagioclase compositions between different layers overlap in terms of An/Ab ratio. Anorthite in different layers ranges from An_1 to An_{36} and albite ranges from Ab_{64}- Ab_{96}. This is applicable in both mafic and leucocratic portions. Despite the fact that the ranges in plagioclase compositions within the leucocratic and mafic portions are very similar, the differences in bulk rock Na_2O: CaO ratio between these rocks dictates that average plagioclase in the mafic layers is considerably more anorthitic than average plagioclase in the leucocratic portions.

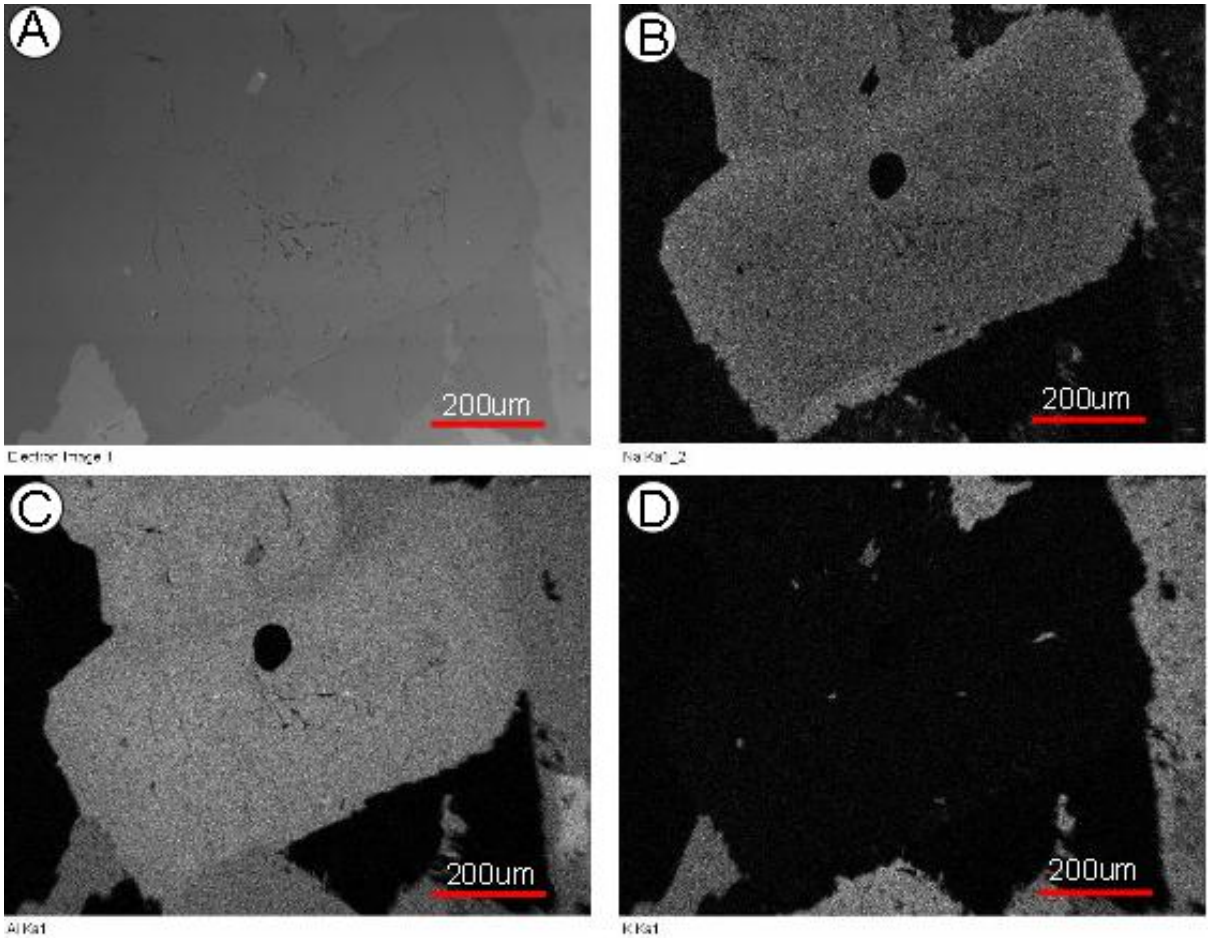

Fig. 16 Chemical maps for plagioclase showing zonation in the mafic portions of the layering. (A) Electron image of the mapped crystal. (B) Na. (C) Al. (D) K.

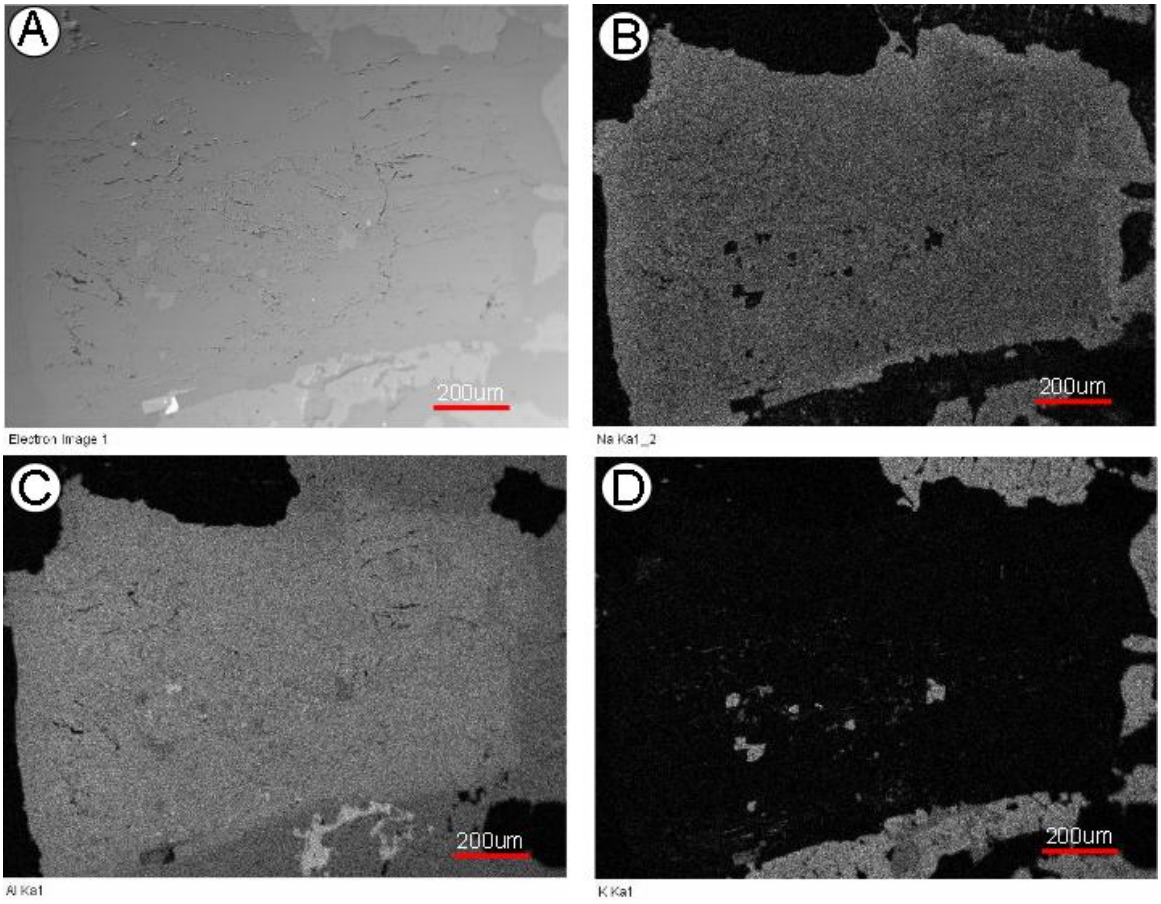

Fig. 17 Chemical maps for plagioclase showing zonation in the leucocratic portion of the layering. (A) Electron image of the crystal. (B) Na. (C) Al. (D) K.

Table 4. Representative data for plagioclase in the mafic portions of the layering.

Sample Name		SiO_2	Al_2O_3	CaO	Na_2O	K_2O	Total	Si	Al	Ca	Na	K	An	Ab	Or
LL1	1	62.00	24.03	5.97	8.08	0.29	100.38	2.74	1.25	0.28	0.69	0.02	0.28	0.70	0.02
	2	62.38	23.43	5.00	8.51	0.21	99.54	2.77	1.23	0.24	0.73	0.01	0.24	0.75	0.01
	3	59.71	24.88	6.95	7.43	0.22	99.19	2.68	1.32	0.33	0.65	0.01	0.34	0.65	0.01
	4	63.97	22.44	4.12	9.20	0.30	100.03	2.83	1.17	0.20	0.79	0.02	0.20	0.79	0.02
	5	62.74	22.29	4.08	9.05	0.28	98.69	2.82	1.18	0.20	0.79	0.02	0.20	0.79	0.02
	6	62.77	23.37	5.14	8.61	0.27	100.17	2.78	1.22	0.24	0.74	0.02	0.24	0.74	0.02
	7	63.82	23.03	4.52	8.87	0.31	100.55	2.81	1.19	0.21	0.76	0.02	0.22	0.77	0.02
	8	60.72	24.84	6.74	7.60	0.24	100.13	2.70	1.30	0.32	0.65	0.01	0.32	0.66	0.01
	9	60.90	24.76	6.80	7.59	0.20	100.25	2.70	1.29	0.32	0.65	0.01	0.33	0.66	0.01
LL3	1	59.08	25.34	6.55	7.66	0.16	98.81	2.66	1.35	0.32	0.67	0.01	0.32	0.67	0.01
	2	58.97	25.17	6.51	7.59	0.24	98.58	2.67	1.34	0.32	0.67	0.01	0.32	0.67	0.01
	3	60.56	25.33	6.43	7.72	0.39	100.49	2.68	1.32	0.31	0.66	0.02	0.31	0.67	0.02
	4	67.92	19.67	0.36	11.49	0.11	99.73	2.98	1.02	0.02	0.98	0.01	0.02	0.98	0.01
	5	60.06	24.73	6.04	7.82	0.29	99.05	2.70	1.31	0.29	0.68	0.02	0.29	0.69	0.02
	6	61.36	24.59	5.93	8.17	0.34	100.39	2.72	1.28	0.28	0.70	0.02	0.28	0.70	0.02
	7	64.55	22.29	3.05	9.90	0.20	100.04	2.85	1.16	0.14	0.85	0.01	0.14	0.85	0.01
	8	64.92	22.31	3.06	9.95	0.20	100.44	2.85	1.15	0.14	0.85	0.01	0.14	0.85	0.01
	9	64.25	22.34	3.15	9.57	0.19	99.53	2.84	1.16	0.15	0.82	0.01	0.15	0.84	0.01

LL13B	1	58.54	25.70	7.38	7.10	0.34	99.11	2.64	1.36	0.36	0.62	0.02	0.36	0.62	0.02
	2	59.58	25.15	6.68	7.60	0.34	99.41	2.67	1.33	0.32	0.66	0.02	0.32	0.66	0.02
	3	60.72	24.36	6.02	8.04	0.24	99.41	2.72	1.28	0.29	0.70	0.01	0.29	0.70	0.01
	4	60.36	24.55	5.88	8.06	0.32	99.26	2.71	1.30	0.28	0.70	0.02	0.28	0.70	0.02
	5	59.11	25.29	6.82	7.55	0.17	99.04	2.66	1.34	0.33	0.66	0.01	0.33	0.66	0.01
	6	59.34	25.40	6.71	7.59	0.19	99.28	2.66	1.34	0.32	0.66	0.01	0.32	0.66	0.01
	7	59.54	25.14	6.55	7.57	0.20	99.15	2.68	1.33	0.32	0.66	0.01	0.32	0.67	0.01
	8	64.08	21.84	3.16	9.81	0.17	99.10	2.85	1.15	0.15	0.85	0.01	0.15	0.84	0.01
	9	65.96	20.73	1.62	10.38	0.22	99.07	2.92	1.08	0.08	0.89	0.01	0.08	0.91	0.01

Table 5. Representative data for plagioclase in the leucocratic portions of the layering.

Sample Name		**SiO_2**	**Al_2O_3**	**CaO**	**Na_2O**	**K_2O**	**Total**	**Si**	**Al**	**Ca**	**Na**	**K**	**An**	**Ab**	**Or**
LL6	1	63.11	22.88	3.80	9.26	0.28	99.38	2.81	1.20	0.18	0.80	0.02	0.18	0.80	0.02
	2	61.31	24.62	5.66	8.28	0.26	100.14	2.72	1.29	0.27	0.71	0.01	0.27	0.72	0.01
	3	61.22	24.63	5.78	8.16	0.32	100.11	2.72	1.29	0.27	0.70	0.02	0.28	0.71	0.02
	4	59.28	25.91	7.18	7.28	0.25	99.94	2.65	1.36	0.34	0.63	0.01	0.35	0.64	0.01
	5	63.30	23.07	3.95	9.13	0.42	99.98	2.80	1.20	0.19	0.78	0.02	0.19	0.79	0.02
	6	61.37	24.03	5.23	8.39	0.33	99.35	2.74	1.26	0.25	0.73	0.02	0.25	0.73	0.02
	7	59.98	25.46	6.64	7.54	0.31	99.92	2.67	1.34	0.32	0.65	0.02	0.32	0.66	0.02
	8	59.53	25.62	7.01	7.39	0.29	99.94	2.66	1.35	0.34	0.64	0.02	0.34	0.65	0.02
	9	59.55	25.60	6.97	7.65	0.12	99.89	2.66	1.35	0.33	0.66	0.01	0.33	0.66	0.01
	10	59.52	25.56	7.14	7.33	0.27	99.94	2.66	1.35	0.34	0.63	0.02	0.34	0.64	0.02
LL9	1	61.05	24.46	5.66	8.16	0.33	99.67	2.72	1.28	0.27	0.71	0.02	0.27	0.71	0.02
	2	61.71	23.53	4.81	8.60	0.34	99.08	2.76	1.24	0.23	0.75	0.02	0.23	0.75	0.02
	3	62.72	23.37	4.44	8.94	0.36	99.83	2.78	1.22	0.21	0.77	0.02	0.21	0.77	0.02
	4	66.29	20.99	1.83	10.70	0.22	100.03	2.91	1.09	0.09	0.91	0.01	0.09	0.90	0.01
	5	67.52	20.11	0.66	11.17	0.17	99.75	2.96	1.04	0.03	0.95	0.01	0.03	0.96	0.01
	6	65.76	21.55	2.30	10.30	0.27	100.23	2.89	1.12	0.11	0.88	0.02	0.11	0.88	0.02
	7	62.15	23.72	4.77	8.76	0.28	99.67	2.76	1.24	0.23	0.75	0.02	0.23	0.76	0.02
	8	60.51	24.61	6.06	7.95	0.28	99.52	2.71	1.30	0.29	0.69	0.02	0.29	0.69	0.02
	9	60.70	24.53	6.05	7.92	0.30	99.51	2.71	1.29	0.29	0.69	0.02	0.29	0.69	0.02
	10	60.05	24.94	6.49	7.78	0.20	99.52	2.69	1.31	0.31	0.68	0.01	0.31	0.68	0.01
LL11A	1	65.95	20.88	1.53	10.66	0.34	99.46	2.91	1.09	0.07	0.91	0.02	0.07	0.91	0.02
	2	65.84	20.68	1.47	10.81	0.27	99.11	2.92	1.08	0.07	0.93	0.02	0.07	0.92	0.02
	3	66.17	21.00	1.60	10.83	0.34	100.04	2.91	1.09	0.08	0.92	0.02	0.07	0.91	0.02
	4	65.79	21.31	1.99	10.47	0.50	100.06	2.89	1.10	0.09	0.89	0.03	0.09	0.88	0.03
	5	65.03	21.34	2.20	10.01	0.42	99.04	2.89	1.12	0.10	0.86	0.02	0.11	0.87	0.02
	6	60.18	24.52	5.80	7.99	0.22	98.70	2.71	1.30	0.28	0.70	0.01	0.28	0.70	0.01
	7	59.53	25.08	6.55	7.69	0.14	99.10	2.68	1.33	0.32	0.67	0.01	0.32	0.67	0.01
	8	60.77	24.93	5.81	8.11	0.29	99.95	2.70	1.31	0.28	0.70	0.02	0.28	0.70	0.02
	9	60.86	24.88	6.08	8.08	0.23	100.18	2.70	1.30	0.29	0.70	0.01	0.29	0.70	0.01
	10	59.29	25.61	6.94	7.39	0.20	99.43	2.66	1.35	0.33	0.64	0.01	0.34	0.65	0.01

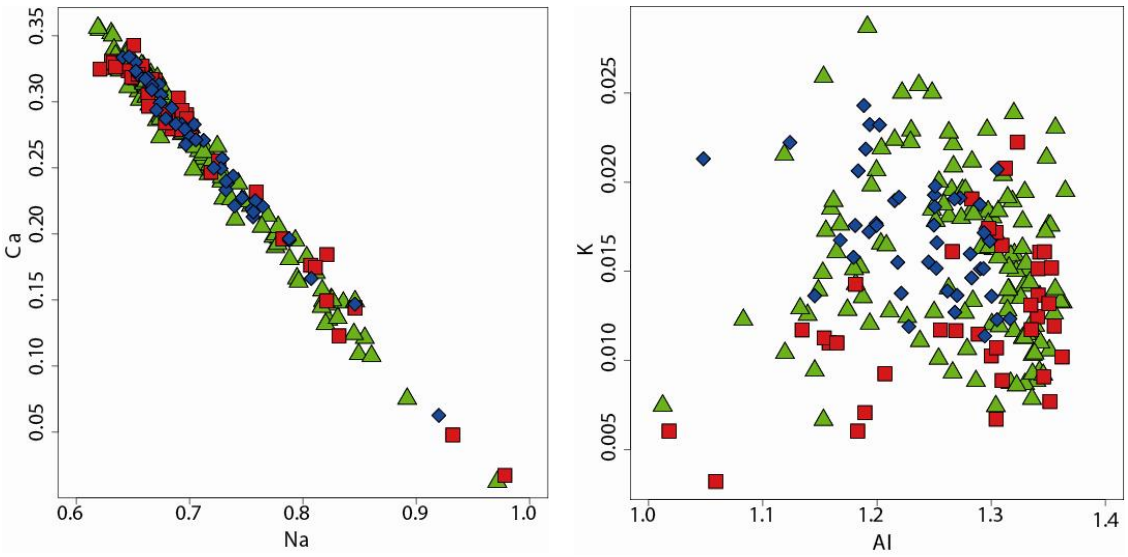

Fig. 18 Harker diagrams displaying elements Ca/Na and K/Al in the plagioclase in the mafic portions. The blue diamonds represent LL1, the red squares represent LL3 and the green triangles represent LL13B.

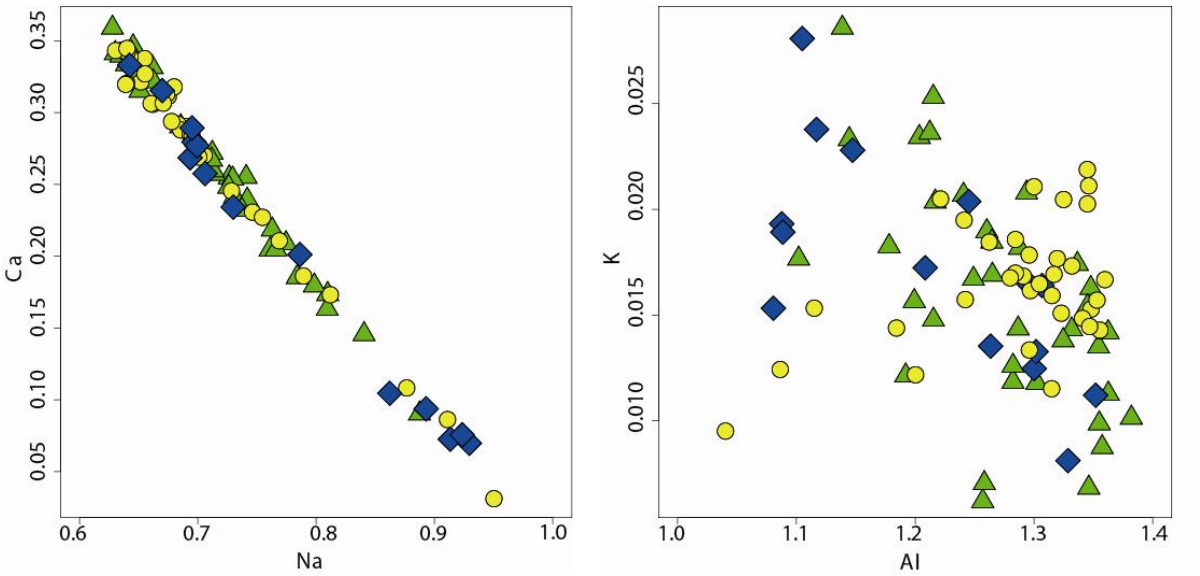

Fig. 19 Harker diagrams displaying elements Ca/Na and K/Al in the plagioclase in the leucocratic portions of the layers.

K-feldspar chemistry

K-feldspar megacrysts from the layering and Llandudno granodiorite was analyzed. The data for the analysis is presented in appendices 3. K-feldspar megacrysts that are abundant in the Llandudno granodiorite are also present in the layering, though in much lower abundance.

This megacrysts are limited to a few layers within the whole layered sequence. From the data analyzed, K-feldspar megacrysts are enriched in Ba, Rb, Sr and Pb. The REE patterns for trace elements in K-feldspar megacrysts were normalized to Llandudno granodiorite, and indicated in Fig. 20 and 21. These patterns for the layered zones and the Llandudno granodiorite do not show any significant difference; in fact they are quite similar. This data confirms with our conclusion that megacrysts in the layering and the Llandudno granodiorite are similar. Furthermore, Sr and Eu anomaly were plotted against distance of the crystals from the rim to the rim. The diagrams shown in Fig. 22 indicate that the megacrysts crystals in the layering and the Llandudno granodiorite are zoned, and that the patterns for all this plots ranges mostly to 1 for both megacrysts in layering and Llandudno granodiorite. From this, we can further argue that our earlier conclusion in fact is consistent with the data.

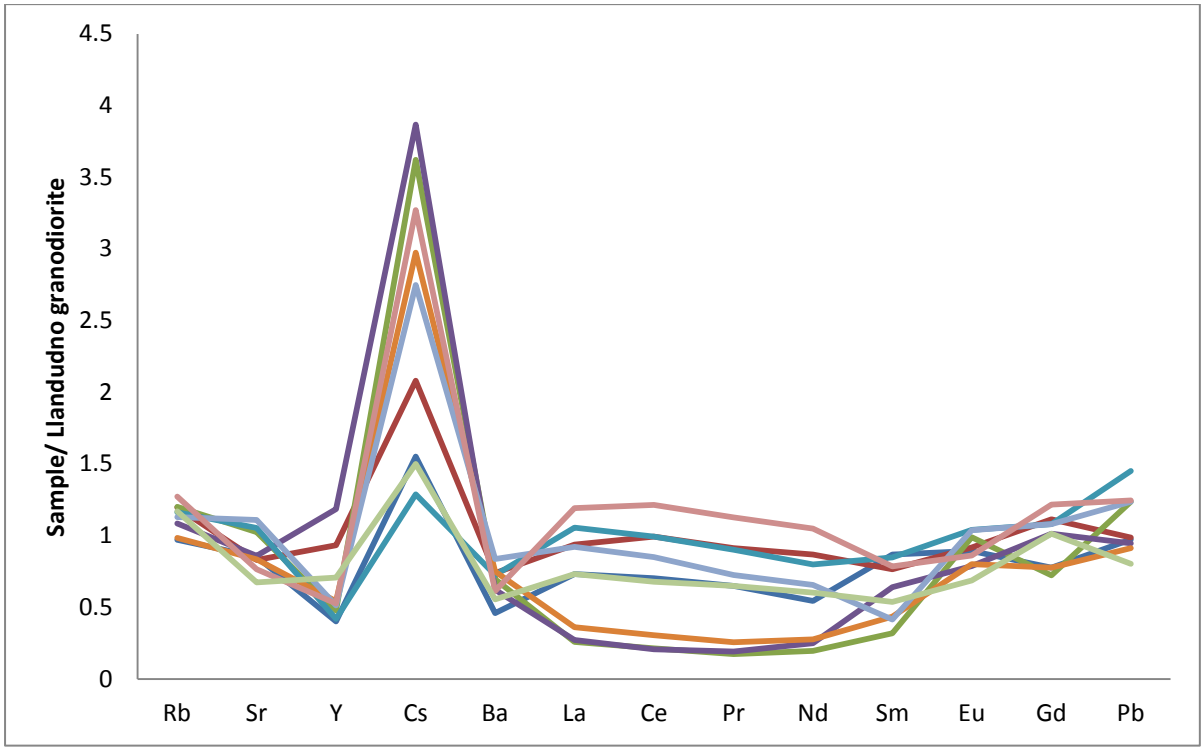

Fig. 20 Rare earth elements in K-feldspar from the layering normalized to Llandudno granodiorite.

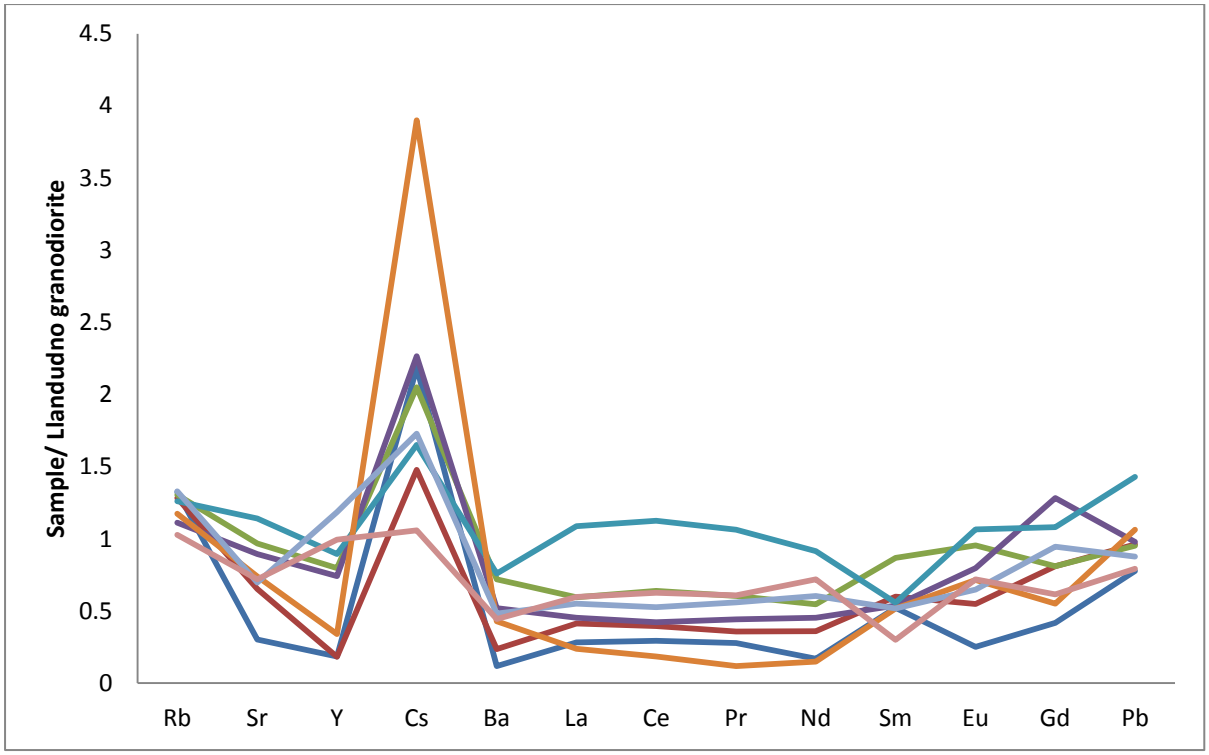

Fig. 21 Rare earth elements in K-feldspar from the Llandudno granodiorite normalized to Llandudno granodiorite.

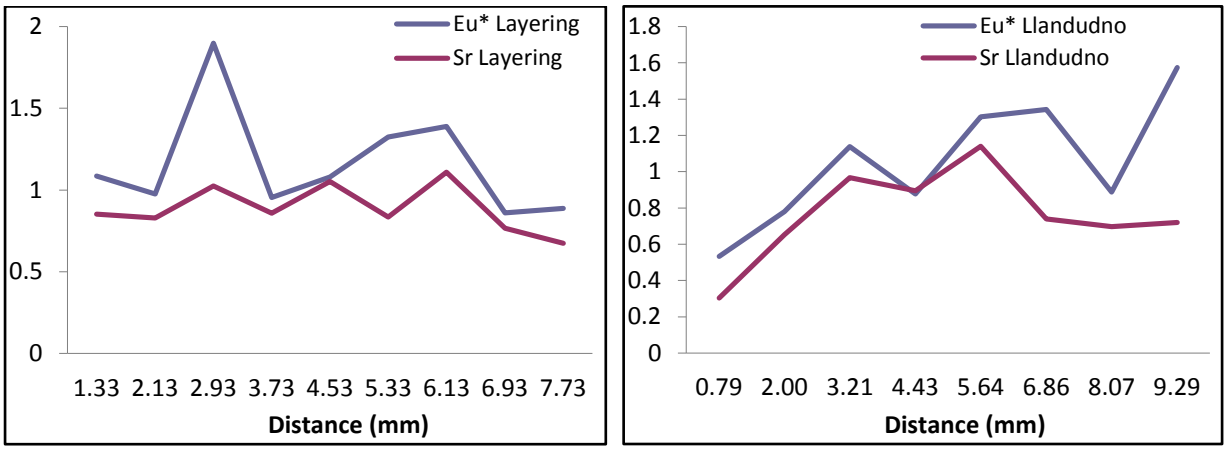

Fig. 22 Zonation diagrams of Eu* and Sr anomaly in the K-feldspar megacrysts in the layering and the Llandudno granodiorite.

Apatite chemistry

The REE patterns in the apatite in all the rocks are essentially flat, or upwardly convex in linear-scale plots (Fig. 23). They show very pronounced negative Eu anomalies, with Nd also showing a slight negative anomaly. The relatively flat slopes of the pattern probably reflect

crystallisation of other accessory phases such as monazite and zircon. The enrichment of the HREEs may be due to the few HREE-rich accessory phases that are competing for these elements in the melts as apatite crystallise. Known minerals such as amphibole and xenotime that concentrate the HREEs are not present in this rocks; zircon which occur as peritectic entrained phases is lesser of competition in concentrating HREE. In this case the Eu anomaly is interpreted to be as a result of enrichment of other elements relative to Eu due to co-entrainment of zircon and monazite, since there is accumulation of plagioclase in both the mafic and leucocratic portions of the layering.

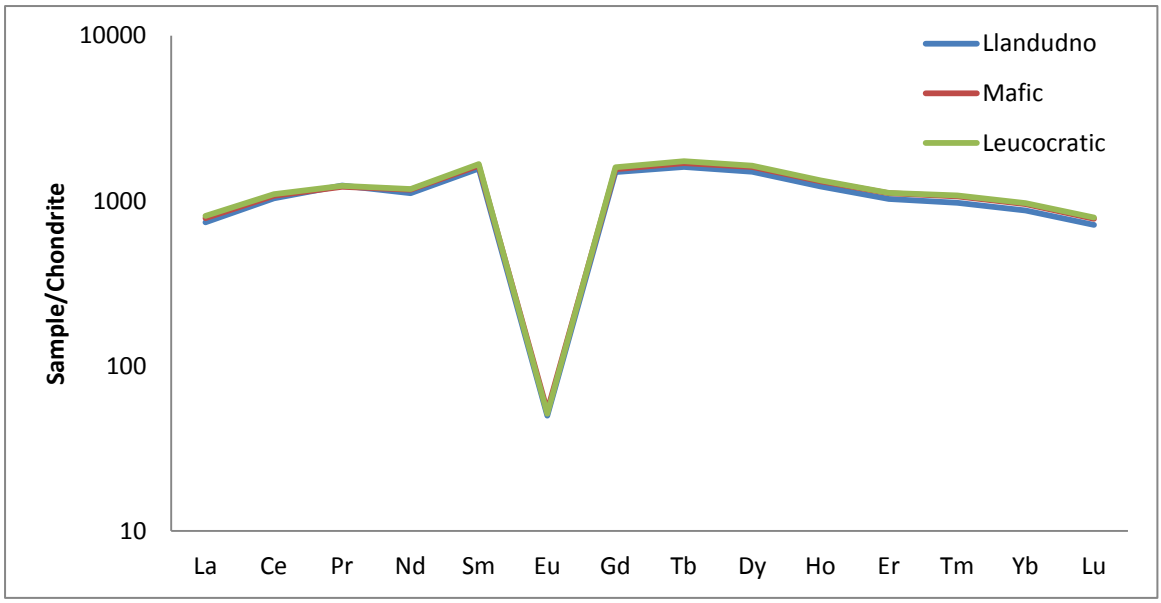

Fig. 23 Rare earth elements patterns of apatite in the Llandudno granodiorite, mafic layers and leucocratic layers.

Monazite chemistry

Monazite REE patterns for mafic, leucocratic and Llandudno granodiorite are significantly similar (Fig. 24). These display enrichment in LREEs and depletion in HREEs and characterised also as in the case of apatite with a pronounced negative Eu anomaly. The HREEs are more compatible in apatite and zircon than monazite thus the depletion in monazite and enrichment in apatite. The lack of monazite xenocrysts in the rocks indicate that during partial melting, entrained monazite had sufficient time to dissolve. As a result of this the melt is rich in LREEs, making it possible for the crystallising monazite to be highly enriched in LREEs.

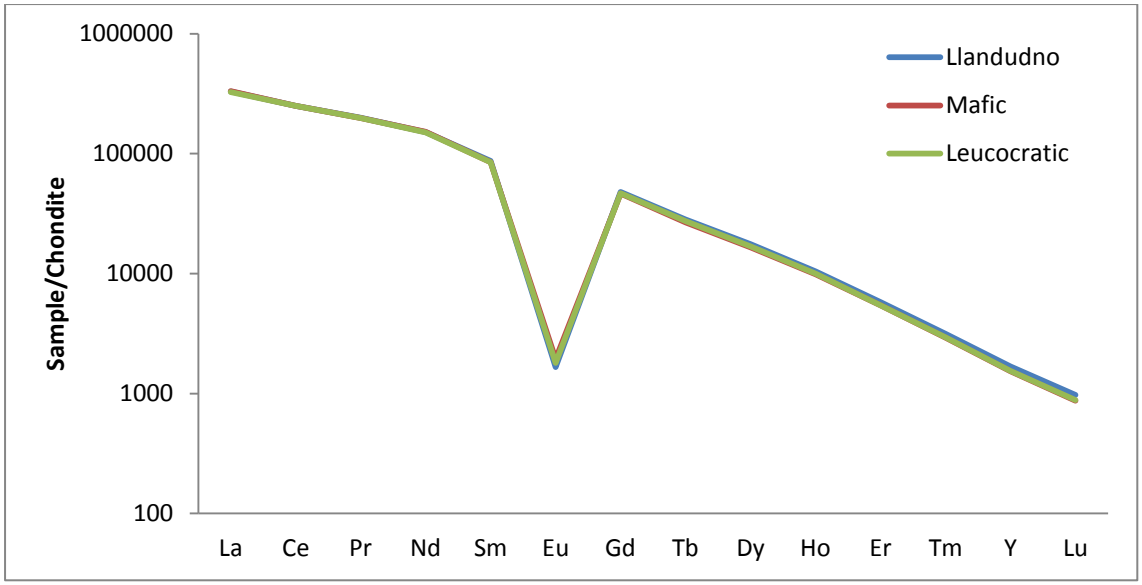

Fig. 24 Monazite rare earth elements patterns of the Llandudno granodiorite, mafic layer and leucocratic layer.

CHAPTER SEVEN

DISCUSSION

Layering is much less prevalent in granitic intrusions than in mafic rocks, although it is reported from some felsic plutons worldwide. This less common occurrence of layering in felsic plutons is generally attributed to the high viscosity of siliceous magmas compared to low viscosity of the mafic magmas (Urbain et al., 1982). The high viscosity suppresses many processes believed to be partially responsible for producing layering in mafic rocks. These include crystal settling, high convection rates, and rapid chemical and thermal diffusion, each of which is promoted by low viscosity (Rockhold et al., 1987). Glazner et al., (2004) has recently focussed attention on the fact that it is very probable that granitic rocks undergo textural modification during and possibly even following their crystallization. The reason for this is the likely common construction of sizable granite magma bodies from many small magma batches intruded over a significant time interval (Glazner et al., 2004). The frequent new arrival of magma serves to keep the magma body above its solidus for protracted periods of time (Petford et al., 2000; Matzel et al., 2006).

In the case of the Peninsula pluton there is considerable evidence to support the modification of early formed rock textures as the magma system matured. Magmatic enclaves found in the Peninsula pluton are also present in the Llandudno granodiorite. These enclaves are characterised by a finer grained matrix than the Llandudno granodiorite and contain about 30 vol. % K-feldspar phenocrysts that are similar in size and texture to that of the Llandudno granodiorite (e.g. Farina et al. 2012). These enclaves are interpreted to reflect more rapidly cooled early magmas that have subsequently been largely digested by the larger magma volume assembled as the pluton grew. The layering exposed at Llandudno also appears to have been part of a larger structure or structures. In particular, the well exposed southern termination of the main lens of well-preserved layering can be seen to feather out into diffuse biotite schlieren that disappear into the Llandudno granodiorite. Biotite schlieren are common in the pluton with almost every sizable outcrop has evidence of biotite schlieren that define layering to some degree. In the best developed cases there is clear alternation between biotite rich layers that are separated by more leucocratic granite. Typically these features are between 1 to 3 metres in length along strike and only consist of 1 to 3 repetitive layers, but in well preserved examples the textures in the biotite rich portions are markedly similar to the textures in the well preserved mafic portions of the layers. These features are interpreted to

represent digested disrupted layers and are taken as evidence that the layered structures seem to have formed a more significant part of the inventory of early formed textures in the Peninsula pluton or could have formed in response to an existing gradient of some variable that produced layers grading to schlieren. Consequently, understanding the petrogenesis of the layers very likely may provide significant insights into the petrogenesis of the pluton.

Composite layering in granites

Rhythmic layering in Llandudno granodiorite is in some aspects similar to that exhibited by many layered mafic intrusions in that it is predominantly planar. Within the Llandudno granodiorite, the sequence of formation is not evident in the layered sequence, though the sharp lower contacts associated with the cumulate textures in the lower portion and the way in which these textures grade over a short distance into the leucocratic portions is indicative that each layer formed from the mafic to the leucocratic portion of the layering. It is possible that this feature of the Llandudno granodiorite provides a relatively unique insight into the formation of layering in granites. If the leucocratic portion of the layers represents a relatively melt-dominated magma, as the Si-rich, low MgO + FeO and relatively high Na_2O:CaO ratio compositions suggest, from which the minerals which form the mafic portion segregated, then it is possible that in other instances this magma might drain away after depositing the mafic portion. In this case mafic portions would be produced that are either overlain by other mafic layers or intersperses with granite of similar composition and texture to the host granite. These phenomena are perhaps more common in granite than the composite layering observed at Llandudno.

The petrogenesis of the layers

Petrographic evidence

The textures of the mafic and leucocratic portions of the layering are visibly different. The mafic portions show clear orthocumulate texture with euhedral biotite grains, while the leucocratic portions show coarse grained granitic texture with phenocrystic quartz. These textures coupled with the field relations and gradational internal contact within layers indicates that the mafic and leucocratic portions formed concurrently. The euhedral biotite crystals occur as occasional inclusions within euhedral plagioclase in the mafic portions. Consequently, biotite is interpreted to have crystallised first, either directly from the melt or by early reaction of entrained peritectic minerals. Plagioclase crystallised subsequently and it

is likely the magma intruded Llandudno granodiorite with biotite, plagioclase and accessory minerals in suspension. The absence of any fracture at the upper or lower contact of the layering indicates that the Llandudno granodiorite was partially crystallised at this time. Flow alignment of K-feldspar megacrysts is common in the Llandudno granodiorite, and this is developed adjacent to the layering and in some areas at a steep angle to the layering. There is no disruption to the layering leading to the interpretation that the megacrysts had crystallised prior to the formation of the layering. This is consistent with the interpretation that the megacrysts that do occur within the layering are inherited from the Llandudno granodiorite. The mafic portions of the layers are interpreted to have formed by separation of biotite and plagioclase from the melt, with biotite, in particular, trapping and concentrating zircon, monazite and apatite as inclusions. This is interpreted to have been due to gravitational settling, assisted by biotite trapping a filtering out plagioclase into the mafic layer. Orthopyroxene would have formed a minor component of the ferromagnesian assemblage in the mafic layers, prior to its reaction with the cooling melt to form biotite. The rate of settling of crystals was modelled to gain insight into the rate of differentiation (Dosseto and Turner, 2011). They assumed that spherical olivine crystals with radius 0.1 cm settling in basaltic melt would settle at rate of 1m per day using Stokes' Law, while feldspar crystals in rhyolitic melt would settle much slower at rate of 2 cm/year. Assuming that a spherical biotite crystal with 0.1 cm radius in granitic melt; the crystal will settle at a slower rate of 0.69 cm/year within a 10 cm settling distance. Gravity settling is driven by the difference in density, ρ, between the crystal and the liquid and resisted by the liquid viscosity. The viscosity is reported to be due to the amount of the Fe in the liquid whilst viscosity is a function of silica content, water and alkali contents and temperature (Dosseto and Turner, 2011). Considering that the granodioritic melt in Llandudno is high in silica content, contain considerable amount of water and alkali contents this will then increase the viscosity of the melt, thus making the settling time for the biotite to be slower. This seems to be in agreement with the calculated settling rate. The leucocratic portions consisting mainly of coarse grained quartz phenocrysts are interpreted to have crystallised from the remaining melt after the separation of the mafic layers. These quartz phenocrysts are not present in the mafic portions, thus the deduction that they crystallised later when the remaining melt was silica rich after the mafic portion was formed. The leucocratic portion of the layering shows textural and compositional difference from the Llandudno granodiorite. The texture observed is different to what is seen in the Llandudno granodiorite which is mainly K-feldspar megacrystic. This is another indication that the layering was formed by a magma that is compositionally different from the

Llandudno granodiorite, and that the difference is not just the biotite and plagioclase accumulation seen in the textures. Plagioclase shows oscillatory zoning probably attributed to the changing temperature as the new magma cools down.

The whole rock chemistry case for the layers representing injection of magma different to the average magma which constructed the Cape Granodiorite

In general, the magmas which formed the Peninsula pluton are considered to be derived from the partial melting of a higher grade equivalent of the Malmesbury Group metasediments (Harris et al., 1997). The mineralogy of the layered zones confirm that the magma from which they formed was certainly peraluminous and granitic. However, if the compositions of entire layers are representative of the composition of the magma from which the layered rocks formed, this magma was more felsic than the hosting Llandudno granodiorite and at the same water content and temperature would have consisted of a lower proportion of crystals. As crystal accumulation is involved in shaping the mafic portions of the layers, it is unlikely that magma loss from the layered structures would have driven the composition of individual layers to more leucocratic values. Thus the felsic character of the complete layers is probably a reflection of the fact that the original magma was felsic. The bulk composition of the layered rocks suggests that the magma from which they formed was different from the magma which formed the Cape Granodiorite. This is most strongly indicated by the higher SiO_2 content, the lower $MgO+FeO^T$ and Al_2O_3 content of the complete layers, as well as their substantially more REE enriched compositions and different REE slopes (Fig. 12). Collectively this evidence suggests that the layering was produced by the injection of peraluminous granitic magma that was different in composition to the magmas from which the rest of the Cape Granodiorite was assembled. Since the Peninsula pluton is made of different facies, the difference in composition of the layering and the Llandudno granodiorite could mean that the source that formed the layering may possibly be similar to one of the other three facies in the Peninsula pluton.

The mineral chemical case for each layer forming from a new injection of magma.

There is variation in the composition of the early formed biotite Mg# {100(MgO/(FeO+MgO))} between the mafic portions of the different layers (Fig. 14). Biotite Mg# changes within layers from the base to the top (Fig. 14). In a general way biotite Mg# appears to decrease from the lower layers (e.g. L1 = 44, L3 = 41) towards the top (e.g. L6 = 36, L13 = 36) (Fig. 25). Biotite compositions vary significantly between the basal mafic

portion and leucocratic portion of individual layers (e.g. LL1 = 44 - 41, LL6 = 37- 34 respectively). The difference in biotite composition between the basal portions of adjacent layers suggests that each layer represents a separate magma. The biotite compositions within each layer, coupled with the biotite textures, suggest that the mafic portions of the layers largely represent an accumulation of early formed crystals that were in the magma batch at the time of injection and that these crystals mostly consisted of biotite with orthopyroxene (now reacted to biotite). The more restricted and overlapping range in biotite compositions within the leucocratic portions is taken to indicate that these biotite crystals formed from the melt following intrusion into the Llandudno granodiorite.

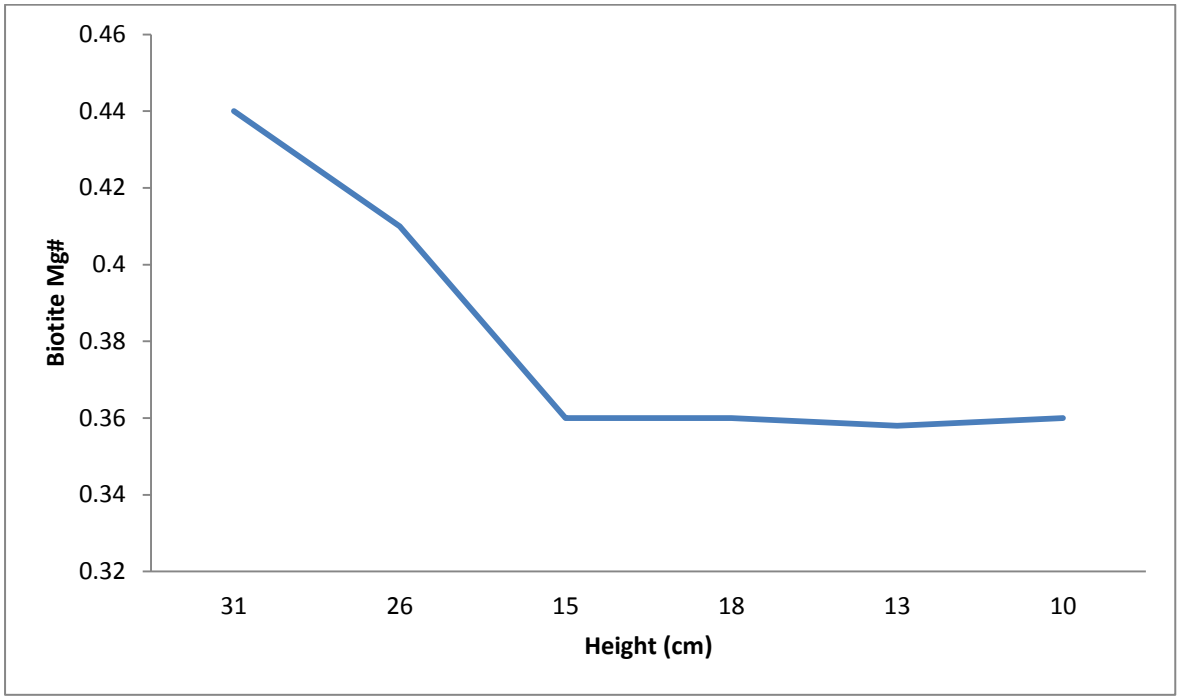

Fig. 25 Diagram illustrating the biotite Mg# and height within the layering.

The trapped liquid shift effect is an important mechanism of post cumulus modification of cumulate mineral Mg# in mafic cumulates (Cawthorn et al., 1992). Consequently, the influence of the trapped interstitial liquid on biotite composition in the mafic portion of the layers was investigated. This was achieved using the measured biotite compositions in the mafic portions and using the bulk rock composition of the overlying leucocratic portion as a proxy for the interstitial liquid composition. Cumulate biotite and interstitial liquid proportions were estimated via observation of the thin sections. An example is presented in Table. 6 and illustrates that with 40% biotite and 20% interstitial liquid, the Mg# of the

cumulus biotite is not shifted significantly by the crystallization of the interstitial liquid. This is due to the fact that granitic melts are low in FeO + MgO, as well as the fact that the Mg#s of biotite in the mafic portions and the whole rock composition of the leucocratic portions are similar (Fig. 26). Fig. 26 shows the results of this calculation for three samples. These findings strongly suggest that the differences in the Mg#s of biotite between the different mafic portions reflect original differences in the compositions of biotite crystallised within the different layers.

Table 6. Results of calculation

Elements (wt %)	**Biotite**	**Interstitial liquid**
MgO	8.32	0.47
FeO	25.44	1.39
Mg#	39.8	37.4
Biotite proportion in cumulate	0.35	
Liquid proportion in cumulate		0.25
Change in Mg# of cumulate Bt due to interstitial liquid crystallization		
Mg# cumulate Bt	36.8	
Mg# Biotite post interstitial liquid crystals	36.7	

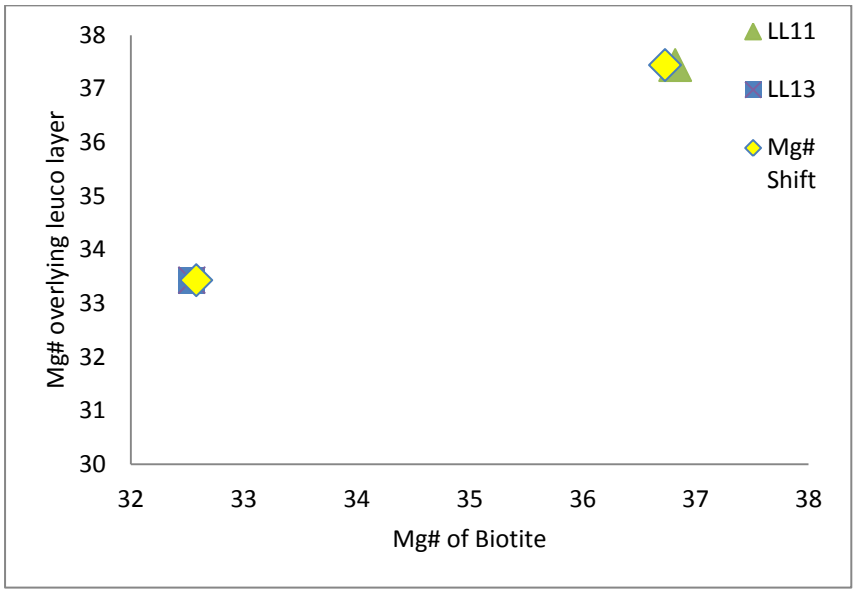

Fig. 26 Graph representation showing the Mg# of biotite in the mafic portion, the Mg# of the assumed interstitial liquid (taken from the bulk composition of the associated leucocratic layer), as well as the effect of the crystallization of the interstitial liquid on biotite composition.

Layering, magmatic enclaves and the construction of the Peninsula pluton

The field relations in the Llandudno area provide insight into some of the processes involved in the formation of the pluton. The preservation of mafic enclaves in the Llandudno granodiorite and other magmatic enclaves in the pluton, that are compositionally similar to the pluton, yet that have textures indicative of more rapid crystallizations, as well as the existence of the layering attest to a magma body that has grown through successive pulses of magma. The magmatic enclaves and the layering occupy opposite ends of this time spectrum. These enclaves are interpreted to represent early magma contributions that cooled and crystallised more rapidly than the main body of the pluton. They quite commonly contain garnet and K-feldspar phenocrysts in a range of sizes that are typically similar in size and texture to those in the host granite. Within the layering, K-feldspar phenocrysts much less variable in size are generally slightly smaller than the crystals in the Llandudno granodiorite. They are interpreted to have been inherited from the Llandudno granodiorite during injection of the magma which formed the layering. The relationship of the layering to flow fabrics within the megacrystic Llandudno granodiorite suggests the magmas which formed the layering intruded late in the crystallization history of the host Llandudno granodiorite.

CHAPTER EIGHT

CONCLUSIONS

Layering in granites is quite a rare and intriguing feature. There are many mechanisms proposed for the formation of layering, although there is little consensus about these mechanisms amongst researchers. This study found that the layering in the Llandudno granodiorite is composed of a basal mafic portion of the layer with a sharp lower intrusive contact which evolves through a relatively abrupt gradational contact into an upper leucocratic portion. This mafic-leucocratic pair was interpreted to represent a single layer due to the basal sharp contact and a diffuse upper contact. The layers seem to have formed sequentially, though the order of formation either from top to bottom or underplating is unknown. Biotite in the mafic portion of the layer show cumulate-like texture, and constitute approximately 50vol. % of the rock. The biotite Mg# in the mafic portion of the layers decreases from the bottom to the top of the layered sequence. The differences in the biotite composition in the basal mafic portion of the layer suggest that each layer represents a separate magma injection. The different composition and texture observed suggest that the mafic portion of the layer was formed by the accumulation of minerals that were most likely in suspension within the magma batch at the time of injection. The upper portion of the layer represents the products of crystallisation from the melt after the separation of the mafic portion. The layering appears to have been part of the larger structure, as seen by the digestion of the end of the layering at Llandudno, the existence of the three separate lenses of layering at Llandudno and the widespread occurrence of biotite schlieren within the pluton. These schlieren are interpreted to represent the remains of digested layering that formed earlier in the plutons history via a similar process to that describes at Llandudno. Thus, the layering at Llandudno provides a snapshot into pluton assembly via incremental addition of magma, which has been preserved because the magma injected into the pluton very late in its crystallization history.

REFERENCES

Barbey, P., Gasquet, D., Pin, C., Bourgeix, A.L., (2008). Igneous banding, schlieren and mafic enclaves in calc-alkaline granites: The Budduso pluton (Sardinia): Lithos, 104, 147–163.

Barbey, P., (2009). Layering and schlieren in granitoids: a record of interactions between magma emplacement, crystallisation and deformation in growing plutons: Geologica Belgica, 12(3-4), 109-133.

Barrière, M., (1981). On curved laminae, graded layers, convection currents and dynamic crystal sorting in the Ploumanac'h (Brittany) subalkaline granite: Contributions to Mineralogy and Petrology, 77, 214-224.

Burgess, S.D., Miller, J.S., (2008). Construction, solidification and internal differentiation of a large felsic arc pluton: Cathedral Peak granodiorite, Sierra Nevada Batholith, in Annen, C., and Zellmer, G.F., (eds), Dynamics of crustal magma transfer, storage and differentiation: Geological Society of London Special Publication, 304, 203–234.

Cawthorn, R. G., Sander, B. K., Jones, I. M., (1992). Evidence for the trapped liquid shift effect in the Mount Ayliff Intrusion, South Africa. Contributions to Mineralogy and Petrology, 111(2), 194-202.

Chu, M. F., Wang, K. L., Griffin, W. L., Chung, S. L., O'Reilly, S. Y., Pearson, N. J., Iizuka, Y., (2009). Apatite composition: tracing petrogenetic processes in Transhimalayan granitoids. Journal of Petrology, 50(10), 1829-1855.

Clarke, D.B., Clarke, G.K.C., (1998). Layered granodiorites at Chebutco Head, South Mountain batholith, Nova Scotia: Journal of Structural Geology, 20, 1305–1324.

Clemens, J.D.,Wall, V.J., (1981). Origin and crystallization of some peraluminous (S-type) granitic magmas: Canadian Mineralogist, 19, 111–131.

Clemens, J.D., Benn, K., (2010). Anatomy, emplacement and evolution of a shallow-level, post-tectonic laccolith: the Mt Disappointment pluton, SE Australia: J Geol Soc, 167,915–941.

Clemens, J.D., Stevens, G., Farina, F., (2011). The enigmatic sources of I-type granites: The peritectic connexion: Lithos, 126, 174-181.

Clemens, J.D., Stevens, G., (2012). What controls chemical variation in granitic magmas? Lithos, 126, 317-329.

Da Silva, L.C., Gresse, P.G., Scheepers, R., McNaughton, N.J., Hartmann, L.A., Fletcher, I., (2000). U-Pb SHRIMP and Sm-Nd age constraints on the timing and sources of the Pan-African Cape Granite Suite, South Africa: J Afr Earth Sci 30,795–815.

Dosseto, A., Turner, S.P., (2011). Magma cooling and differentiation-Uranium-series Isotopes. In: Dosseto, A., Turner, S.P., Van Orman, J.A., (eds). Timescales of Magmatic processes: from core to atmosphere. Wiley-Blackwell, Chichester West Sussex, UK; Hoboken, NJ, 160-180.

Eggins, S., (2003). Laser ablation ICP-MS analysis of geological materials prepared as lithium borate glasses: Geostand Geoanal Res, 27,147–162.

Farina, F., Dini, A., Innocenti, F., Rocchi, S., Westerman, D. S., (2010). Rapid incremental assembly of the Monte Capanne pluton (Elba Island, Tuscany) by downward stacking of magma sheets. Geological Society of America Bulletin, 122(9-10), 1463-1479.

Farina, F., Stevens, G., Villaros, A., (2012). Multi-batch, incremental assembly of a dynamic magma chamber: the case of the Peninsula pluton granite (Cape Granite Suite, South Africa): Mineralogy and Petrology, 1-24.

Glazner, A.F., Bartley, J.M., Coleman, D.S., Gray, W., (2004). Are plutons assembled over millions of years by amalgamation from small magma chambers? GSA Today, 14, 4–11.

Glazner, A.F., Bartley, J.M., Coleman, D.S., Boudreau, A., Walker, J.D., (2007). Questioning the sedimentary paradigm for granites. In AGU Fall Meeting Abstracts, 1, 08.

Gresse, P.G., Chemale, Jr., F., da Silva, L.C., Walraven, F., Hartmann, L.A., (1996). Late- to post-erogenic basins of the Pan-African/Brasiliano collision orogen in southern Africa and southern Brazil: Basin Research, 8, 157- 171.

Harris, C., Faure, K., Diamond, R.E., Scheepers, R., (1997). Oxygen and hydrogen isotope geochemistry of S- and I-type granitoids: the Cape Granite Suite, South Africa: Chem Geol 143, 95–114.

Holdaway, M.J., (2000). Application of new experimental and garnet Margules data to the garnet–biotite geothermometer: American Mineralogist, 85, 881–892.

Irvine, T.N., Andersen, J.C.O., Brooks, C.K., (1998). Included blocks (and blocks within blocks) in the Skaergaard intrusion: Geologic relations and the origins of rhythmic modally graded layers: Geological Society of America Bulletin, 110, 1398-1447.

Klemme, S., Günther, D., Hametner, K., Prowatke, S., Zack, T., (2006). The partitioning of trace elements between ilmenite, ulvospinel, armalcolite and silicate melts with implications for the early differentiation of the moon: Chemical Geology, 234(3), 251-263.

Mahan, K.H., Bartley, J.M., Coleman, D.S., Glazner, A.F., Carl, B.S., (2003). Sheeted intrusion of the synkinematic McDoogle pluton, Sierra Nevada, California: Geological Society of America Bulletin, 115, 1570–1582.

Matzel, J. E., Bowring, S. A., Miller, R. B., (2006). Time scales of pluton construction at differing crustal levels: Examples from the Mount Stuart and Tenpeak intrusions, North Cascades, Washington. Geological Society of America Bulletin, 118(11-12), 1412-1430.

Miller, R.B., Paterson, S.R., (1999). In defense of magmatic diapirs: Journal of Structural Geology, 21, 1161–1174.

Moore, J.G., Sisson, T.W., (2008). Igneous phenocrystic origin of K-feldspar megacrysts in granitic rocks from the Sierra Nevada batholith. Geosphere, 4(2):387–400.

Morisset, C., Scoates, J. S., Weis, D. A., (2010). Partitioning of trace elements during exsolution in ilmenite-hematite series minerals by LA-ICP-MS. In AGU Fall Meeting Abstracts, 1, 2291.

Moyen J.F., Stevens G., Kisters A., (2006). Record of mid-Archaean subduction from metamorphism in the Barberton terrain, South Africa: Nature, 442, 559–562.

Naney, M.T., Swanson, S.E., (1980). The effect of Fe and Mg on crystallization in granitic systems: American Mineralogist, 65, 639–653.

Naslund, H. R., McBirney, A. R., (1996). Mechanisms of formation of igneous layering. In: Cawthorn, R. G. (ed.) Layered Intrusions. Amsterdam: Elsevier, 1-43.

Reid, J.B., Murray, D.P., Hermes, O.D., Steig, E.J., (1993). Fractional crystallization in granites of the Sierra Nevada: how important is it? Geology 21 (7), 587–590.

Rockhold, J.R., Nabelek, P.I., Glascock, M. D., (1987). Origin of rhythmic layering in the Calamity Peak satellite pluton of the Harney Peak Granite, South Dakota: The role of boron: Geochimica et Cosmochimica Acta, 51(3), 487-496.

Rozendaal, A., Gresse P.G., Scheepers, R., Le Roux, J.P., (1999). Neoproterozoic to early Cambrian crustal evolution of the Pan- African Saldania Belt, South Africa: Precambrian Res, 97, 303–323.

Paterson, S.R., Kenneth Fowler, T., (1993). Re-examining pluton emplacement processes: Journal of Structural Geology, 15(2), 191-206.

Paterson, S.R., Kenneth Fowler, T., Miller, R.B., (1996). Pluton emplacement in arcs: a crustal-scale exchange process. Trans. R. Geol. Soc. Edinburgh: Earth Sci. 87, 115–123.

Paterson, S.R., Vernon, R.H., Žák, J., (2005). Mechanical instabilities and physical accumulation of K-feldspar megacrysts in granitic magma, Tuolumne Batholith, California, USA: Journal of the Virtual Explorer, 18(1), 1-18.

Paterson, S.R., (2009). Magmatic tubes, pipes, troughs, diapirs, and plumes: late-stage convective instabilities resulting in compositional diversity and permeable networks in crystal-rich magmas of the Tuolumne batholith, Sierra Nevada, California: Geosphere, 5, 496–527.

Pearce, N,J.G., Perkins, W.T., Westgate, J.A., Gorton, M.P., Jackson, S.E., Meal, C.R., Chenery, S.P., (1997). A compilation of new and published major and trace element data for NIST SRM610 and NIST SRM612 glass reference materials: Geostand Newslett, 21, 115–144.

Petford, N., Cruden, A.R., McCaffrey, K.J.W., Vigneresse, J.L., (2000). Granite magma formation, transport and emplacement in the Earth's crust: Nature, 408, 669–673.

Pupier, E., Barbey, P., Toplis, M. J., Bussy, F., (2008). Igneous layering, fractional crystallization and growth of granitic plutons: the Dolbel Batholith in SW Niger: Journal of Petrology, 49, 1043-1068.

Scheepers, R., Rozendaal, A., (1992). Relationship of the Riviera W- (MO-Cu) deposit to magmatism in the south-western Cape Province, South Africa. In: Abstracts Geocongress 1992: Geological Society South Africa, 339-341.

Scheepers, R., (1995). Geology, geochemistry and petrogenesis of Late Precambrian S-, I- and A-type granitoids in the Saldania belt, Western Cape Province South Africa: J Afr Earth Sci, 21, 35–58.

Scheepers, R., (2000). Granites of the Saldania mobile belt, South Africa: radioelements and P as discriminators applied to metallogeny: Journal of Geochemical Exploration 68(1), 69–86.

Scheepers, R., Armstrong, R.A., (2002). New U-Pb SHRIMP zircon ages of the Cape Granite Suite: implications for the magmatic evolution of the Saldania Belt: S Afr J Geol, 105, 241–256.

Scheepers, R., Poujol, M., (2002). U-Pb zircon age of Cape Granite Suite ignimbrites: characteristics of the last phases of the Saldanian Magmatism: S Afr J Geol, 105, 163–178.

Seaman, S.J., Scherer, E.E., Standish, J.J., (1995). Multistage magma mingling and the origin of flow banding in the Aliso lava dome, Tumacacori Mountains, southern Arizona: J. Geophys. Res, 100, 8381–8398.

Sha, L. K., Chappell, B. W., (1999). Apatite chemical composition, determined by electron microprobe and laser-ablation inductively coupled plasma mass spectrometry, as a probe into granite petrogenesis: Geochimica et Cosmochimica Acta, 63(22), 3861-3881.

Solgadi, F., Sawyer, E.W., (2008). Formation of Igneous layering in granodiorite by gravity flow: a field, microstructure and geochemical study of the Tuolumne Intrusive Suite at Sawmill Canyon, California: Journal of Petrology, 49 (11), 2009-2042.

Stevens, G., Villaros, A., Moyen, J.F., (2007). Selective peritectic garnet entrainment as the origin of geochemical diversity in S-type granites: Geology 35(1), 9–12.

Urbain, G., Bottinga, Y., Richet, P., (1982). Viscosity of liquid silica, silicates and alumino-silicates: Geochimica et Cosmochimica Acta, 46(6), 1061-1072.

Vigneresse, J.L., Barbey, P., Cuney, M., (1996). Rheological transitions during partial melting and crystallization with application to felsic magma segregation and transfer: Journal of Petrology, 37(6), 1579–1600.

Villaros, A., Stevens, G., Moyen, J.F., Buick, I.S., (2009a). The trace element composition of S-type granites: evidence for disequilibrium melting and accessory phase entrainment in the source: Contrib Mineral Petrol, 158, 543–561.

Villaros, A., Stevens, G., Buick, I.S., (2009b). Tracking S-type granite from source to emplacement: clues from garnet in the Cape Granite Suite: Lithos, 112(3–4), 217–235.

Villaros, A., Buick, I.S., Stevens, G., (2011). Isotopic variations in S-type granites: an inheritance from a heterogeneous source: Contrib Mineral Petrol, 163, 243–257.

Weinberg, R.F., Sial, A.N., Pessoa, R.R., (2001). Magma flow within the Tavares pluton, north-eastern Brazil: compositional and thermal convection: Geological Society of America Bulletin, 113 (4), 508–520.

Wiebe, R.A., (1996). Mafic-silicic layered intrusions: The role of basaltic injections on magmatic processes and the evolution of silicic magma chambers: Royal Society of Edinburgh Transactions, Earth Sciences, 87, 233–242.

Wiebe, R.A., Collins, W.J., (1998). Depositional features and stratigraphic sections in granitic plutons: implications for the emplacement and crystallization of granitic magma: Journal of Structural Geology, 20 (9–10), 1273–1289.

Wiebe, R.A., Jellinek, M., Markley, M.J., Hawkins, D.P., Snyder, D., (2007). Steep schlieren and associated enclaves in the Vinalhaven granite, Maine: possible indicators for granite rheology: Contrib Mineral Petrol, 153, 121–138.

Žák, J., Paterson, S.R., (2005). Characteristics of internal contacts in the Tuolumne Batholith, central Sierra Nevada, California (USA): implications for episodic emplacement and physical processes in a continental arc magma chamber: Geological Society of America Bulletin, 117, 1242-1255.

Žák, J., Paterson, S.R., Memeti, V., (2007). Four magmatic fabrics in the Tuolumne batholith, central Sierra Nevada, California (USA): implications for interpreting fabric patterns and

evolution of magma chambers in the upper crust: Geological Society of America Bulletin, 119, 184-201.

Žák, J., Klomínský, J., (2007). Magmatic structures in the Krkonoše-Jizera Plutonic Complex, Bohemian Massif: Evidence for localized multiphase flow and small-scale thermal-mechanical instabilities in a granitic magma chamber: Journal of Volcanology and Geothermal Research, 164, 254–267.

APPENDICES

Appendix 1. Representative LA ICP MS trace element data for apatite and monazite normalised to chondrite. The words 'Mafic' and 'Leucocratic' relate to the mafic portion of layers and the leucocratic portion of layers respectively. Analytical details are provided in the main text.

Rock Type	La	Ce	Pr	Nd	Sm	Eu	Gd	Tb	Dy	Ho	Er	Tm	Yb	Lu
	Apatite													
Host Granite	739	1033	1236	1109	1567	50	1491	1597	1500	1217	1026	972	871	713
Mafic	784	1072	1213	1168	1628	53	1550	1689	1601	1307	1112	1061	953	777
Leucocratic	808	1096	1231	1178	1665	51	1595	1735	1632	1330	1117	1074	965	790
	Monazite													
Host Granite	329753	250437	198810	151168	87030	1658	47905	28316	17641	10429	5774	3156	1680	974
Mafic	331289	250437	198136	151961	85073	1933	46488	26662	16512	9894	5423	2924	1532	872
Leucocratic	324849	250437	197593	150618	84635	1802	46820	27329	16798	9979	5435	2939	1543	880

Appendix 2. Mineral chemistry of individual K-feldspar megacrysts taken from three separate layers within the layered rocks (L) and within the Llandudno granodiorite (G) adjacent to the layering. The first and last compositions in each sequence represent the rims and the cores are represented by the analyses towards the middle of the sequence. Analytical and sampling details are provided within the text.

Sample	Spectrum	Na_2O	Al_2O_3	SiO_2	K_2O	CaO	BaO	Total	Na	Al	Si	K	Ca	Ba	An	Ab	Or
L1	1	2.62	18.11	65.94	12.28	0.00	0.38	99.32	0.23	0.98	3.02	0.72	0.00	0.01	0.00	0.24	0.76
	2	0.51	17.83	65.01	15.51	0.00	0.57	99.43	0.05	0.98	3.02	0.92	0.00	0.01	0.00	0.05	0.95
	3	0.57	17.84	65.95	15.39	0.00	0.35	100.09	0.05	0.97	3.03	0.90	0.00	0.01	0.00	0.05	0.95
	4	0.44	17.94	65.50	15.80	0.00	0.33	100.00	0.04	0.98	3.02	0.93	0.00	0.01	0.00	0.04	0.96
	5	0.53	18.10	64.95	15.49	0.17	0.57	99.81	0.05	0.99	3.01	0.92	0.01	0.01	0.01	0.05	0.94
	6	0.80	18.08	65.82	15.14	0.00	0.49	100.33	0.07	0.98	3.02	0.89	0.00	0.01	0.00	0.07	0.93
	7	1.75	18.41	66.14	13.93	0.13	0.49	100.85	0.15	0.99	3.01	0.81	0.01	0.01	0.01	0.16	0.83
	8	0.32	17.96	65.68	15.72	0.00	0.51	100.19	0.03	0.97	3.03	0.92	0.00	0.01	0.00	0.03	0.97
	9	1.09	17.87	66.08	15.17	0.17	0.00	100.38	0.10	0.96	3.03	0.89	0.01	0.00	0.01	0.10	0.89
L2	1	0.83	17.64	65.01	15.85	0.00	0.00	99.33	0.08	0.97	3.02	0.94	0.00	0.00	0.00	0.07	0.93
	2	0.44	17.64	64.40	16.14	0.12	0.35	99.09	0.04	0.97	3.01	0.96	0.01	0.01	0.01	0.04	0.95
	3	1.11	17.51	64.90	15.15	0.13	0.23	99.03	0.10	0.96	3.02	0.90	0.01	0.00	0.01	0.10	0.89
	4	0.52	17.15	64.08	16.14	0.15	0.41	98.46	0.05	0.95	3.02	0.97	0.01	0.01	0.01	0.05	0.95
	5	0.37	17.61	64.75	16.09	0.16	0.40	99.39	0.03	0.97	3.02	0.96	0.01	0.01	0.01	0.03	0.96
	6	0.31	17.55	65.04	16.45	0.00	0.22	99.57	0.03	0.96	3.03	0.98	0.00	0.00	0.00	0.03	0.97
	7	0.40	17.43	64.36	16.24	0.00	0.00	98.43	0.04	0.97	3.02	0.97	0.00	0.00	0.00	0.04	0.96
	8	0.98	17.67	65.25	15.56	0.00	0.00	99.46	0.09	0.97	3.02	0.92	0.00	0.00	0.00	0.09	0.91
	9	0.44	17.60	64.66	16.15	0.00	0.00	98.86	0.04	0.97	3.02	0.96	0.00	0.00	0.00	0.04	0.96
L3	1	1.74	18.02	64.64	14.07	0.00	0.64	99.10	0.16	0.99	3.01	0.83	0.00	0.01	0.00	0.16	0.84
	2	1.12	17.80	64.78	15.21	0.14	0.60	99.65	0.10	0.97	3.01	0.90	0.01	0.01	0.01	0.10	0.89
	3	2.15	18.05	66.13	13.59	0.14	0.33	100.39	0.19	0.97	3.02	0.79	0.01	0.01	0.01	0.19	0.80
	4	2.52	17.99	66.33	13.08	0.17	0.00	100.09	0.22	0.97	3.02	0.76	0.01	0.00	0.01	0.22	0.77
	5	0.93	17.87	66.02	15.95	0.00	0.00	100.77	0.08	0.96	3.02	0.93	0.00	0.00	0.00	0.08	0.92
	6	0.62	17.86	65.50	16.11	0.13	0.00	100.22	0.05	0.97	3.02	0.95	0.01	0.00	0.01	0.05	0.94
	7	2.03	17.99	66.31	14.02	0.00	0.00	100.35	0.18	0.97	3.03	0.82	0.00	0.00	0.00	0.18	0.82
	8	0.42	17.77	65.76	16.36	0.00	0.00	100.30	0.04	0.96	3.03	0.96	0.00	0.00	0.00	0.04	0.96
	9	0.44	17.83	65.97	16.37	0.16	0.00	100.76	0.04	0.96	3.02	0.96	0.01	0.00	0.01	0.04	0.95

G1	1	1.04	18.17	66.43	13.72	0.13	0.00	99.49	0.09	0.98	3.04	0.80	0.01	0.00	0.01	0.10	0.89
	2	1.10	17.97	66.20	14.97	0.00	0.00	100.24	0.10	0.97	3.03	0.87	0.00	0.00	0.00	0.10	0.90
	3	0.98	18.03	65.89	15.27	0.00	0.23	100.39	0.09	0.97	3.02	0.89	0.00	0.00	0.00	0.09	0.91
	4	0.51	18.07	65.81	15.68	0.16	0.40	100.63	0.05	0.98	3.02	0.92	0.01	0.01	0.01	0.05	0.95
	5	0.44	18.12	66.32	15.92	0.00	0.00	100.80	0.04	0.97	3.03	0.93	0.00	0.00	0.00	0.04	0.96
	6	1.94	18.07	67.01	13.39	0.00	0.22	100.63	0.17	0.97	3.04	0.77	0.00	0.00	0.00	0.18	0.82
	7	0.61	17.59	65.17	15.54	0.15	0.26	99.32	0.05	0.96	3.03	0.92	0.01	0.00	0.01	0.06	0.94
	8	0.83	18.05	65.93	15.35	0.00	0.37	100.53	0.07	0.98	3.02	0.90	0.00	0.01	0.00	0.08	0.92
	9	0.95	18.00	65.41	15.13	0.11	0.38	99.98	0.08	0.98	3.02	0.89	0.01	0.01	0.01	0.09	0.91
G2	1	0.71	17.66	65.64	15.43	0.12	0.00	99.57	0.06	0.96	3.03	0.91	0.01	0.00	0.01	0.07	0.93
	2	2.34	18.27	66.20	13.46	0.00	0.53	100.79	0.21	0.98	3.01	0.78	0.00	0.01	0.00	0.21	0.79
	3	1.08	18.13	66.58	14.49	0.00	0.42	100.71	0.10	0.97	3.03	0.84	0.00	0.01	0.00	0.10	0.90
	4	0.97	18.08	66.26	15.43	0.12	0.00	100.87	0.09	0.97	3.02	0.90	0.01	0.00	0.01	0.09	0.91
	5	1.36	18.09	65.54	14.77	0.12	0.23	100.10	0.12	0.98	3.01	0.87	0.01	0.00	0.01	0.12	0.87
	6	0.73	17.97	65.32	15.82	0.12	0.28	100.23	0.07	0.98	3.01	0.93	0.01	0.01	0.01	0.07	0.93
	7	1.89	18.04	66.31	13.14	0.13	0.00	99.51	0.17	0.97	3.03	0.77	0.01	0.00	0.01	0.18	0.82
	8	0.36	17.63	65.36	15.97	0.33	0.31	99.96	0.03	0.96	3.02	0.94	0.02	0.01	0.02	0.03	0.95
	9	2.28	18.02	66.29	13.90	0.00	0.24	100.73	0.20	0.97	3.02	0.81	0.00	0.00	0.00	0.20	0.80
G3	1	1.11	17.73	65.05	14.87	0.00	0.56	99.32	0.10	0.97	3.02	0.88	0.00	0.01	0.00	0.10	0.90
	2	0.65	17.89	65.16	15.32	0.12	0.37	99.51	0.06	0.98	3.02	0.91	0.01	0.01	0.01	0.06	0.93
	3	0.86	18.03	65.92	14.71	0.00	0.57	100.09	0.08	0.98	3.03	0.86	0.00	0.01	0.00	0.08	0.92
	4	1.98	18.17	66.12	13.62	0.00	0.33	100.22	0.18	0.98	3.02	0.79	0.00	0.01	0.00	0.18	0.82
	5	0.72	17.93	65.70	15.81	0.13	0.43	100.71	0.06	0.97	3.02	0.93	0.01	0.01	0.01	0.06	0.93
	6	0.68	17.68	64.99	15.68	0.00	0.26	99.28	0.06	0.97	3.02	0.93	0.00	0.00	0.00	0.06	0.94
	7	0.52	17.79	64.34	15.60	0.19	0.61	99.05	0.05	0.98	3.01	0.93	0.01	0.01	0.01	0.05	0.94
	8	2.62	18.13	66.15	12.03	0.15	0.49	99.58	0.23	0.98	3.03	0.70	0.01	0.01	0.01	0.25	0.75
	9	1.26	18.01	65.82	15.03	0.12	0.44	100.69	0.11	0.97	3.02	0.88	0.01	0.01	0.01	0.11	0.88

Appendix 3. LA ICP MS trace element profiles across individual K-feldspar megacrysts from three separate layers within the layered rocks (L) and from three K-feldspar megacrysts sampled within the Llandudno granodiorite (G) adjacent to the layering. All compositions are normalised to the average megacryst composition in sample G3. The first and last compositions in each sequence represent the rims, with the cores represented by the analyses towards the middle of the sequence. Analytical and sampling details are provided in the text.

Element		Rb	Sr	Y	Cs	Ba	La	Ce	Pr	Nd	Sm	Eu	Gd	Pb	Eu*	Distance (mm)
L1	1	0.97	0.85	0.40	1.55	0.46	0.73	0.70	0.65	0.54	0.87	0.89	0.78	0.97	1.09	1.33
	2	1.20	0.83	0.93	2.08	0.74	0.94	0.99	0.91	0.87	0.76	0.92	1.11	0.99	0.97	2.13
	3	1.20	1.02	0.48	3.62	0.70	0.26	0.21	0.17	0.19	0.32	0.99	0.72	1.24	1.90	2.93
	4	1.08	0.86	1.19	3.87	0.62	0.27	0.21	0.19	0.25	0.64	0.79	1.01	0.95	0.95	3.73
	5	1.16	1.05	0.42	1.29	0.73	1.06	0.99	0.90	0.80	0.85	1.04	1.08	1.45	1.08	4.53
	6	0.98	0.84	0.54	2.97	0.75	0.36	0.30	0.26	0.28	0.43	0.80	0.78	0.91	1.32	5.33
	7	1.13	1.11	0.51	2.75	0.84	0.92	0.85	0.73	0.65	0.41	1.04	1.08	1.24	1.39	6.13
	8	1.27	0.77	0.53	3.27	0.61	1.19	1.21	1.13	1.05	0.79	0.86	1.22	1.25	0.86	6.93
	9	1.17	0.67	0.71	1.50	0.55	0.73	0.68	0.65	0.60	0.54	0.69	1.01	0.80	0.89	7.73
L2	1	1.16	0.95	1.46	3.48	0.81	0.88	0.90	0.84	0.80	1.07	1.03	0.88	1.33	1.06	0.71
	2	0.96	0.84	0.40	1.38	0.77	0.76	0.75	0.67	0.60	0.81	0.83	0.72	0.98	1.09	1.86
	3	1.20	0.68	0.31	1.71	0.46	0.30	0.27	0.22	0.24	0.37	0.66	0.50	0.86	1.50	3.00
	4	1.19	0.72	0.38	1.67	0.48	0.26	0.24	0.15	0.26	0.38	0.71	1.01	1.31	1.02	4.14
	5	1.28	0.75	0.35	3.82	0.47	0.23	0.19	0.18	0.20	0.24	0.74	0.76	1.01	1.48	5.29
L3	1	1.05	0.92	0.33	1.00	0.21	0.27	0.29	0.26	0.29	0.56	1.00	1.01	0.80	1.27	6.28
	2	1.02	0.83	0.30	0.89	0.26	0.19	0.21	0.23	0.22	0.31	0.75	0.88	0.88	1.27	9.47
	3	1.08	0.83	0.36	0.98	0.35	0.26	0.35	0.41	0.40	0.52	0.85	1.18	0.80	1.01	12.65
	4	0.83	0.71	0.23	1.66	0.26	0.23	0.26	0.25	0.30	0.52	0.72	1.11	0.61	0.89	15.84
	5	1.12	0.90	0.32	3.18	0.49	0.47	0.51	0.52	0.42	0.43	0.81	1.25	0.95	0.96	19.03
	6	1.09	0.93	1.96	3.51	0.53	0.43	0.40	0.45	0.47	0.50	0.88	1.38	0.90	0.94	22.21

G1	1	1.33	0.30	0.19	2.19	0.12	0.28	0.29	0.28	0.17	0.52	0.25	0.42	0.78	0.53	0.79
	2	1.28	0.65	0.18	1.48	0.24	0.41	0.40	0.36	0.36	0.60	0.55	0.81	0.96	0.78	2.00
	3	1.30	0.97	0.80	2.05	0.72	0.60	0.64	0.60	0.55	0.87	0.96	0.81	0.95	1.14	3.21
	4	1.11	0.89	0.74	2.27	0.52	0.45	0.42	0.44	0.45	0.54	0.80	1.28	0.98	0.88	4.43
	5	1.26	1.14	0.89	1.65	0.76	1.09	1.13	1.06	0.91	0.56	1.07	1.08	1.43	1.30	5.64
	6	1.17	0.74	0.34	3.90	0.43	0.24	0.18	0.12	0.15	0.52	0.72	0.55	1.06	1.34	6.86
	7	1.33	0.70	1.19	1.73	0.48	0.55	0.53	0.56	0.60	0.52	0.65	0.95	0.88	0.89	8.07
	8	1.03	0.72	1.00	1.06	0.44	0.60	0.63	0.61	0.72	0.30	0.72	0.61	0.79	1.57	9.29
G2	1	1.45	0.69	0.24	5.90	0.49	0.43	0.41	0.36	0.32	0.46	0.73	0.56	0.91	1.42	1.06
	2	1.12	0.76	0.46	4.01	0.70	0.41	0.29	0.22	0.17	0.54	0.83	0.57	0.87	1.49	2.55
	3	0.85	1.11	0.51	0.45	0.93	0.88	0.88	0.74	0.82	0.64	1.17	1.15	0.93	1.31	4.04
	4	0.94	1.33	0.94	0.76	1.12	1.22	1.29	1.26	1.22	0.79	1.34	1.28	1.17	1.30	5.53
	5	0.96	0.72	0.51	0.77	0.49	0.26	0.27	0.26	0.21	0.45	0.71	0.86	0.76	1.07	7.02
	6	1.08	0.92	0.36	1.80	0.48	0.57	0.57	0.58	0.50	0.34	0.88	0.95	1.03	1.37	8.51
	7	0.99	0.83	0.56	0.46	0.49	0.42	0.43	0.41	0.40	0.43	0.83	0.71	0.84	1.45	10.00
	8	1.16	0.97	0.54	2.02	0.56	0.43	0.39	0.33	0.36	0.45	0.99	0.98	1.03	1.39	11.49
	9	1.05	0.77	0.35	0.60	0.47	0.28	0.31	0.31	0.33	0.41	0.75	0.88	0.77	1.16	12.98
	10	1.28	1.06	0.47	3.22	1.10	1.08	1.00	0.95	0.86	0.41	1.13	0.64	1.42	2.15	14.47
	11	1.06	0.84	0.41	2.05	0.57	0.85	0.86	0.90	0.65	0.35	0.88	0.78	0.84	1.55	15.96
G3	1	1.18	0.97	1.79	2.56	1.16	1.27	1.26	1.28	1.19	0.66	1.13	1.32	0.91	1.14	1.77
	2	0.99	0.94	0.64	0.58	0.97	0.91	0.90	0.83	0.97	0.39	0.95	0.61	0.96	1.90	3.10
	3	1.04	0.92	0.93	0.90	1.01	0.93	0.95	1.00	0.91	1.26	0.88	0.64	0.99	0.92	4.42
	4	1.00	0.98	0.76	0.69	1.02	0.95	0.91	0.94	0.97	0.81	0.93	1.15	1.04	0.95	5.75
	5	1.04	0.94	1.43	1.08	0.85	0.98	0.99	1.05	1.04	1.63	0.91	1.35	1.08	0.61	7.08
	6	0.98	0.92	0.62	0.75	0.89	0.82	0.84	0.83	0.87	0.99	0.89	1.08	0.98	0.86	8.41
	7	0.91	1.07	0.92	0.75	0.98	1.05	1.02	0.98	0.99	1.10	1.09	1.08	1.02	1.00	9.73
	8	0.87	1.26	0.91	0.69	1.13	1.08	1.13	1.09	1.06	1.16	1.23	0.78	1.03	1.27	11.06